LOW VELOCITY IMPACT RESPONSE OF LAMINATED TEXTILE COIR-ARAMIDS/EPOXY HYBRID COMPOSITES SUBJECTED TO TRANSVERSE PENETRATION LOADING

by

AZRIN HANI BINTI ABDUL RASHID

Thesis submitted in fulfilment of the

requirements for the degree of

Doctor of Philosophy

April 2015

ACKNOWLEDGEMENTS

First and above all, all praise is for Allah SWT, the most gracious and the most merciful, for providing me this opportunity and granting me the capability to complete what I have started. This acknowledgement is a tribute to the individuals who have assisted and inspired me in the undertaking and the completion of this research. My deepest and sincerest gratitude goes to my supervisor, Assoc. Prof. Dr. Roslan Ahmad and my co-supervisor, Prof. Ir. Dr. Mariatti Jaafar@Mustapha for their warm encouragement, inspiration, thoughtful guidance, critical comments and invaluable support throughout the duration of the thesis project.

My special appreciation is dedicated to University Tun Hussein Onn Malaysia (UTHM), Johor and the Ministry of Education Malaysia for providing the scholarship through the IPTA Academic Training Scheme (SLAI) during my period of study. I am greatly indebted to the academic and management staffs of University Sains Malaysia (USM) and UTHM, as well as the laboratory staffs who have assisted me during the experimental stages and supported me in many ways. I am also most thankful for the support of my research fellows and colleagues.

Last but not least, I would like to express my gratefulness to my beloved family for their support and understanding throughout the journey. To my parents, from the bottom of my heart, thank you for your amazing endless love and support. To my beloved husband and kids, for all that we have been through, there is nothing more I could say except thank you for the patience. All of you are my motivation to be a better person every day. I dedicate my thesis to my lovely family.

TABLE OF CONTENTS

Page

LIST OF TABLES

LIST OF FIGURES

LIST OF SYMBOLS

Symbols	Descriptions
NaOH	Sodium hydroxide
E_a	Energy absorbed
E_m	Energy absorbed at maximum load point
E_p	Propagation energy
E_r	Residual energy
E_t	Total impact energy
U_{tot}	Total fracture energy
P_{peak}	Peak load
δ_{peak}	Total displacement to peak load
δ_{tot}	Maximum displacement
t_{peak}	Time at peak load
t_{tot}	Total time to penetration
DI	Ductility index
ε	Inter-yarn fabric porosity
d	diameter
m	Mass
t	Thickness
SEA_{peak}	Specific energy absorbed to peak load
SEA_{tot}	Specific total energy absorbed
wt%	Weight percentage
R^2	Coefficient of determination
Tex	Unit of measure for the linear mass density of fibres
epi	Ends per inch
ppi	Picks per inch
dpi	Dots per inch

LIST OF ABBREVIATIONS

Notations	Descriptions
AFTA	ASEAN Free Trade Area
ANOVA	Analysis of variance
ASTM	American Standard Testing Material
CFRP	Carbon fibre-reinforced polymer
DF	Degree of freedom
DOE	Design of experiment
FRP	Fibre-reinforced polymer
GFRP	Glass fibre-reinforced polymer
MS	Mean square
MW	Molecular weight
NF	Natural Fibre
PMC	Polymeric (plastic) matrix composites
PVA	Polyvinyl alcohol
SEM	Scanning electron microscope
SS	Sum of squares
TGRT	Tukey's group range test
UHMPE	Ultra high molecular weight polyethylene
UTM	Universal Testing Machine

RESPON HENTAMAN HALAJU RENDAH KE ATAS KOMPOSIT HIBRID TEKSTIL BERLAMINAT SERAT KELAPA-ARAMID/EPOKSI YANG DIKENAKAN BEBAN TUSUKAN MELINTANG

ABSTRAK

Hibrid bagi gentian sintetik dan gentian semula jadi dalam sistem komposit telah mendapat perhatian dalam bidang penyelidikan disebabkan oleh kesedaran terhadap alam sekitar. Gentian sabut kelapa diketahui mempunyai potensi yang tinggi sebagai rintangan hentaman, iaitu gentian yang rapuh membantu menyebarkan tenaga hentaman ke kawasan yang lebih luas. Fokus kajian ini ialah untuk menentukan jika terdapat sebarang penambahbaikan dalam tindak balas terhadap hentaman disebabkan oleh penggabungan serat Kevlar yang berprestasi tinggi dan gentian sabut kelapa dalam urutan susunan berlamina tertentu. Dalam kajian ini, eksperimen kuasi-statik dijalankan pada kelajuan 1.25 mm/s, dan ujian hentaman halaju rendah dijalankan dengan menggunakan penghentam berbentuk hemisfera 12.7 mm pada kelajuan yang berbeza-beza, iaitu daripada 5 m/s ke 17 m/s. Perisian Matlab digunakan untuk penyesuaian lengkung bagi data mentah, manakala ANOVA dan DOE melalui perisian Minitab digunakan bagi pemeriksaan statistik untuk menyokong hasil kajian. Kawasan komposit yang rosak dinilai menggunakan teknik analisis imej oleh peralatan pemprosesan imej daripada perisian Matlab. Analisis morfologi bagi permukaan yang retak disebabkan oleh hentaman juga diperhatikan menggunakan SEM. Pada peringkat permulaan, tindak balas hentaman optimum terhadap komposit epoksi serat kelapa bagi pelbagai reka bentuk yang diperkukuhkan, kaedah pembuatan komposit, pengubahsuaian fabrik dan ketumpatan fabrik telah ditentukan. Dapatan menunjukkan tindak balas hentaman boleh dikawal

secara berkesan dengan parameter-parameter bahan yang berubah. Gentian sabut kelapa dalam bentuk struktur yang ditenun dengan ketumpatan tinggi, dirawat menggunakan larutan NaOH 6% dan dibuat menggunakan kaedah pengacuan mampatan didapati berkesan dalam menyerap dan menyebarluaskan tenaga hentaman. Spesifikasi serat kelapa tersebut kemudiannya digunakan dalam lamina hibrid. Komposit hibrid epoksi sabut kelapa/Kevlar yang mengandungi tiga lapisan luaran lamina bagi enam konfigurasi susunan yang berbeza telah dihasilkan. Komposit hibrid (dua lapisan sabut dan satu lapisan Kevlar) dikenal pasti mempunyai penyerapan jumlah tenaga khusus yang sama seperti Kevlar berlamina 100% (pada tiga lapisan). Secara kesimpulannya, komposit hibrid epoksi sabut kelapa/Kevlar menunjukkan peningkatan dalam tindak balas hentaman. Ia juga memberikan penjimatan kos bahan serta menyumbang ke arah teknologi hijau yang memberikan manfaat besar kepada industri dan komuniti.

LOW VELOCITY IMPACT RESPONSE OF LAMINATED TEXTILE COIR-ARAMIDS/EPOXY HYBRID COMPOSITES SUBJECTED TO TRANSVERSE PENETRATION LOADING

ABSTRACT

The hybrid of natural and synthetic fibres in a composite system has gained interest in research field due to the environmental consciousness. Coir natural fibre has been found to have a high potential as impact resistance, in which brittle fibre helps to spread the impact energy over a wider area. The focus of the study is to determine if any improvement in impact response exists as a result of combining high performance Kevlar synthetic fibre and coir natural fibre in a specified laminated stacking sequence. In this research, quasi-static experiments were conducted at the speed of 1.25 mm/s, and low velocity impact tests were conducted using a 12.7 mm hemispherical impactor at the speed varying from 5 m/s to 17 m/s. Matlab software was used for curve fitting of the raw data, whereas ANOVA and DOE via Minitab software were employed for statistical examination to support the results. The area of the damaged composite was evaluated using the image analysis technique by Matlab image processing tool. The morphology analysis of the impact fractured surfaces was also observed by SEM. At the beginning stage, the optimum impact responses of coir epoxy composites subjected to different reinforcement architecture, composite manufacturing method, fabric modification and fabric density were determined. The findings showed that the impact responses could be effectively controlled by varying material parameters. Coir fibre in the form of woven structure with dense structure, treated using 6% of NaOH solution and

manufactured by compression moulding method was found to be effective in absorbing and propagating impact energy. The respective coir was then used in hybrid laminates. Coir/Kevlar epoxy hybrid composites consisted of three interply laminates layers at six different stacking configurations were developed. It was observed that the hybrid composite (two coir layers and one Kevlar layer) had equivalent specific total energy absorption as 100% Kevlar laminate (at three layers). It can be concluded that the hybrid of coir/Kevlar-epoxy laminated composites had shown an improved in impact response. It also provides cost-effective materials and contributes towards green technology which will be of great benefit to the industry and community.

CHAPTER 1

INTRODUCTION

1.0 Background

Laminated composite structure is an assembly of fibrous individual thin sheets of materials impregnated with crosslinked resin, or so called the binder, to provide required engineering properties such as in-plane stiffness, bending stiffness, strength, as well as coefficient of thermal expansion (Powell, 1994). Particularly in laminated textile fibre composite structure, layers of natural or artificial fibre structure in the form of flexible fabrics is employed and combined with the binder. Textile structures offers advantages such as subtle conformability, improved dimensional stability and deep draw shapeability are important for their efficient use in structural applications (Naik, 1994; Mallick, 1988). The orientation of fibres and stacking sequence of various textile layers can be controlled to create an extensive range of mechanical and physical properties of the composite laminate. Therefore, the uniqueness of laminated textile composite is visible as it can be tailored to fit an application (Zampaloni et al., 2007; Mallick, 1988).

Textile reinforced composite materials exhibit anisotropy. The properties may differ considerably depending on the plane or geometric axis on which they are evaluated. Textile composites are among typical high energy absorption materials. They absorb and mitigate kinetic energy effectively as they combine the valuable properties of both high performance fibres and polymer resins. Textile composites have high capability to provide protection from an impact at reduced weights.

Besides, they offer higher specific strengths (tensile strength divided by density) than their metal counterparts. Fibres used for high speed impact resistance include fibreglass, aramid fibre, woven and braided composites, as well as polyethylene fibre composites (Srivastava et al., 2011; Qiao et al., 2008).

The interest in using natural fibres (NFs) as reinforcements in polymer composites to replace synthetic fibres has increased due to the need for sustainable development and growing environmental consciousness and awareness. The most dominant use of natural fibre composites by far can be found in interior parts of the automotive industry (Anon, 2013). Figure 1.1 shows the use of natural fibres for composites in the European Automotive Industry in 2012 for the total volume of 80,000 tonnes. Coir offer advantages such as low price, unlimited and sustainable availability, low density, and low abrasive wear of processing machinery. Most importantly, coir are biodegradable, recyclable, carbon dioxide neutral and their energy can be recovered in an environmentally acceptable manner (Verma et al., 2013; Karthikeyan and Balamurugan, 2012). Coir can achieve high specific strength properties though they have poor strength properties due to low density (Begum and Islam, 2013; Satyanarayana et al., 1990). During a landfill or combustion process at the end of their life cycle, the released amount of carbon dioxide from the fibres is neutral with respect to the embraced amount during their growth. Compared to synthetic fibres, the abrasive nature of coir is much lesser. Advantages with respect to processes, material recycling and technical of composite materials in general could be reached. There is also the potential advantage of weight saving as the density of coir is much lower compared to most synthetic fibres.

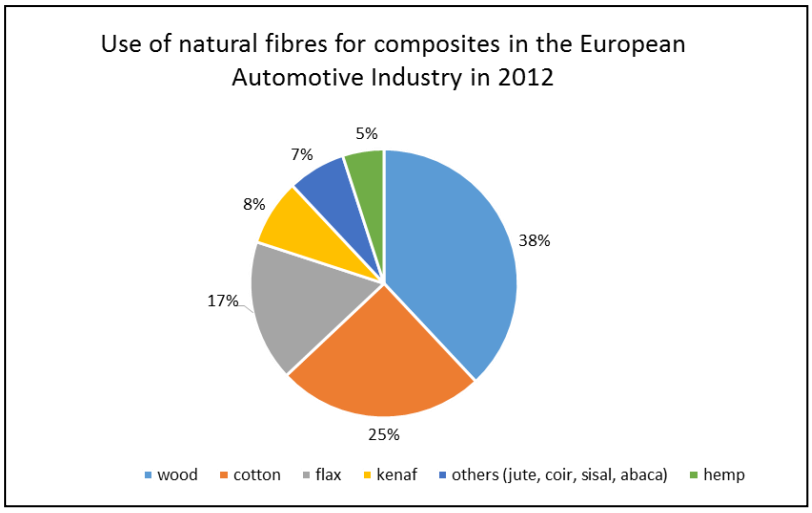

Figure 1.1: Use of natural fibres for composites in the European Automotive Industry in 2012 for the total volume of 80,000 tonnes (Anon, 2013)

NFs, at its early exposure, were used as discontinuous structure reinforcement. Until 1900s, realizing the advantages offered by continuous woven structure, efforts were made to explore its potentials (Othman and Hassan, 2013; Kamiya et al., 2000). The results displayed that continuous NF structure reinforcement had improved mechanical properties by a factor of three to four compared to the discontinuous structure (Goutianos et al., 2006). Complementary works also showed that properties like fracture toughness, ductility index and damage area of continuous reinforcement NF composite were significantly improved (Zhang et al., 2013; Kushwaha and Kumar, 2010; Liu and Hughes, 2008; Kim and Sham, 2000).

Heterogeneous and anisotropic properties exhibited by laminated textile composite have the capability to mitigate damage when impacted due to various mechanisms to transform the kinetic energy from penetrator into actions that can change the materials response, for instance plastic deformation, buckling, opening extensive crack surfaces and spreading (de-localizing) the damage zone, and other

dynamic instabilities (Qiao et al., 2008). Impact resistance is defined as the ability of a material to absorb energy during fracture. The total fracture energy absorbed by a material during impact should correspond to the amount of damage in one or more modes of rupture. Higher energy absorption also indicates the toughness of the material (Iqbal and Gupta, 2008; Lu and Yu, 2003; Stronge, 2000). In aeronautical applications for instance, the key factor that affects the design allowable is the sensitivity of composite materials to low velocity. Low impact energy levels results in barely visible damage, which can lead to significant strength loses. Hence, extensive research effort is needed to explore the relationship between impact parameters, extent of failure, failure modes and residual-strength retention after impact (Wang et al., 2014; Xiao et al., 2014; Quaresimin et al., 2013; Caprino and Lopresto, 2001).

In the nature of impact energy absorption application, none of the research has proven that NF alone is able to outperform the properties of high strength and modulus of synthetic fibres. Studies conducted by Jayabal et al. (2011) had shown that the mechanical properties of woven coir/polyester composites had improved significantly with the presence of glass fibre in the composite system. Kang and Kim (2000) mentioned that energy absorption capabilities of brittle fibre composites are less than those of ductile fibre-reinforced composites. As reported by Sathishkumar et al. (2014), Jawaid and Abdul Khalil (2011) and Hariharan and Abdul Khalil (2005), hybridizing lignocellulosic fibres with a stronger and more corrosion-resistance synthetic fibre enhances the strength, stiffness, moisture and fire resistance behaviour of the lignocellulosic composite. It is in agreement with the research by Kushwaha and Kumar (2010) and Mishra et al. (2003) where they found that the

addition of a little amount of synthetic fibres to NF boosted the mechanical properties of the resulting hybrid composites. Previous research had also hypothesised that brittle materials in the front layer could slow down the impactor and spread the impact energy over a wider area. The back layer of the ductile materials absorbs the impact energy (Ramakrishnan, 2009).

The need for hybrid composite materials that serve as the motivation for this research had been realized due to these findings and issues. Hybridization is expected to trim certain materials weaknesses while keeping its advantages. This research intends to explore the potential of coir in working with high performance Kevlar aramids fibre in order to absorb energy from penetration impact and to investigate the damage failure after impact. This research is also driven towards sustainability by reducing the amount of synthetic fibre and substituting it with NF, besides maintaining its quality.

1.1 Problem Statement

Aramids fibre are seen to replace ballistic nylon and glass fibre as a superior energy absorbing capacity material including its greater flexible wearability, mobility and also lightweight (Wambua et al., 2007). However, there is increasing concern that the use of synthetic polymer is causing some serious drawbacks such as high cost, poor recycling and non-biodegradable. Such effects are not in line with the global mission of green, safe and sustainable environment. Moreover, researchers claimed that the use of synthetic products threatens the NF industry (Satyanarayana et al., 1990). Its employment is restricting the utilization of NF in the fibre industry,

which is basically a rural/cottage industry, leads to the displacement of labour. Hence, there is a crucial need to seek opportunities to diversify the uses of these NFs. NFs are gaining attention as a viable alternative to synthetic composite as they are environmentally sound and have very low raw material costs (Begum and Islam, 2013; Justizsmith et al., 2008).

Fibres from the coconut fruit crust, which are currently disposed as an unwanted waste might be seen as an alternative recyclable materials for use in polymeric matrix composite (Monteiro et al., 2008). According to Wei and Gu (2009), of almost 55 billion coconuts harvested annually in the world, only 15% of the husk fibres are actually recovered for use. Moreover, Rout et al. (2001) claimed that the traditional coir products take only a small percentage of the potential total world production of coconut husk. Hence, new applications for coir is needed. NF can be reused to reinforce the composites in an effort to prevent wasting the coir fibre, substituting typical or synthetic composites. They could also be used together in high performance applications owing to their advantages.

It has been reported that the rate of deforestation in Malaysia increased due to the high demand for timber industry. The land area of Malaysia covered with forest decreased by 14.2% from 2006 to 2009 (Akber Basri et al., 2014). To curb the issues of deforestation and biodiversity preservation, it is necessary to explore and expand the potential usage of non-wood crop like coir so that the destruction and the damage to the forest and environment can be minimised. The outcomes of the research and emerging new applications for coir are of relevance and may open the opportunity for more plantations in Malaysia and tropical countries in general. Sivapragasam

(2008) in his report mentioned that more than 80000 households of Malaysian rural population are involved in coconut plantation. Hence, the need for coconut crop rehabilitation is crucial to avoid unemployment. Moreover, besides kenaf, coconut may also become a substitute for tobacco. The introduction of ASEAN Free Trade Area (AFTA), which comes into effect in 2010 had negative impact on tobacco planters (Akber Basri et al., 2014).

Most previous research had proven that NF hybrid composites promote low specific weight and cost-saving besides reducing the amount of non-biodegradable materials of the end product. Therefore, hybridization is crucial to be implemented as energy absorbing materials. As reported by Jawaid and Abdul Khalil (2011), the hybridization of lignocelluloses fibres with glass fibres have been studied extensively by researchers throughout the world, which shows an outstanding hybrid performance. However, none was reported on the hybrid of Kevlar aramids and coir fibre. Hence, the properties of coir/Kevlar hybrid must be completely evaluated and appropriate design data should be established to understand its performance behaviour so as to commercialize and expand the use of this new material. Quaresimin et al. (2013) agreed that very few data have been collected related to energy absorption capability of composites, although they have become the main concern in most of the design industry.

1.2 Thesis objectives

Generally, there are several areas requiring further studies concerning the use of natural fibre/synthetic hybrid composites for impact energy absorption such as in

protective applications. To address this need, the objectives of this thesis were as follows:

a) To identify the impact response of coir composites subjected to different reinforcement architecture, manufacturing method, fabric modification and fabric density.

b) To investigate the effects of laminate stacking configuration on the quasi-static and low velocity impact behaviour of hybrid (coir/aramid) composite.

c) To examine the effects of impact incident rate towards the impact response of hybrid (coir/aramid) composites laminates.

d) To evaluate the damage morphology and damage extent of novel hybrid (coir/aramid) composites under transverse puncture impact.

1.3 Scope of research

Figure 1.2 illustrates the general flow chart of the scope of the research. This thesis involved an extensive experimental (empirical) analysis, coupled with the use of existing theoretical and numerical formulae. A multi-level full factorial design was implemented in this research as a systematic and efficient way to distinguish the interactions between many factors. Moreover, analysis of variance (ANOVA) was employed to determine the significant factors that predominantly influence the impact and energy absorption behaviours of the composites. The structure of NF (fabric) used for composite reinforcement in this research was self-designed based on the existing design concept. However, the design was accomplished to suit the physical characteristic of the natural yarns received.

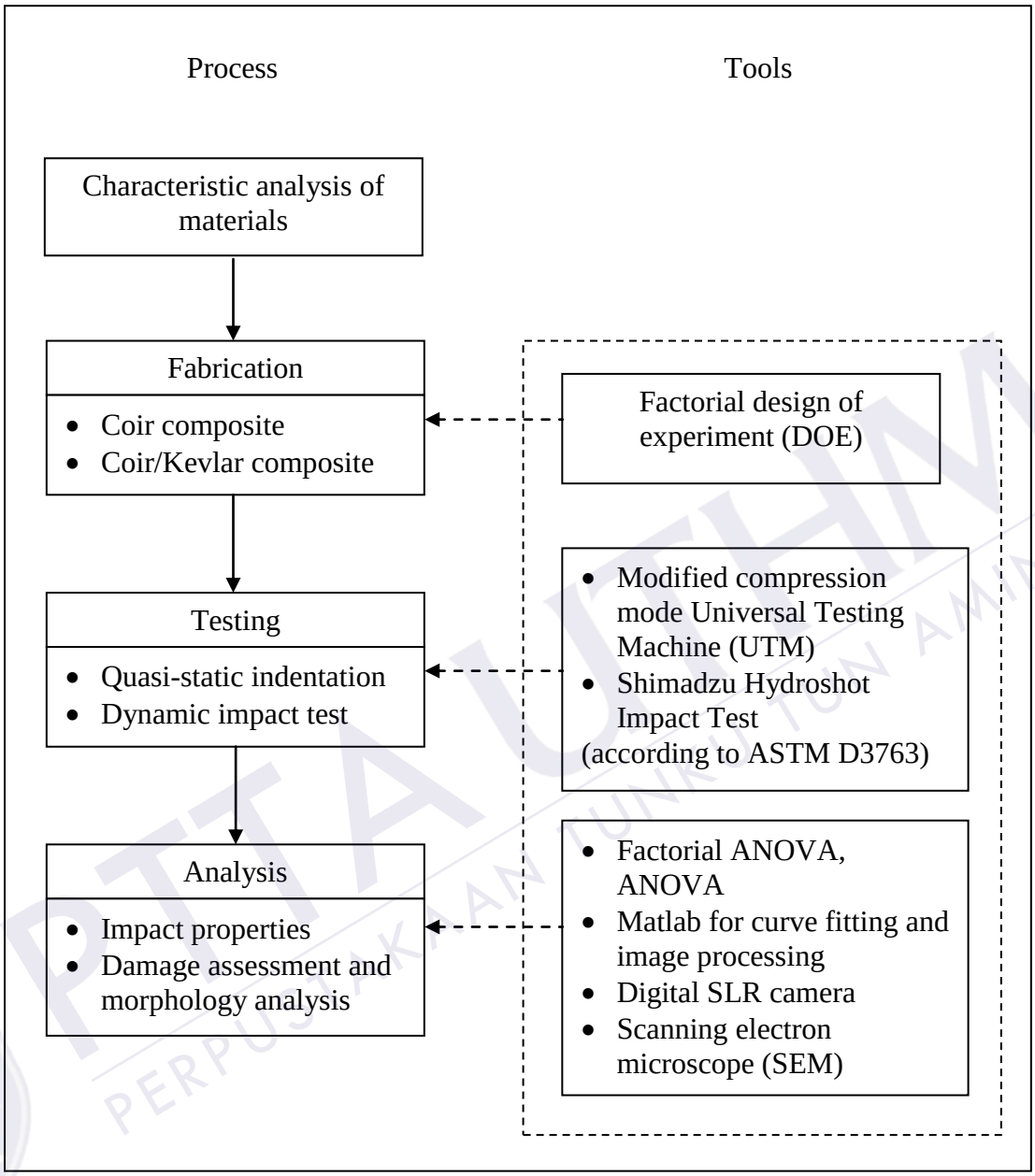

Figure 1.2: The general flow chart of the scope of the research

Impact analysis on composite materials was conducted through two modes; dynamic and quasi-static loadings. The low velocity penetration impact was conducted according to ASTM D3763 using Shimadzu Hydroshot Impact Test Machine. On the other hand, the quasi-static indentation was conducted using a

Universal Testing Machine (UTM) by compression mode. The impactor of the static indentation test was modified to equate it with the impactor of the dynamic impact. Impact responses such as the first material damage, the peak load, the total displacement, the absorbed energy, the propagation energy, the ductility index and the impact strength were gathered and could be defined through the load-displacement curve. The composites' strain rate dependency was evaluated by varying the low velocity impact speed at four levels; 5, 9, 13 and 17 m/s.

The fractured surface of the composites after impact loading was observed to examine the relationship between the damaged mode and the impact behaviour. An image analysis procedure was developed in order to determine the area of composites damaged. A flatbed scanner was used to scan the damaged samples and the images were processed using Matlab software with the image-processing tools. Samples were scanned at 600 dpi (dots per inch). Besides, some of the fractured composite images were captured through a Digital SLR camera. Programming commands were developed in the software to remove unwanted particles, detect the damaged edges and calculate the respective areas and perimeters. The morphology of the impact fracture surfaces of the composites was observed by a scanning electron microscope (SEM) at room temperature. It was performed by using Hitachi Tabletop Microscope TM-1000. A gold coating of a few nanometres in thickness, coated the impact fracture surfaces. The samples were viewed both in the horizontal and upright directions to the fractured surface.

1.4 Contributions of the research

The thesis has various contributions towards furthering the understanding on the response of coir/Kevlar textile hybrid composite under quasi-static and low velocity dynamic impact loadings. The contributions are briefly summarized as follows, while the specific results are detailed in Chapter 4 and the final conclusions are expressed in Chapter 5.

(1) The coir textile structure with optimum impact strength to be used as reinforcement in composite was identified. The understanding on impact responses for woven, cross-ply and angle-ply coir composite was gained in term of how the geometrical parameters of such structures could be used to control the absorbed energy. Such knowledge is useful for design purposes.

(2) The composite manufacturing method that contributed to good fibre-matrix bonding of coir-epoxy composite was obtained. Such information is important to enhance the impact response and the energy absorption behaviour of the designed composite.

(3) It is well understood that the response of NF composites can be significantly influenced by fibre modification and structural density. However, most of the documented researches regarding the effects of NF treatment were found on fibre form. Less research concerning NF treatment in the form of woven fabric structure was reported. The optimum treatment percentage for NF modification conducted on textile fabric and the appropriate fabric density to resist penetration impact were discovered in this research.

(4) The results of optimum hybrid stacking sequence of three layers coir/Kevlar composites could be used to control the stacking sequence arrangement of a particular hybrid composite with increasing layers. This knowledge can then be used to control energy absorption of hybrid composites.

(5) The research modelled the response of impact speed on hybrid composite. The knowledge generated shows how the energy absorption of such structures is influenced by various loadings and configurations of the composite structures. The empirical models allow the prediction of the response of coir/aramids hybrid composite under quasi-static and low velocity impact penetration loading.

(6) This research contributes to the knowledge of the damage morphology and damage extent of the novel hybrid (coir/Kevlar) composites under impact penetration loading.

(7) Coir/Kevlar hybrid composite material introduced in this study is capable of retaining the advantages of its elements and disabling some of its disadvantages.

1.5 Structure of thesis

The inscription of the thesis has been divided into five chapters. Chapter 1 gives the general information about the idea of the research as a whole, including the problems and issues related. Chapter 1 also highlights the main aims and objectives of the research, besides emphasizing on the research contributions. Chapter 2 provides a review of the literature related to the aims and objectives of the thesis. Areas where further research is required were identified, thereby positioning the aims

of this thesis. Topics reviewed include low velocity impact and energy absorption, analysis and testing of impact performance, fibre-reinforced polymer (FRP) composite for impact resistance and laminated textile composites (with particular focus on anisotropic textile structure). Chapter 3 embraces a whole experimental procedure, including the information on raw materials, tool fabrication, sample preparation, characterisation, testing and analysis method. Chapter 4 involves the interpretation of the results and findings for all research objectives in order to gain a better understanding. Finally, Chapter 5 summarizes and concludes the results of the present study and proposes some recommendation for future works.

CHAPTER 2

LITERATURE REVIEW

This chapter reviews the pertinent background literature to the research conducted in this thesis. Areas where relevant research is lacking are identified, thereby establishing the need for further investigation.

The topics addressed in the literature review are broadly contained as follows:

(1) Impact and energy absorption (E_a) behaviour

(2) Fibre-reinforced polymer (FRP) composite

(3) Laminated textile composites

2.1 Low velocity impact and energy absorption behaviour

Impact is defined as the relatively sudden forcible contact to another object or part of a material's structure. Contact force develops as the impactor objects indents the target object (Chai and Manikandan, 2014; Reid and Zhou, 2000). Impact can be generally categorized into low, medium and high velocities. Most researchers classify low velocity as impact below 10 m/s (Balasubramani and Boopathy, 2012; Cantwell and Morton, 1991). Low velocity impact is one of the causes of damaged in composite's body. It is probably induced by the dropping of tools due to careless handling during manufacture and in-service incidents such as flying debris, striking of objects and birds strike. Soldiers are sometimes hit by foreign objects or objects that are thrown in the air into other objects at low velocities. Observing situations

like the failures of aircraft and aerospace structures due to impact damage and the increasing number of vehicle accidents, which cause body injuries demands an active research on impact resistant materials. High performance design and high energy absorbing materials and structures are crucial in civil and military applications. In the aerospace industry for instance, design and development of new composite wing structures are essential to resist hail and bird impacts (Qiao et al., 2008; Bolukbasi and Laananen, 1995). Even at low velocities, the damage induced within a structure can be significant and may cause serious structural degradation (Rahman, 2013). Thus, the analysis of composite structures subjected to low velocity impact is considered very important for any engineering application.

The capacity to absorb and dissipate energies under impact loading is denoted as the impact properties of a materials (Mallick, 1988). Energy absorbing materials refers to materials that can control the release of energy in various ways. Energy can be transferred into different forms, however it is never lost. Things that can impair any object or machine can be avoided by adjusting the absorbed energy and released energy (Lu and Yu, 2003; Stronge, 2000). Designing energy absorbing materials is a challenging job since many mechanisms occur simultaneously to weaken the material. The failures include dynamic cracks and delamination, wave propagation, dislocation generation, thermal effects, growth and motion, etc. which happen at different material scales and combination during impact (Qiao et al., 2008). The damage mechanism between ductile and brittle composite materials is different. Ductile materials are found to perform better energy absorption than brittle materials (Kang and Kim, 2000). Lu and Yu (2003) highlighted the major applications of energy absorption (E_a) as follows:

a) E_a to improve vehicles crashworthiness

b) E_a structures for highway safety

c) E_a structures for protection against industrial accidents

d) E_a for personal safety

e) E_a structures/materials for packaging

Several phenomena occur upon impact like elastic, plastic wave propagation, fracture and fragmentation, shock, as well as spallation and perforation. Most composites absorb impact energy in elastic deformation. Plastic deformation is rarely seen as composite materials experiencing through damage mechanisms. Impact may affect the maintainability and the design of a composite body or structures besides causing an abrupt decrement of the structure's residual strength (Xiao et al., 2014; Balasubramani and Boopathy, 2012). In low velocity impact, damages in FRP laminated composites comprises three principle failure modes, namely (i) interlaminar delaminations or damage, (ii) intralaminar damages between fibres, which includes transverse matrix cracking and fibre-matrix interface debonding, and (iii) intralaminar damage across fibre, namely fibre fracture (Zhang et al., 2013; Reid and Zhou, 2000). Delamination is found to be the most crucial damage in laminated composites as reported in Richardson and Wisheart (1996) and Kim and Sham (2000) because some may not be detectible on impacted surface. Delamination is a crack formed in the resin rich area between two neighbouring layers. It is observed to occur if the threshold energy is reached and matrix crack is present.

2.1.1 Analysis on impact and energy absorption properties

This section provides overview on the fundamentals of impact and energy absorbing properties analysis as they provide the understanding on impact mechanics.

2.1.1.1 Load-displacement curve

During low velocity impact, useful information on the failure process can be recorded in the load-displacement curve (Mohmmed et al., 2014; Abrate et al., 2013). Information such as material stiffness (the initial slope of a load-displacement), maximum load, yield point, energy at maximum load, propagation energy (energy after maximum load), ductility index, and total energy absorbed can be obtained from this curve. Observations can be made on the shape of the curve and the characteristic points related to the performance of the material under dynamic load. Figure 2.1 (a) illustrates a typical view of the load-displacement curve for laminated composites with some characteristic points. On the other hand, Figure 2.1 (b) shows four different curves for carbon fibre-reinforced polymer (CFRP) laminates at different thickness. The end of the elastic phase where a load drops, denoted by point "a" in Figure 2.1 (a), indicates the pre-initial fracture region of the laminated composite materials. Additionally, the load drop is clearly visible as the thickness of the material rose as displayed in Figure 2.1 (b). Thinner material structure shows almost a linear trend under very low displacement value and the pre-initial fracture region almost does not exist. During impact, the first damage type is believed to be matrix crack. Usually, there is only a slim reduction in laminate rigidity as the load increases again after the first damage. The occurrence of matrix crack gradually

initiates delamination and fibre breakage, which dramatically changes the local and global composite stiffness and influences the load-time response. All of the energy that exceeds the latter is used for damage propagation. The failure that occurs along the laminate thickness reduces the residual strength of the composite structure, resulting in a series of load drops and oscillations in the load-displacement curves (Abrate et al., 2013; Mallick, 1988).

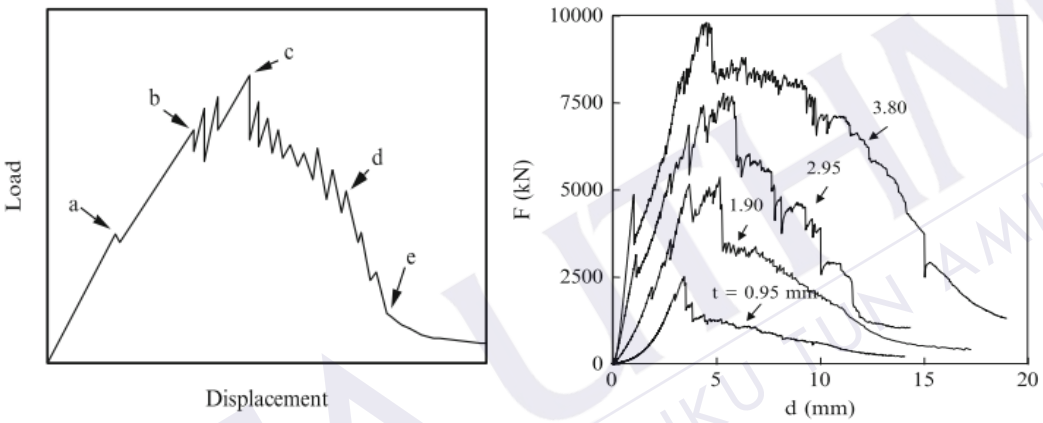

(a) (b)

Figure 2.1: (a) Schematic view of the impact load-displacement curve at penetration and (b) load-displacement curve of materials of different thicknesses (Abrate et al., 2013)

Damage initiation at or near the peak load ("b" and "c") is termed as the initial fracture region. It is usually caused by interlaminar shear failure or tensile failure at the outermost fibre. The maximum peak load provides an indication of the load required to initiate the failure, therefore activating the energy absorption process. In the range of "b" to "d", the different damages propagate through all of the layers, which are progressively broken until (point "d") a complete perforation occurs. The rapid decrease from "d" to "e" illustrates the penetration process. This region is normally called the complete fracture region. Beyond point "e", the friction between the impactor and the penetrated samples has slowed down the contact force,

whereby the energy here is dissipated by friction. For a totally penetrated sample, the total energy absorbed or the energy needed to completely penetrate the laminate is given by the area under the load-displacement curve at the penetration point (point "e") (Abrate et al., 2013; Mallick, 1988). Ursenbach et al. (1995) demonstrated a clear picture (Figure 2.2) of the various stages of plate response as described in this section.

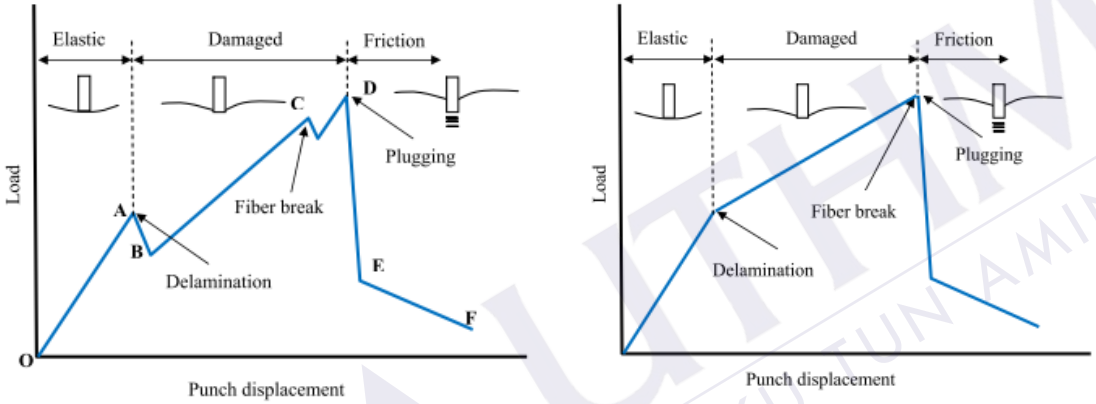

(a) (b)

Figure 2.2: Stages of plate response after impact (Ursenbach et al., 1995)

2.1.1.2 Energy absorption characteristic

In an energy absorbing system, determining the suitable energy absorbers is essential to accommodate a wide range of applications. Energy absorbed (E_a) causing a complete penetration event is calculated using Equation 2.1 (Othman and Hassan, 2013).

$$E_a = E_t - E_r \tag{2.1}$$

E_t is the total impact energy and E_r is the residual energy. Several failure mechanisms during energy absorption process in the composite structure includes (Reid and Zhou 2000):

a) Fibre failure, U_f

b) Resin crazing or cracking, U_m

c) Fibre/resin debonding, U_d

d) Fibre pull-out from the matrix across a failure surface, U_p

e) Fibre relaxation and stress distribution to the matrix, U_r

f) Multiple fibre failure, U_{mf}

g) Multiple matrix failure, U_{mm}

h) Delamination, U_{del}

However, not all mechanisms necessarily happen in a single failure occurrence. The total fracture energy is given by Equation 2.2.

$$U_{tot} = U_f + U_m + U_d + U_p + U_r + U_{mf} + U_{mm} + U_{del} \quad (2.2)$$

The impact energy introduced to a composite specimen is approximately equivalent to the impactor's kinetic energy immediately before contact. During an impact test, the energy absorbed by the specimens can be calculated from the load-displacement curves (Jacob et al., 2002). For an impact having a closed load-displacement curve, the absorbed energy is equal to the area within the load-displacement curve. Whereas for an impact event having an open load-displacement curve, the absorbed energy is equal to the area bounded by the load-displacement curve and the displacement axis (Liu, 2004). Fundamentally, through basic mechanics, the total energy absorbed, E_t is defined as an integration of a load-

displacement curve and calculated at the penetration point given by the expression in Equation 2.3.

$$E_t = \int_0^{\delta \max} p\delta \, d\delta \tag{2.3}$$

P is an immediate impact load, while δ and δ_{max} are the present and maximum achievable impact distances, respectively. The energy absorbed at the maximum load point is symbolised as E_m. Propagation energy, E_p or fracture propagation energy occurs in the crack propagation phase given by Equation 2.4.

$$E_p = E_t - E_m \tag{2.4}$$

On the other hand, the ductility index (*DI*) is calculated using Equation 2.5.

$$DI = E_p / E_m \tag{2.5}$$

Specific energy absorption capacity (*SEA*) is the most essential characteristic of energy absorbers. *SEA* is given by Equation 2.6. It is expressed as energy absorbed per unit mass, where E_t is the total absorbed energy and m is the original mass (undeformed).

$$SEA = E_t / m \tag{2.6}$$

SEA is an indicator to measure the weight efficiency of an energy absorber material, mainly when weight reduction is crucial. Materials having higher *SEA* has more

efficient impact absorber in terms of its weight (Zarei and Kroger, 2006; Santosa et al., 2001). The weight-saving, however, must not compromise its structural or safety performance.

2.1.2 Quasi-static and low velocity impact test for composite materials

The similarities between quasi-static loading and low velocity impact have been examined by several researchers. The stress wave of low velocity impact is minimal, thus can be considered to be quasi-static (Mantena et al., 2001). Studies by Curtis et al. (2000), Li et al. (2012) and Xiao et al. (2014) indicated that the load-displacement characteristics and the damage appearance of the two tests have similarities. Kaczmarek and Maison (1994) agreed that the propagation and delaminated area are similar for both static and low velocity tests. Zhang et al. (2000), in their investigations on bamboo/aluminium laminated composites, showed similar failure processes and global deformation between static indentation experiment and impact loading at speeds lower than 3.5 m/s. Moreover, Caprino et al. (2003) added that the penetration energy and material indentation of plates are unaffected under low velocity and static loading. A conclusion can be made that static models can be used to predict the response of low velocity impact. However, in an indentation behaviour study by Hachemane et al. (2013), they found that impact loading on sandwich laminates dissipate 11% more energy than that of the static test.

2.1.2.1 Quasi-static indentation

In quasi-static testing, the test specimen is crushed at a constant speed. Crashworthy structures or materials usually depend on the speed at which they are

crushed. Therefore, quasi-static test is inappropriate to simulate strain rate sensitive materials. The results is not applicable in dynamic situation, although the materials show good energy absorption after quasi-static test (Chathbai, 2007). Shengqing and Boay (2013) performed quasi-static indentation tests to investigate the damage and failure mode maps for composite sandwich panels. Zhang et al. (2000) investigated the damage and deformation behaviour of bamboo/aluminium laminated composites under static loading at different speeds. On the other hand, Curtis et al. (2000) conducted a static test to measure the strain distributions of the composite tubes. Fan et al. (2010) investigated the failure modes and energy absorption properties of woven textile sandwich panels under quasi-static loading. Most researchers examined the failure mechanism by quasi-static test method. Quasi-static test can be performed using a standard universal testing machine with the crosshead moving at a speed usually in the range of 3-5 mm per minute.

2.1.2.2 Low velocity impact

There are various test methods for low velocity impact response on composite materials as reported in previous literature (Dhakal et al., 2014; Mohmmed et al., 2014; Ho and Lau, 2012; Aktas et al., 2009; Sevkat et al., 2009; Ellis, 1996; Cantwell and Morton, 1991). The most often used test methods include the Charpy pendulum, the Izod pendulum, the falling weight (drop-weight) fixtures and drop dart tests as well as the hydraulic machines designed to perform both in-plane and out-of-plane testing.

Charpy and Izod pendulum impact tests are initially designed for testing metallic materials (refer to Figure 2.3). They are among the early impact tests on

composite materials (Ellis, 1996; Cantwell and Morton, 1991). Although the Charpy and Izod tests are both simple to use and can be instrumented, they have several disadvantages. The specimens used are short and thick, and are not representative of common engineering components. The standard test method that are commonly used for the tests are ASTM A370, ASTM E-23 and ASTM D256. The applicability of these tests method is contestable. Bader and Ellis (1974) claimed that the Charpy impact energy of carbon fibre-reinforced plastic (CFRP) varied with specimen geometry. However, both Charpy and Izod tests are suitable for impact ranking purposes as well as a stepping stone in determining the dynamic toughness of composite materials (Cantwell and Morton, 1991).

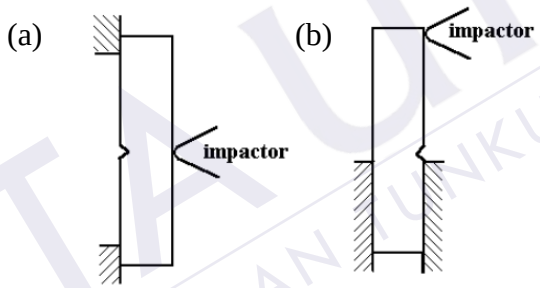

Figure 2.3: Schematic of; (a) Charpy pendulum test and (b) Izod pendulum test

Another common low velocity test method is the drop weight impact test. At a predetermined height, an impactor of specific weight is dropped to strike the test specimen supported in the horizontal plane. Greater range of specimen geometries can be tested, allowing more complex specimens to be tested. It is also possible to use different impactor shapes. This test method has advantages over Charpy and Izod impact tests.

The impact test method using hydraulic test machine is capable of determining the puncture properties of rigid plastics at different test velocities. This may provide a measure for the rate sensitivity of the materials. The hydraulic testing machine shall consist of two assemblies, one fixed and the other driven by hydraulic to achieve the required impact velocity. Most low velocity impact tests for plastic materials are conducted according to ASTM D3763 (Pramanik and Mantena, 2012; Duan et al., 2003; Mantena et al., 2001). Pramanik and Mantena (2012) performed a low-velocity punch-shear test at 3 m/s on nano-reinforced and sandwich composites of various materials. Duan et al. (2003), on the other hand, conducted a multiaxial impact test on glassy polymer acrylonitrile-butadiene-styrene (ABS) and semicrystalline polymer alloy of polycarbonate and polybutylene-terephthalates (PBT) at different ranges of impact velocities (1 m/s to 4.2 m/s). Mantena et al. (2001) conducted low-velocity test on glass-resin composites where specimen support fixtures are in accordance with ASTM D3763.

2.1.3 Influence of constituent properties on the impact response of composite materials

The energy absorption behaviour of composite materials and structures is influenced by numerous factors as discussed by Abrate et al. (2013), Balasubramani and Boopathy (2012), Feraboli et al. (2009) and Lu and Yu (2003). The factors may be classified as follows:

a) Composite materials and properties

b) Fabrication conditions

c) Structure, geometry and dimensions of the structural components

d) Test conditions

e) Temperature

Moreover, these factors can be categorised into internal and external factors. Internal factors are factors that depend on the material itself such as matrix content and type, fibre type and architecture, orientations of fibre, thickness and stacking sequence of the laminate. Then, external factors include those related to impact conditions, for instance the specimen's dimensions and geometry, impactor type and fixture or constraint conditions.

An early study by Caprino and Lopresto (2001) had shown that fibre volume and tup diameter have significant influence on penetration energy, whereas factors like resin content and type, fibre architecture, orientations and stacking sequence play a secondary role on the response. Jayabal and Natarajan (2010) agreed that fibre content plays a major role in improving impact properties. Their research on coir-polyester composites reported that the optimum value of impact strength could be reached at a fibre weight of 29%. They also reported that higher impact properties are obtained for a long fibre reinforcement. Jang et al. (1989) highlighted several approaches to enhance the impact resistance of composite materials. These include matrix and reinforcement modifications (i.e. fibre treatment), improvement of fibre/matrix interfacial adhesion, lamination design, through-the-thickness reinforcements (utilization of stitching, 3-D weaving and braiding), inclusion of interlaminar layers, fibre hybridization and utilization of high-strain fibres.

Weave density has a decisive influence on the utilisation of fabric for some technical applications. The density of woven structure is measured per unit dimension. It has an effect on yarn crimp and fabric areal density (Lim et al. 2012). Yarn crimp is the degree of yarn undulation resulting from interweaving. According to Peled et al. (1998), woven densities on warp and weft direction also influence the penetrability of the matrix into the fabric. Lim et al. (2012) investigated the effects of weaving density of aramid fabrics on ballistic impact resistance and concluded that higher crimp deteriorates tensile strength. Other research by Abou Nassif (2012) demonstrated that fabric breaking load increases with the increase of weft density, although breaking elongation is decreased.

A number of studies on the effects of stacking sequence have been reported so far (Zhoa et al., 2009; Belingardi and Vadori, 2003; Jang et al., 1989). Examinations show that stacking sequence plays an important role in controlling delamination and plastic deformation in composite laminates (Jang et al., 1989). A research on carbon-epoxy laminates by Belingardi and Vadori (2003) indicated that the stacking sequence of $[0/90]_i$ exhibited greater value for maximum force. Moreover, Zhoa et al., (2009) claimed that the quasi-isotropic laminates of $[(0/45/90/-45)_2]_s$ demonstrated higher energy absorption due to bending, and larger in-plane stiffness and shear rigidity than those of angle-ply laminates. It can be concluded that the geometry design stage of fibres in a composite is very important to consider in designing impact resistant materials.

Belingardi and Vadori (2003) and Park and Jang (2003) reported that maximum force has linear dependency on laminate thickness. As the thickness

increases, the resistance to impact is more effective. On the other hand, the impact energy of thin laminates is controlled by the huge displacement and delamination area, while for thick laminates, the energy is dominated by the maximum load (Park and Jang, 2003).

Most researchers claimed that the energy absorbed by a specimen initially increases with increasing impact energy and velocity, but it will become almost constant at a certain value (Dehkordi et al., 2010; Iqbal and Gupta, 2008; Belingardi and Vadori, 2003; Mantena et al., 2001), which shows that materials are substantially independent from strain rate. However, Dhakal et al. (2012) found that the increase in low velocity incident rate gives rise in the laminated materials damage area. They also reported that hemispherical impactor shape is able to resist higher impact load compared to flat and conical impact shapes. As for high velocity impact, Zhoa et al. (2009) claimed that the affected area of impact reduces with increasing striking velocity.

2.2 Fibre-reinforced polymer (FRP) composite

Composite material consists of reinforcement from fibres, particles, flakes, and/or fillers embedded in a cured resin or known as the matrix. The overall mechanical properties of the composite material are improved by the presence of reinforcement, while the matrix holds the reinforcement together to form the desired shape. A fibre-reinforced polymer (FRP) composite material is prepared principally by varying the volume of fibre reinforcement, which is then embedded in a matrix material. Some examples of thermosets matrices are epoxy, unsaturated polyester,

polyamide and phenolic, whereas thermoplastics matrices include nylon, polyethylene, polypropylene, etc. As for reinforcement fibre, the most common fibres used are glass, carbon, aramid, UHMPE (ultra high molecular weight polyethylene), boron, and NFs such as flax, wood, kenaf, jute, hemp, coir, etc. Both matrices and reinforcement fibres can also be combined to provide the most appropriate properties for a specific application.

2.2.1 Kevlar aramids fibre composite

A new era in composite materials is achieved by the presence of high performance synthetic fibres. The physical properties of this type of innovative composite material greatly outperform those of the matrix material alone. Synthetic FRP composite encompasses high strength and high stiffness, besides having long fatigue life and adaptability to the intended function of the structure. It is also often known to be wear- and corrosion-resistant, and have good appearance, temperature-dependent behaviour, environmental stability and thermal insulation and conductivity. The specific properties of these materials make it highly desirable in primary and secondary structures in military and civilian aircraft, transportation industry and other related industries (Begum and Islam, 2013). The strength and stiffness of few selected synthetic fibre materials are displayed in Table 2.1. The common metallic structural materials such as aluminium, titanium and steel are also listed for comparison purposes.

Aramid fibres, which is developed during the 1960s were first commercially introduced by DuPont in the 1970s. At its early exposure, it was used as a

replacement for steel in racing tyre. Its trade name is Kevlar. Kevlar is a very important reinforcer for advanced composites as it possesses a high degree of toughness, high tensile strength-weight ratio and low specific gravity compared to other reinforcing fibres. It also promotes good impact/ballistic performance (Reis et al., 2012). However, the major drawbacks of Kevlar 29 are its low compressive strength and difficulty in machining (Mallick, 1988). Moreover, Reis et al. (2012) added that Kevlar does not fail by brittle cracking. It fails by a series of small fibril failures where the fibrils are molecular strands that make up each aramid fibre and are oriented in the same direction as the fibre itself. These many small failures absorb high amount energy and, therefore resulting in very high toughness. The tensile strength of aramids is comparable to cast metals. In additions, they exhibit low creep and low water absorption. Therefore, these materials are suitable for metal replacement (Fink, 2008).

Table 2.1: Synthetic fibre/wire and common structural metallic material properties (Bhattacharyya and Fakirov, 2012; Akil et al., 2011; Jones, 1999)

Material	Density, ρ (g/cm^3)	Tensile strength, S (MPa)	S/ρ (10^6 cm)	Tensile stiffness, E (GPa)	E/ρ (10^8 cm)
Aluminum	2.68	620	2	73	3
Titanium	4.71	1900	4	115	3
Steel	7.81	4100	5	207	3
E-glass	2.55	3400	14	72	3
S-glass	2.49	4800	20	86	4
Carbon HS	1.50	5700	38	280	19
Carbon HM	1.50	1900	13	530	35
Berylium	1.85	1700	9	300	17
Boron	2.57	3400	14	400	17
Graphite	1.41	1700	12	250	18
Kevlar	1.44	4500	31	120	8

The advantage of Kevlar aramid fibre over other polymeric fibres is the cost-effective performance at reduced weight. Glass fibres, for instance, are cheaper but have lower strength and modulus with increasing weight. As a reinforcement, Kevlar fibre is substituting glass fibre in many aerospace and marine applications where high tensile strength and light weight are vital. Besides, it is also resistant to local damage usually caused by dropped hand tool or bird strike (Mallick, 1988). Carbon fibre, despite having the highest strength and modulus among the three fibre types, demonstrates the lowest elongation and is more expensive than aramids. Aramid fibres have a unique combination of high strength and modulus with low density and high elongation, resulting in improved impact resistance (Bhattacharyya and Fakirov, 2012). Kevlar composites have also been extensively utilized in lightweight armour structures ranging from military helmets and ballistic panel to large scale vehicle systems such as land vehicles, and naval vessels besides aircraft and spacecraft (Gustin et al., 2005). Applications in aerospace for instance can be found for landing gear doors, aircraft cabin and jet engines. Other typical applications of Kevlar composite materials include monoque bodies for Formula 1 racing cars, squash and badminton racket, tennis, table tennis, cricket bats and hockey sticks, helicopter rotor blades and kayaks/kenu.

2.2.2 Natural fibre (NF) composite

NFs may be classified into plant, animal and mineral fibres (Jawaid and Abdul Khalil, 2011). Plant fibres can be categorised into cellulose and lignocellulose fibres, extracted from either the plants' bast, seed, leaf, fruit, etc. Examples of fibres derived from plants include flax, hemp, jute, abaca, sisal, coir, cotton, bamboo, etc. Animal

fibres comprise of silk and wool, whereas asbestos goes under mineral fibres. Generally, the density of NFs is lesser than most synthetic fibres. Table 2.2 demonstrates the physico-mechanical properties of NFs. Some synthetic fibre properties are also listed as comparison. The specific strength and specific modulus of NFs, for instance, are comparable or even superior to E-glass fibres. Many NFs have higher specific modulus compared to E-glass fibres. Hence, it is often said that there is an opportunity for NFs to replace synthetic fibre like aramids and E-glass fibre (Ayrilmis et al., 2011; Wirawan et al., 2009).

2.2.2.1 Coir composite

Coir is a NF extracted from the husk (mesocarp) of a coconut fruit (Cocos Nucifera L.) (refer to Figure 2.4). 'White coir' fibres are extracted from unripe nuts, while 'brown coir' is extracted after the ripening of the coconut (Defoirdt et al., 2010). Brown fibre was found to be stronger than white coir fibre (Wang and Huang, 2009). Plantations of coconut spread all over the world in tropical and sub-tropical regions, and is an important item in the economy of many of these regions. Coir is abundantly available in India, who is the second largest producer in the world after the Philippines. Out of 55 billion coconuts produced annually in the world, only 15% of the husk fibres are recuperated for use, while others are left abandoned (Verma et al., 2013; Karthikeyan and Balamurugan, 2012). Malaysia is listed amongst the top ten world's coconut producer with the total coconut production of 382000 metric tonnes (in year 2007). Coconut is the fourth important commercial plant in Malaysia in terms of total planted area and the total plantation area recorded of about 109,185 hectares in 2007 (Sivapragasam, 2008).

Table 2.2: Physico-mechanical properties of natural fibres and some synthetic fibres (Akil et al., 2011; Faruk et al., 2012)

Fibres	Density (g/cm^3)	Diameter (µm)	Tensile strength (MPa)	Young's modulus (GPa)	Elongation at break (%)
Flax	1.5	40-600	345-1500	27.6	2.7-3.2
Hemp	1.47	25-500	690	70	1.6
Jute	1.3-1.49	25-200	393-800	13-26.5	1.16-1.5
Kenaf	1.2	-	930	53	1.6
Ramie	1.55	-	400-938	61.4-128	1.2-3.8
Nettle	-	-	650	38	1.7
Sisal	1.45	50-200	468-700	9.4-22	3-7
Henequen	-	-	-	-	-
PALF	-	20-80	413-1627	34.5-82.5	1.6
Abaca	1.5	-	430-760	-	-
Oil palm EFB	0.7-1.55	150-500	248	3.2	25
Oil palm mesocarp	-	-	80	0.5	17
Cotton	1.5-1.6	12-38	287-800	5.5-12.6	7-8
Coir	1.15-1.46	100-460	131-220	4-6	15-40
E-glass	2.55	<17	3400	73	2.5
Kevlar	1.44	-	3000	60	2.5-3.7
Carbon	1.78	5-7	3400-4800	240-425	1.4-1.8

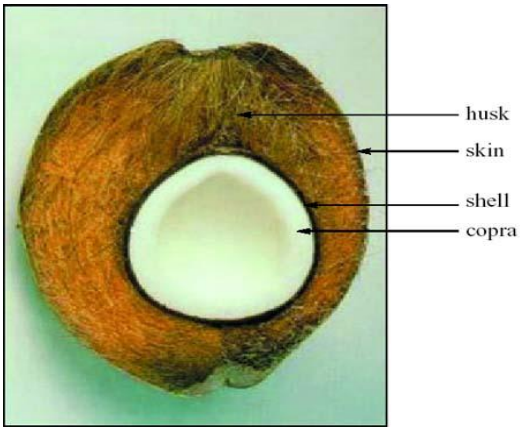

Figure 2.4: Coconut fruit

Culinary is found to be the main use of coconut. After extraction, coir is usually disregarded. Regions or industries that consume high amount of coconut, therefore, face a big problem to appropriately dispose this waste, since husks take a lengthy time to degrade. Increasing attention is currently paid on coconut fibre, which is now being commercially used. Coir-reinforced rubber materials have found widespread application (Karthikeyan and Balamurugan, 2012). In the production of automobile seat cushion for instance, coir has been blended with natural rubber latex (Monteiro et al., 2008). Wang and Huang (2009) in their research on coir/rubber composites found that fibre loading of higher than 60% may reduce the tensile strength of the composites. Meanwhile, they also concluded that temperature variation between 130-160^{o}C has no significant influence on tensile strength. Besides, coir as reinforcement in polymer-matrix composites have been used in many other aspects. They have been tested as helmets, roofing and post-boxes (Monteiro et al., 2008). Monteiro et al. (2008) carried out experiments on coir/polyester composite by varying the range of fibre weight fractions. They obtained two different products, which were rigid composites for fibre loading of less than 50% wt, and agglomerates composites for fibre loading higher than 50% wt.

Yuhazri and Dan (2007) used coir in the manufacturing of motorcycle helmet. Coir were used as reinforcement and epoxy resins as the thermoset matrix materials. It was found that coir performed well and is a suitable reinforcement in epoxy resin matrix. A study by Wambua et al. (2003) found that the impact strength of coir composites was greater than that of kenaf and jute composites, although its mechanical properties were the lowest among them. Moreover, as conveyed by Ali (2010), applications of coir in civil engineering technology are encouraging. He reported that coir is the most ductile and energy absorbent material. Coir are broadly used as construction materials such as roofing materials, corrugated slabs, plaster, cement board, wall panelling system, house construction and slope stabilization. It is also noted that coir is an excellent reinforcement for polymer concrete, as it has the ability to withstand high fracture toughness on high impact strength (Wong et al., 2010).

The automotive sector has also shown interest in coir due to its hard-wearing quality and high hardness (less fragile than glass fibre), good acoustic resistance, non-toxic, resistant to microbial and fungi degradation, moth-proof, more resistant to moisture compared to other NFs, withstand heat and salt water, as well as not easily combustible (Ayrilmis et al., 2011). The presence of lignin layer, yet low contents of cellulose and hemicellulose in coir compared to other NFs improves the dimensional stability of the composites. It is reported that increased amounts of cellulose and hemicellulose initiates higher water uptake to the fibre (Ayrilmis et al., 2011). Prices of some NFs and synthetic fibres are represented in Table 2.3. It can be observed that the price for NFs is very low as compared to synthetic fibres. Instead, when compared among NFs, coir is found to have comparatively lower price.

Table 2.3: Density and cost (in US Dollar) of some NFs, synthetic fibres and steel (Akil et al., 2011; Mohanty et al., 2000)

Fibre	Density (g/cm^3)	Cost (kg^{-1})
Flax	1.4-1.5	~$0.40-$0.55
Hemp	1.48	~$0.40-$0.55
Jute	1.3-1.45	~$0.40-$0.55
Sisal	1.45	~$0.40-$0.55
Ramie	1.50	~$0.44-$0.55
Pineapple leaf	1.53	~$0.40-$0.55
Cotton	1.5-1.6	~$0.44-$0.55
Coir	1.15	~$0.40-$0.55
Kenaf	1.4	~$0.40-$0.55
Softwood	1.4	~$0.44-$0.55
Hardwood	1.4	~$0.44-$0.55
E-glass	2.5	~$2
S-glass	2.5	~$2
Kevlar	1.44	~$20-$50
Carbon	1.78	~$200
Steel	7.81	~$30

2.2.2.2 Treatment of natural fibre

The hydrophilic nature of coir in composites results in poor compatibility with hydrophobic resins. The limited amount of cellulose, but high lignin content in coir fibre restricts the penetration of matrix resins into the fibre. Therefore, in order to improve the resin-fibre interfacial bonding, a process to remove the surface layer of lignin is needed. This can be done through fibre modification or so called the treatment process (Karthikeyan and Balamurugan, 2012; Harish et al., 2009). Rout et al. (2001) agreed that the treatment of fibres aimed to better and more stable bond between fibre and matrix. Composite materials which have good mechanical properties can be obtained if there is an effective wetting of fibres by matrix and satisfactory dispersion of fibres in the matrix (Rout et al., 2003).

Various treatment methods are present nowadays. Physical treatment method is when the treatment does not change or modify the chemical composition of the fibres. In fact, physical treatment generally improves fibre interface and increases mechanical bonding between fibre and matrix. On the other hand, Corona treatment is a technique for surface oxidation activation. Corona releases treatment on cellulose fibre to change the surface energy. Another similar treatment is the plasma treatment. The type and nature of gases used in plasma treatment will contribute to different surface modifications (Faruk et al., 2012). Chemical treatment is considered to be one of the methods in modifying a fibre's surface properties. Chemical treatments include alkali, acetylation, silane, benzoylation, maleated coupling agents, acrylation, isocyanates, permanganate, etc. All of the treatment types are targeted to improve the adhesion between fibre surface and polymer matrix as well as to increase fibre strength using different chemical agents (Li et al., 2007). The most used chemical methods are alkaline treatment or mercerisation. The chemicals disrupt the hydrogen bonding in the fibre structure, which results in enhancing the surface roughness. Moreover, certain amounts of wax, lignin and oils covering the external surface of the fibre cell wall are also removed.

Research by Karthikeyan and Balamurugan (2012) showed an improvement of about 15% in impact strength for alkali treated coir in coir/epoxy composite compared to untreated fibre. 6% alkali treated composite was found to exhibit the best impact strength. The result also agreed with a study by Rahman and Khan (2007) whereby they concluded that alkali treatment decreased the hydrophilicity of coir fibre, improved interfacial bonding and gave substantial rise in tensile properties of the fibre. They observed that NaOH solution of around 10-30% gives the best

performance effects. Research on the effects of alkali treatment has also been conducted on other NFs. As reported by Prasanna and Subbaiah (2013), alkali treatment increases the mechanical properties of Palmyra-banana fibre composite, while the surface morphology of the fractured samples showed good fibre-matrix bonding. An increase in flexural strength by about 36% of the treated kenaf/epoxy composites was also indicated in investigations done by Yousif et al. (2012). In terms of the thermal stability of the coir, Khan and Alam (2012) reported an improvement on the fibre after treated with alkali. However, the treatment was conducted at above 180^{o}C, thereby reducing the tensile strength compared to untreated fibre. De Weyenberg et al. (2003) examined the effects of alkali treatment and diluted epoxy on flax fibre composite and concluded that the combination treatment enhanced the bending strength and stiffness in both longitudinal and transverse directions.

2.2.3 Hybrid natural fibre/synthetic composites

Although NF has a promising mechanical properties, they still have disadvantages such as lower impact strength compared to synthetic fibre, poor moisture resistant, which causes swelling of the fibres, poor wettability and restricted processing temperature (Jawaid and Abdul Khalil, 2011; Sindhu et al., 2007). Results from a study by Harish et al. (2009) indicated that coir/epoxy composites exhibit relatively lower mechanical properties than glass fibre-reinforced polymer (GFRP) laminate specimens. They suggested that the hybrid between coir and other cellulosic fibre has a potential for new applications. The statement was supported in a research by Jayabal et al. (2011) who found that the incorporation of synthetic fibre plies

improved the properties of coir composites. Both researchers clearly justified the reasons why hybridisation is needed.

Hybrid composites consist of a merger of two or more fibres in a polymer matrix or a mixture of different matrices in a single reinforcing fibre. Hybrid composites can also be a combination of both approaches. Possible combinations of hybrid composites include artificial–artificial, natural–natural and natural–artificial fibre types. The main aim for hybridization is the capability in tailoring the properties to suit the needs of the applications (Santulli, 2007). Reddy et al. (2008) agreed that the insertion of synthetic fibres to NFs composites make it more suitable for technical applications. A blend properties of strength, stiffness and ductility may be accomplished by hybrid composites which cannot be achieved by a single fibre reinforcement composite (Nunna et al., 2012). Researchers started exploring NF-based hybrid due to the consciousness of the adverse effects of synthetic fibre on the environment and high cost of synthetic fibre type. Previous researches had proven that synthetic-natural based hybrid composites leads to the intermediate characteristic between pure natural and pure synthetic fibre based composites (Justizsmith et al., 2008; Santulli et al., 2005).

The rule of mixture (Equation 2.7) can be used to predict the properties of hybrid mixtures composite (Sreekala et al., 2002).

$$P_H = P_1V_1 + P_2V_2 \tag{2.7}$$

P_H refers to the characteristic property to be examined, P_1 and P_2 are the characteristic property of the first system and the second system. V_1 and V_2 are the relative hybrid volume fractions of the first and second system and $V_1+V_2=1$.

A positive or negative hybrid effect in hybrid composites is defined as a positive or negative deviation of a certain mechanical property from the rule of mixtures behaviour. Many positive hybridization effects have been reported so far by the inclusion of synthetic fibre to NF. Wong et al. (2010) reported that the inclusion of glass fibre had improved the impact strength of coir composites at various fibre lengths. Kumar et al. (2009) stated that coir/glass hybrid composites is a promising candidate for structural applications where high strength and stiffness are required. Coir/glass ratio of 1:2 was observed to be an effective positive hybrid. Moreover, research by Mishra et al. (2003) found that the impact performance of sisal/glass hybrid polyester composite increased by 34% with the addition of only 8.5 wt% of glass fibre. On the other hand, Reddy et al. (2008) reported an increase in impact properties of kapok/glass hybrid polyester composites compared to kapok/polyester composite, whereas an increment in flexural strength was almost 70%. A study by Thwe and Liao (2003) indicated that bamboo-glass hybrid reinforced polypropylene composite exhibits better fatigue resistance than pure bamboo fibre composites.

As seen, most of the research involving hybridization with NFs are focusing on glass fibre. Less attention has been made to Kevlar aramids fibre most probably due to the cost and the wetting problem between Kevlar and NFs. Considering the research done by Halvorsen et al. (2006) where they observed on Kevlar/fibreglass as the face sheet in a thermoset polymer epoxy composite, the result showed that the

impact performance increased with the addition of Kevlar fabric layer. It was expected that the impact performance of coir composite would show a tremendous increase if Kevlar was incorporated rather than glass fibre. Experiments showed that factors affecting the mechanical behaviour of hybrid composites are fibre weight or volume fraction, stacking sequence of the fibre layers or hybrid configurations, treatment of fibres, composite manufacturing method and effects of environmental condition (Nunna et al., 2012; Santulli, 2007). Therefore, the methods to promote good interfacial bonding between Kevlar and coir need to be refined.

2.3 Laminated textile composites

Laminated composite materials refer to layers (laminas) of at least two different materials that are stacked together in the thickness (z) direction. Fibres as the prime load-carrier in fibre-reinforced composite laminates can be in two forms; continuous or discontinuous structure (refer to Figure 2.5).

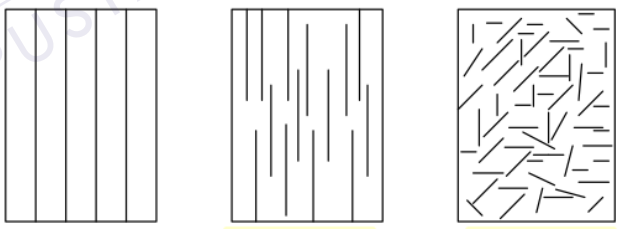

Figure 2.5: Fibre orientations in fibre-reinforced composites (Rahman, 2013); (a) continuous and aligned fibres, (b) discontinuous and aligned fibres and (c) discontinuous and randomly orientated fibres

Although most of the advances in NF composites are focusing on random discontinuous orientation, continuous fibre-reinforced composites are essential for manufacturing materials for instance in load bearing or structural applications

(Goutianos et al., 2006). Composite systems composed of discontinuous reinforcements are considered as single layer composites. It usually produces isotropic composites, although some may yield anisotropic properties. Continuous reinforcements can be either single or multi-layered. Each lamina layer can be either unidirectional or bidirectional (woven) fibre structure and produce orthotropic behaviour (Verma et al., 2013). Unidirectional fibre composite structure is strong in the fibre direction, but weak in the direction perpendicular to the fibre. Bidirectional composite reinforcement, which is also known as woven reinforcement offers a second direction of fibre bundle (yarn) in a single layer to provide more balanced properties. Table 2.4 illustrates the types of continuous multilayer laminate.

The term 'textile' in the laminated composite system can be explained as the combination of a resin system with a textile fibre, yarn or fabric system as reinforcement. The fabric system comprises of laminate types as displayed in Table 2.4. A number of studies varying textile structures and angle ply laminates were conducted to determine the damage resistance and tolerance of composites (Karahan, 2008; Kim and Sham, 2000; Dorey et al., 1978). A research by Kushwaha and Kumar (2010) agreed that the properties are enhanced in woven glass mat reinforced hybrid composites compared to strand mat. Dorey et al. (1978) pointed out that unidirectional (UD) composite structure is better than woven structure in terms of static mechanical properties. Moreover, Karahan (2008) reported that UD non-woven was 16% lighter in weight and more flexible compared to woven for the same number of ply. It was also found that UD contributes to better impact energy absorption and improves ballistic energy propagation compared to woven structure.

Table 2.4: Types of continuous multilayer laminates (Mallick, 1988)

Laminates type	Configuration	Description
Woven	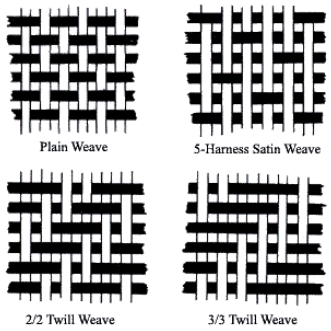	Interlacing two sets of continuous yarns passing over and under each other
Unidirectional	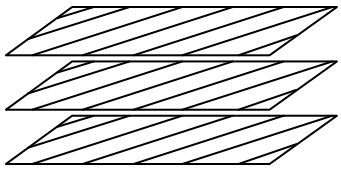	Fibre orientation angle is the same in all laminates
Angle-ply	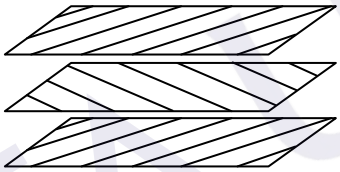	Fibre orientation angles in alternate layers
Cross-ply	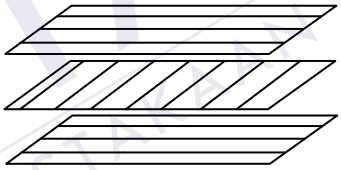	The angles in alternate layers are: …/0^o/90^o/0^o/90^o/…
Symmetric	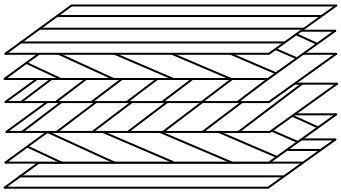	Ply orientation is symmetrical about the centreline of the laminate: i.e: $[0/+45/90/90/+45/0]_S$ S indicates symmetry about the midplane
Quasi-isotropic	Ply orientations: [+60/0/-60] & [+45/0/-45/90] or [0/+60/-60] & [0/+45/-45/90] or $[0/\pm45/90]_S$	Laminates consist of three or more laminas of identical thickness and materials with equal angles between each adjacent lamina

Kim and Sham (2000) claimed that lower maximum load with smaller damage area, higher ductility index and higher residual compression after impact are exhibited by woven fabric laminates over cross-ply laminates. Othman and Hassan (2013) added that better ballistic performance in terms of higher energy dissipation and minimum layer of projectile arrest upon impact are found on cross-ply laminated aramids over woven aramids.

Heterogeneous and orthotropic/anisotropic properties of laminated textile composite are found to deliver great intralaminar and interlaminar strengths, and damage resistance. The structure has the capability to transform kinetic energy from the impactor and reduce damage through several methods, such as opening extensive crack surfaces and spreading (de-localizing) the damage zone, plastic deformation, buckling and other dynamic instabilities that change the material response (Qiao et al., 2008).

2.3.1 Woven reinforcement structure

Woven fabric reinforcement is a textile formed by the weaving process. Woven structure is produced on a loom and made by interlacing two sets of continuous fibre bundles (yarns) passing over and under each other to offer superior dimensional stability in the longitudinal and crosswise directions. According to Cao et al. (2008), textile composites demonstrate excellent properties for high specific-strength products. It is widely used in commercial applications including products for energy absorption, aerospace, automotive and defence research as well as agricultural products. A multi-scale nature of structural fabric is presented in Figure 2.6. It can be

clearly seen that woven fabric structure is formed by yarns, which themselves composed of many micro-scale fibrils or fibres.

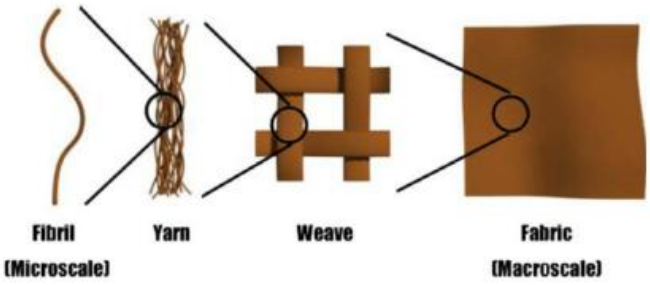

Figure 2.6: Multi-scale nature of structural fabric (Powell and Zohdi, 2009)

The basic operational concept to interlace yarns to produce fabrics on any type of loom is 'shedding', 'picking' and 'beating' (Collier, 2000). These three operations are often called the primary motions of weaving. Shedding involved opening vertical (warp) yarns direction in order to assist horizontal (weft) yarns to get in. 'Harness' (healds) is designed for this specific function. On the other hand, weft insertion of yarns or carrying yarns across the loom is called the 'picking' mechanism. Picking is usually assisted by a 'shuttle' device for simple handloom. Beating is the final process in weaving formation. Beating allows in-coming weft yarns to stay close to the other weft yarns to form fabric. 'Reed' or 'comb' is designed for this purpose. Figure 2.7 illustrates the schematic of weaving device.

Numerous complex weaving loom mechanisms and machines have been developed for mass production since the industrial revolution era. Though numerous machines have been developed, the fundamental of the weaving concept is still within the boundary of the three steps mentioned earlier. Shedding process is vital to defer the pattern of the produced fabric. It can be divided into two categories, which

are fixed shedding and programmable shedding. For fixed shedding, heald frames move in the opposite direction, bringing together all yarns to a respective frame. This action creates a pathway for the shuttle to interlace the yarns. Unlike fixed shedding, programmable shedding has loose heddles and can be solely moved depending on the written program (Onder and Berkalp, 2011).

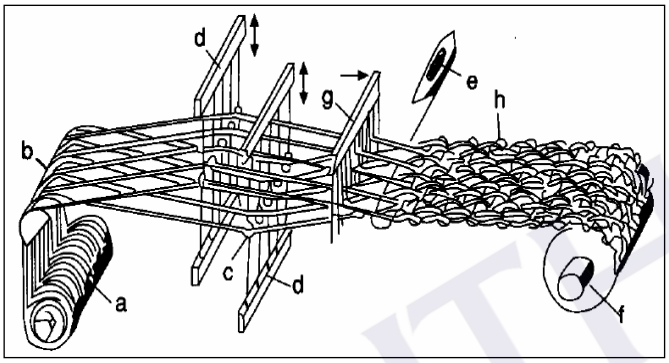

Figure 2.7: Essential parts of a loom; a-weaver's beam, b-back rest, c-healds (heddle), d-heald frames, e-shuttle weft yarn, f-cloth beam, g-reed and h-woven cloth (Onder and Berkalp, 2011)

The easiest picking or wefting process is done by moving the shuttle manually across the warping yarns. The motion of the shuttle can be driven by other mechanisms such as pneumatic or hydraulic drivers. In an advanced design, weft yarn is carried across the loom by means of air jet or water jet. Seyam and El-Shiekh (1990) reported that shuttleless loom is not efficiently weavable for yarns having various thickness. Next, the beating process allows the formation of fabric. The size of the reed or comb that is used to pull yarns close to each other must consider yarn fineness and fabric size. Bigger reed size results in fabrics with porous structure. On the other hand, smaller reed size induces higher friction between the reed wire and yarns end with hairiness problems and loose tensioning of warp yarns. Another issue that must be considered is the balance pulling force of the reed. Any imbalanced

force during the beating process can produce fabric with high porosity as well as fabric disorientation.

2.3.2 Non-woven cross-ply and angle-ply reinforcement structure

Textile materials produced by means other than weaving are called non-wovens. It is normally made from continuous filaments or from staple fibre webs, which is bonded together to strengthen it. It was explained by Dubrovski and Cebasek (2005) that the preferred mechanical properties on non-wovens can be achieved by selecting the proper constructional parameters such as fibre type, composition and orientation, the methods of preforms (webs) construction and the bonding techniques.

Cross-ply and angle ply non-woven structure exhibits better uniformity compared to other compressed staple fibre webs as it offers higher cover or yarn packing in relation to fabric thickness (Dubrovski and Cebasek, 2005). Cross-ply laminates hold plies that are oriented in both 0º and 90º directions. In contrast, angle-ply comprises of continuous filaments or yarns in a certain degree of orientation. In order to produce CP and AP structures, Cheon et al. (1999) and Abraham et al. (2007) introduced a filament winding method where the filament or yarns from bobbin are wound on a rotating reel at a controlled speed. Each layer produces unidirectional structure and by laying two UD layers with a desired angle, CP and AP can be formed. Figure 2.8 shows the schematic of the winding process by Abraham et al. (2007).

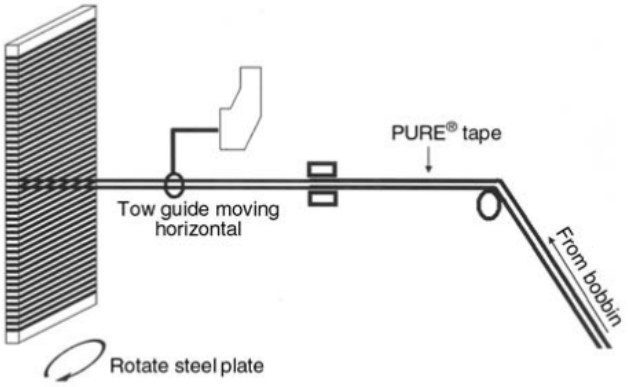

Figure 2.8: Schematic of the tape winding process for the fabrication of UD structure (Abraham et al, 2007)

2.3.3 Textile hybrid laminates

There are several types of hybrid composite laminates as highlighted by Pegoretti et al. (2004) including interply hybrids, intraply hybrids, intimately mixed (intermingled) hybrids, selective placement hybrid and superhybrid composite. Extensive research has been done to explore interply and intraply hybrids. Park and Jang (1997) studied the effects of aramid-UHMPE fibre interply hybrid with changes in the stacking sequence. Pegoretti et al. (2004) examined the effects of interply and intraply hybrids structure on E-glass-PVA composites. Moreover, Dehkordi et al. (2010) investigated the low velocity impact behaviour of basalt-nylon intraply hybrid with changes in nylon volume fraction and energy levels. Wang et al. (2008), on the other hand, studied the effects of fibre arrangement of aramid/basalt interply and intraply hybrids composite. Interply hybrids are the stacking of two or more layers of homogenous materials, whereas, intraply involves two or more types of fibres that are combined in the same layers. It was reported that interply hybrid exhibits greater tensile performance. However, better ductility index is gained by intraply hybrid

compared to interply hybrid composites due to its ability to impede crack propagation (Pegoretti et al., 2004).

2.4 Concluding remarks

Based on the literature review, several needs have been identified as the motivation for the research. The current work intends to focus on the hybrid between NFs and synthetic fibres as previous studies have shown great improvements on the impact response by hybridizing fibre. The merge between NF (coir) and synthetic fibre (Kevlar aramids) becomes the primary intention due to high awareness of the adverse effects of petroleum-based fibres. The incorporation of coir fibres can limit the use of Kevlar synthetic fibres, besides preserving the advantages offered by high strain fibres. Very few attempts have been made to investigate the applicability and compatibility of NFs with Kevlar aramids fibre. Therefore, a novel idea of hybrid composite development is proposed in this research. The exceptional properties of Kevlar aramids fibres are expected to significantly trim down the weaknesses of coir. This research aims at focusing on the assessment of impact response and energy absorption behaviour.

CHAPTER 3

MATERIALS AND METHOD

3.1 Introduction

This chapter introduces the materials used (Section 3.2) and the experimental methods involved in this research. Section 3.3 details the preparatory process of dry continuous fabric/mat, preparation of coir-epoxy composites and preparation of hybrid coir/Kevlar composites. Methods of testing and characterising the produced samples are described in Section 3.4. In Section 3.5, the statistical analysis conducted on the experimental data is explained.

3.2 Materials

3.2.1 Coir yarn

The coir used in the present study is in the form of continuous yarn (Figure 3.1). The coir yarn was used to produce structural woven, cross-ply and angle-ply mats, which provide more balanced properties and structural integrity compared to discontinuous structure mats. Coir yarns were supplied by Btex Engineering Ltd., India. The price of the coir yarn was USD 6 per kilogram. The density of coir as reported in the previous literature is 1.15 g/cm^3 (Akil et al., 2011).

Figure 3.1: Coir yarns

3.2.2 Woven Kevlar 29

Plain woven Kevlar 29 (Figure 3.2) used in this research was supplied by China Beihai Fiberglass Co. Ltd., China. The yarn size is 110 Tex whereas the fabric weight is 200 g/m^2. The price of the materials per meter square was USD 18.

Figure 3.2: Plain woven Kevlar 29

3.2.3 Epoxy resin and curing agent

The matrix used was epoxy DER 332 of density 1.16 g/ml. The epoxy resin was cured with the addition of Jeffamine D-230 hardener. Hardener of density 0.948 g/ml was used as the curing agent. The amount of hardener used was 32% of the

epoxy resin portion. Both the resin and hardener were supplied by Penchem Technologies Sdn. Bhd., Malaysia.

3.2.4 Sodium hydroxide

Laboratory grade sodium hydroxide (NaOH) of 0.1M and a purity of 99.99% was used for alkaline treatment. It is in pellet form and its molecular weight (MW) is 45.55 $g.mol^{-1}$. Strong alkaline solution was formed when the NaOH pallets were dissolved in a solvent such as water. In order to prepare 1% of NaOH, the mixing ratio between NaOH pellets and distilled water is 100:1 by weight.

3.3 Sample preparation methods

Basically, there were three main processes involved in the samples preparation. The first process was the preparation of dry continuous coir fabric/mat that was used as composite reinforcement. This was followed by the second process, which involved the preparation of coir-epoxy composite. The final process was the preparation of coir/Kevlar hybrid composite. The flow chart of the primary sample preparation process is illustrated in Figure 3.3.

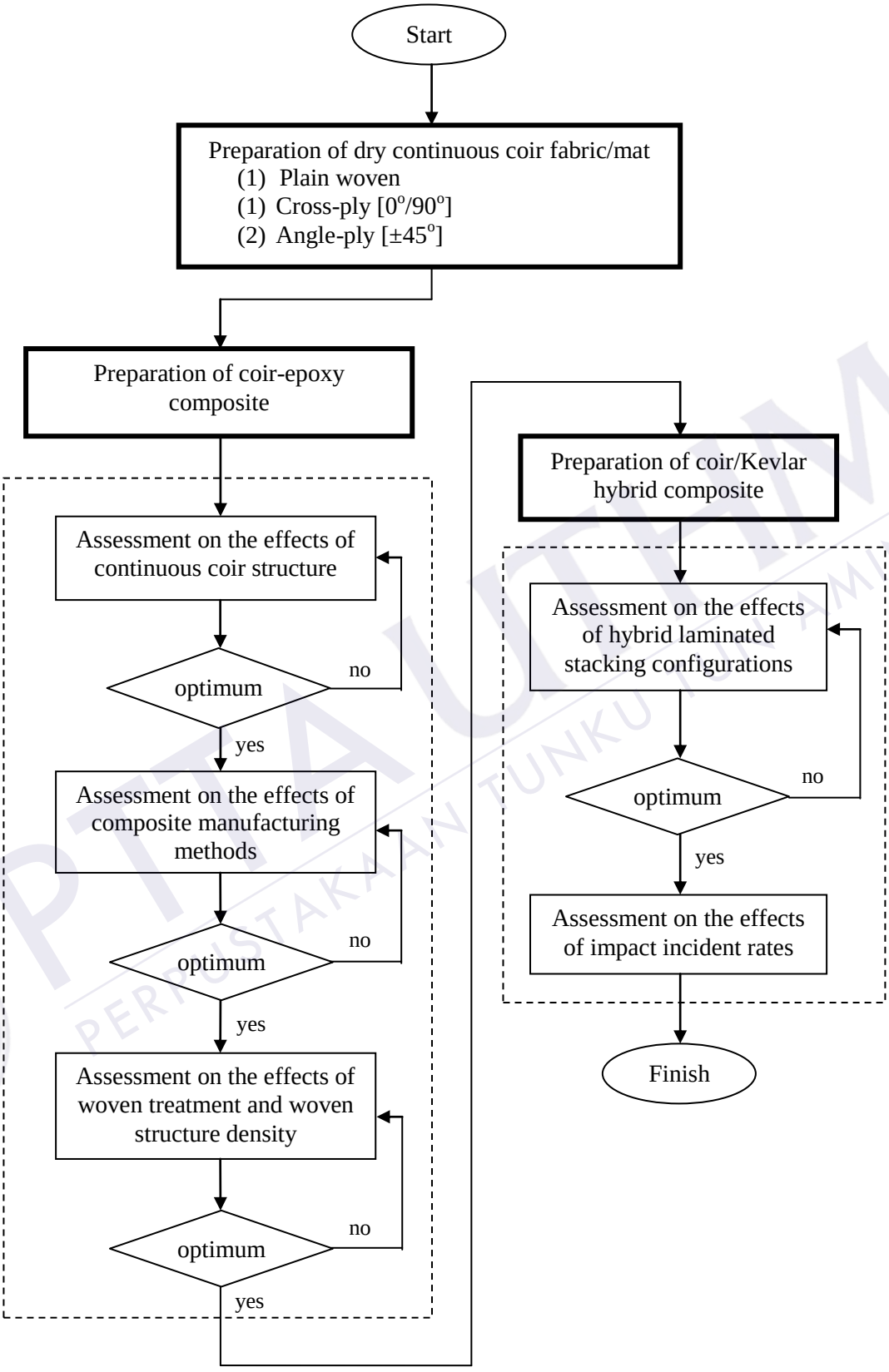

Figure 3.3: Flow chart of the primary sample preparation process

3.3.1 Preparation of dry continuous coir fabric/mat structure

NF yarns were fabricated into three different textile fabric structures, which were plain woven, 0/90 degree cross-ply and +45/-45 degree angle-ply structures. Figure 3.4 illustrates the schematic of the fabric structure.

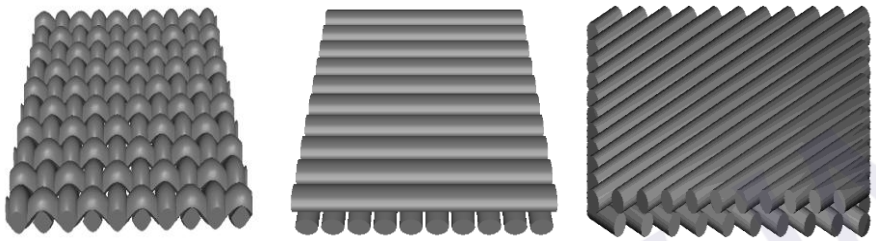

(a) (b) (c)

Figure 3.4: Schematic of; (a) plain woven (b) 0/90 degree cross-ply and (c) +45/-45 degree angle-ply

3.3.1.1 Preparation of plain woven coir fabric structure

Existing weaving device in laboratory was not ideal for respective NF yarns used in this research. Figure 3.5 highlights problems during the woven preparation process. High friction rate rises when installing yarns on the floor loom led to very bad yarn hairiness. The condition became worse when the beating process was done where the hairiness formed fibre hanks, which restricted the movement of the reed. More force was exerted during beating, causing the yarns to loose in tension. Therefore, weft yarns were unable to stay close to each other to form a dense fabric structure. As a result, the yarn interlacing was less dense and the structure was porous. This, in turn, increased inter-yarn flow channel and the permeability of the fabric geometry, which led to deteriorated mechanical properties. This kind of consideration has been stopped, but the weave process continued with a self-design weaving device.

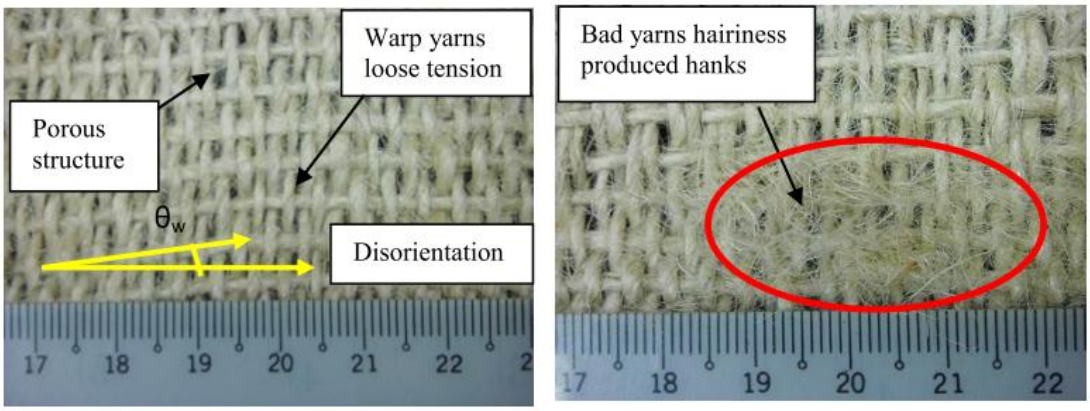

Figure 3.5: Failure of woven fabric

The design objective was not to produce the best weaving device, but rather to design the most reliable lab-scale loom and to produce consistent woven structure. A number of existing looms were referred to, as shown in Figure 3.6, for design assistance and understanding the operating mechanism.

(a) (b)

Figure 3.6: Loom for design reference; (a) table loom and (b) floor loom

Plain woven fabric structure were prepared using fabricated self-designed handloom. The proposed loom design utilizes manual actuation for all the three basic weaving operations; shedding, picking and beating. This prototype manages to produce fabric dimension of 230 mm x 230 mm. The overall size of the weaver is 465 mm x 400 mm x 145 mm (L x W x H). It consists of five major components

which are the base with pin holder, front reed aligner, rear reed aligner and two heald frames (Figure 3.7). The base was made from mild steel to retain the components' positions during weaving. Pin holders were attached at both ends of the base to tie the yarn in Y-axis position or so called warp yarn.

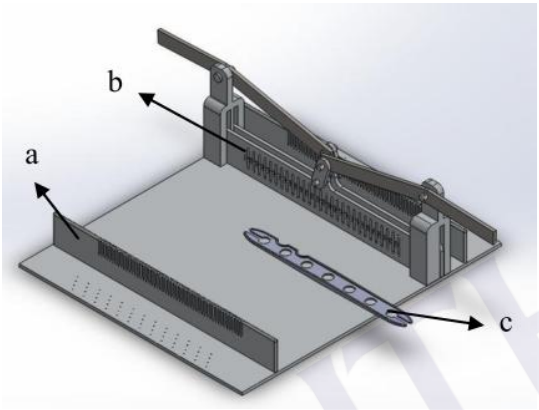

Figure 3.7: Final concept sketch of weaving handloom; a-aligner, b-heald frame, c-shuttle

In order to ensure the aligned yarn is in the right position, an aligner was fixed near the finishing end pin holder. As this prototype was designed for laboratory woven sample, no rolling mechanism was attached at the end pin holder. Heald frames were located 265 mm from the front aligner so that the produced sample would have a length around 230 mm in Y-axis. Both frames were actuated using lever-pivot mechanism. The maximum lift elevation recorded between the two frames was a 10 mm gap. The proposed handloom design was found to eliminate disorientation of yarns and the woven structure produced was less porous. Fabrication of denser, less porous woven structure was achieved using the self-designed handloom. Table 3.1 represents the main parts of the loom and its function. Figure 3.8 on the other hand illustrated the fabricated handloom.

Table 3.1: Main part of self-designed handloom

Parts	Description
(a) Aligner 	To ensure warp yarns are in the right position
(b) Heald frame 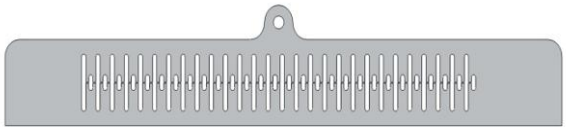	To lift warp yarns
(c) Shuttle 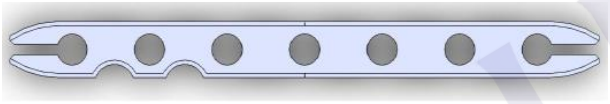	To assist weft yarn insertion

Figure 3.8: Fabricated loom

Fabrics were produced in two different types; Type 1 and Type 2 (refer to Figure 3.9). The black lines in the Figure indicate the distance between the warp

yarns on the fabric. Warp distance on woven fabric Type 2 was closer than in Type 1. The selection of woven type was based on the highest degree of woven density the device can produce as fabric density has significant influence on weaving resistance. A powerful beating motion might obtain higher weaving density, however it may damage and consequently, weaken the fibre, yarn and fabric itself (Lim et al., 2012). Extensive report from previous work has shown that fabric properties are highly affected by the fabric degree of tightness (Seyam and El-Shiekh, 1994). Therefore, the effects of woven tightness (woven density) on composite materials were further assessed in this study as described in Section 3.3.4.3.

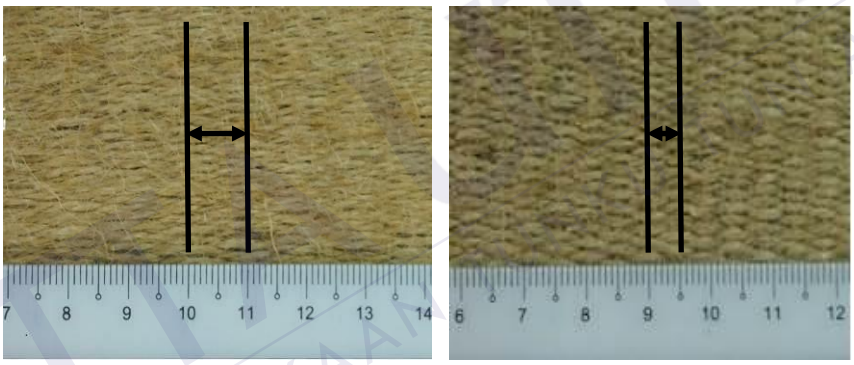

(a) (b)

Figure 3.9: Woven fabric; (a) Type 1 and (b) Type 2

Fabric Type 1 had a warp distance of 10 mm, produced using an aligner size of 10 cm gap between each tooth and heald size of 10 mm gap between each hole. On the other hand, fabric Type 2 (warp distance of 5 mm) was produced using 5 mm gap size between teeth on aligner and 5 mm gap between holes on heald frame. Technically, warp and weft set of the plain woven coir structure for Type 1 was 3 epi (ends per inch) and 31 ppi (picks per inch). On the other hand, Type 2 woven structure exhibited 5 epi and 21 ppi.

3.3.1.2 Preparation of cross-ply and angle-ply coir fabric structure

The process of manufacturing cross-ply and angle-ply structures involved the frame winding method (Figure 3.10). The idea of this method was triggered from a research by Abraham et al. (2007). The overall machine size was 750 mm x 400 mm x 250 mm, whereas the winding frame size was 320 mm x 250 mm. A single phase inverter was used as the speed controller where it allows a winding speed up to 42 RPM. Allowable yarn size to be used on the device was over 800 Tex. Textile preforms for cross-ply and angle-ply structures were then cut into the desired angle to be used as composite reinforcement (Figure 3.11). On average, the fabric density for 0/90 degree cross-ply was recorded as around 17 to 20 yarns per inch, whereas for 45/-45 degree angle-ply, 14 to 16 yarns per inch was found in each direction.

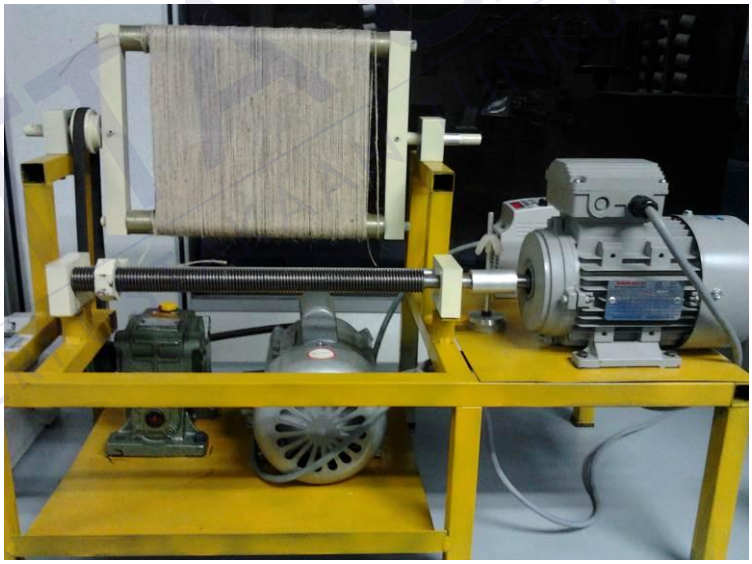

Figure 3.10: Frame winding machine

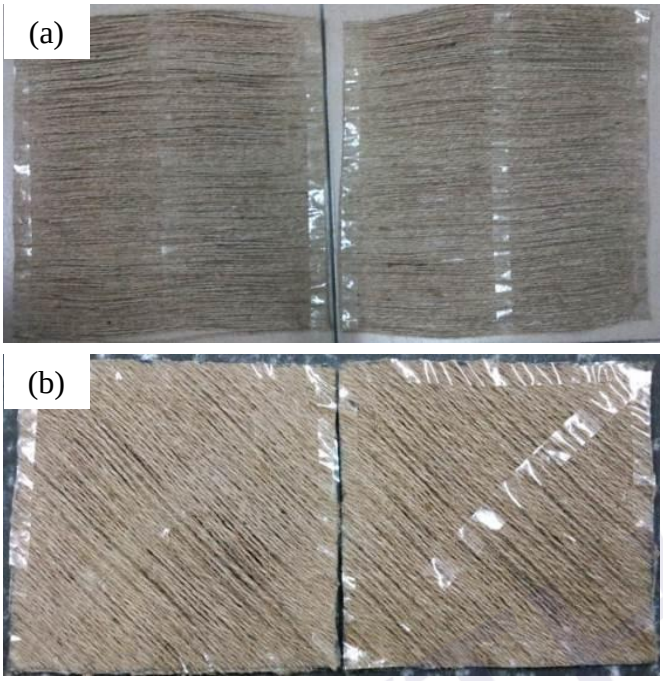

Figure 3.11: Fabric samples for (a) cross-ply arrangement and (b) angle-ply arrangement

3.3.2 Preparation of coir-epoxy composite

3.3.2.1 Effects of laminated textile structure on impact response of coir-epoxy composites

Type 1 imbalanced plain woven, cross-ply (0°/90°) and angle-ply (+45°/-45°) structures were prepared in this research. All of the reinforcement samples involved were in untreated condition. The preparation process of the dry fabric/mat structure has been well explained in Section 3.3.1. Manufacturing of the structural composite samples involved vacuum bagging techniques as discussed in Section 3.3.2.2 (b). The lamina comprised a single ply for imbalanced plain woven structure, whereas for $0^o/90^o$ cross-ply and $+45^o/-45^o$ angle-ply structure, it comprised one set each. The coding and formulation of the composite samples in the present study are summarized in Table 3.2. Analysis of variance (ANOVA) was employed to

determine the significant structural condition that predominantly influenced the impact behaviour of the composites. All samples were subjected to low velocity impact at an impact velocity of 9 m/s. The test set-up is further described in Section 3.4.3.3.

Table 3.2: Samples coding and formulation of the composites with different reinforcement structures

Samples coding	Composites formulation
WC	Woven/Coir
CPC	Cross-ply/Coir
APC	Angle-ply/Coir

3.3.2.2 Effects of different composite manufacturing methods on impact response of woven coir-epoxy composites

In this study, composite materials involved a combination of two different constituent materials, which are the fabric (or mat) structure as the reinforcement and epoxy resin as the matrix. The reinforcement-matrix ratio was fixed at 3:7 by weight ratio. The ratio was chosen based on the previous findings by Arrakhiz et al. (2012) who reported that 30 wt% of coir fibre content shows the optimum set of mechanical properties. Composites exceeding 50 wt% of fibres loading were found to be rigid and agglomerated as claimed by Monteiro et al. (2008). The reinforcement samples were first dried in an oven for 2 hours at 80^{o}C to remove moisture.

a) Composite fabrication via compression moulding method

A 230 mm x 230 mm square mild steel mould was applied with mould release agent, which helped to avoid the specimen from sticking on the mould. The applications of mould release agent need to be dried for at least 30 minutes before the

second layer was applied. Resins were poured and the reinforcement samples were placed in a square mould alternately. The mould was closed and placed in a pressing device. The heating element on the pressing device was turned to 100^{o}C for the first 6 h for pre-cured and the pressing was continued overnight without heating for post-cured. Figure 3.12 illustrates the actual and schematic drawing of the compression moulding apparatus.

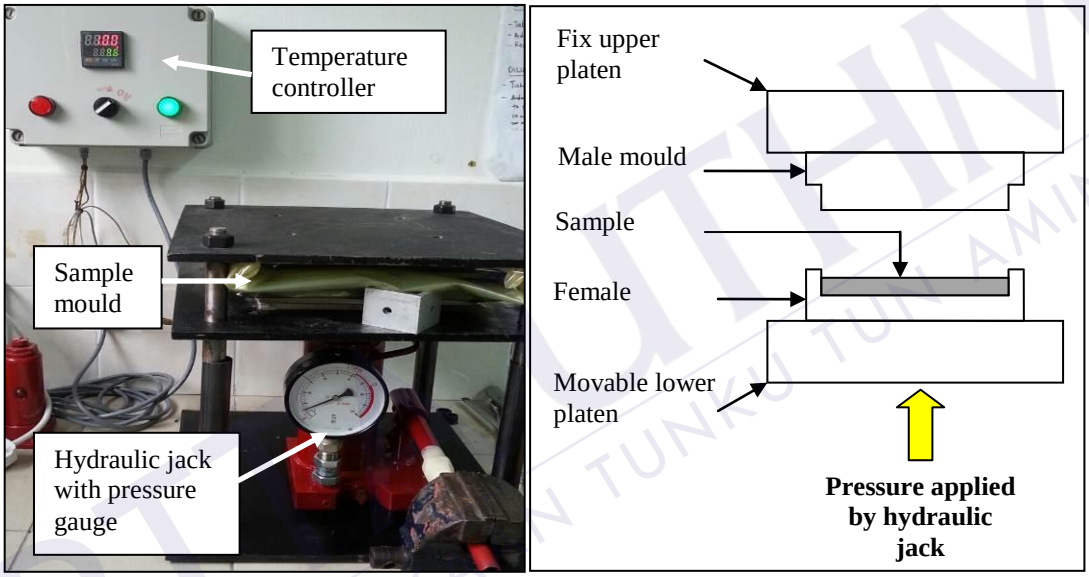

(a) (b)

Figure 3.12: Compression moulding apparatus; (a) actual and (b) schematic diagram

b) Composite fabrication via vacuum bagging method

A schematic diagram and the actual set-up of the vacuum bagging used for the composite panel manufacturing are shown in Figure 3.13. Vacuum bagging assembly contained several parts. The tool plate was usually made of glass and was covered with release film. Tiny holes scattered on the peel ply assisted in the penetration of excess resin. A special cotton filter called “breather” covered the top of the peel ply to avoid the resin from flowing through the vacuum valve. The whole

stack was then covered with a thin bagging film. Sealant tape was used to seal all around it. The suction pressure was set to reach 600 mmHg for about 30 minutes. During the suction process, air flowed out of the bag and excess resin was soaked up by the breather ply. The samples were then left overnight for curing and post-curing for another 6 h at 80^{o}C in the oven.

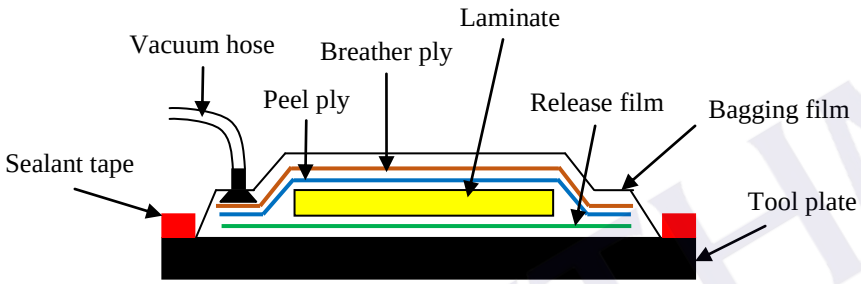

(a)

(b)

Figure 3.13: Vacuum bagging; (a) schematic diagram and (b) actual set-up

Based on the assessment conducted in Section 3.3.2.1, the woven composite structure was selected in this present research due to its tolerable impact properties. Table 3.3 depicts the coding and formulation of the composite samples in the study. Analysis of variance (ANOVA) was employed to determine the manufacturing method that predominantly influenced the impact behaviour of the composites.

Table 3.3: Samples coding and formulation of the composites with different composite manufacturing methods

Samples coding	Composites formulations
CM-WC	Compression moulding/Woven Coir
VB-WC	Vacuum bagging/Woven Coir

3.3.2.3 Effects of woven fabric modification and structure density on impact response of coir-epoxy composites

Woven samples Type 1 and Type 2 mentioned in Section 3.3.1.1 were used in this present research. Moreover, sodium hydroxide (NaOH) was used as the surface treatment of woven coir fabric/mat. The treatment using NaOH had shown some encouraging results on coir fibres as reported in Section 2.2.2.2. However, sufficient concentration of NaOH to be used is essential to ensure optimum mechanical properties of the composites. In order to compare the effects of treatment percentage, the coir fabrics/mats were soaked in three different NaOH concentrations; 6, 9 and 12 %. The percentages were chosen based on the most acceptable range of concentrations used for coconut coir fibre treatment from previous studies (refer Section 2.2.2.2). The soaking process was conducted for 24 hours in a big container and kept in a close room. Later, the fabric/mats were washed thoroughly with tap and distilled water to remove any remaining NaOH solution on the fibre surface. The fabric/mats were finally oven dried for 6 hours at 80 ^{o}C.

Table 3.4 summarizes the samples coding and formulations of the composite sample. Two levels of woven densities (Type 1 and Type 2) were investigated and four levels of treatment percentage (0%, 6%, 9% and 12%) were examined. As both factors had different levels, multi-level factorial design of experiment (DOE) was

performed to investigate the main effect of each factor, as well as the interaction effect between factors on impact response. Randomisation was activated to avoid bias result. Factors and levels assigned for the multi-level factorial design is displayed in Table 3.5. Analysis of variance (ANOVA) was employed to determine the significant factor that predominantly influenced the impact behaviour of the composites.

Table 3.4: Samples coding and formulation of the composites with different woven densities and treatments

Samples coding	Composites formulation
WCT1-0	Woven/Type 1/Treatment 0%
WCT1-6	Woven/Type 1/Treatment 6%
WCT1-9	Woven/Type 1/Treatment 9%
WCT1-12	Woven/Type 1/Treatment 12%
WCT2-0	Woven/Type 2/Treatment 0%
WCT2-6	Woven/Type 2/Treatment 6%
WCT2-9	Woven/Type 2/Treatment 9%
WCT2-12	Woven/Type 2/Treatment 12%

Table 3.5: Factors and levels assigned to the DOE of the effects of woven density and woven treatment

Factor	Level			
Treatment %	0	6	9	12
Woven density	WCT1	-	-	WCT2

3.3.3 Preparation of hybrid coir/Kevlar epoxy composites

The hybrid composites of coir and Kevlar were prepared with different stacking configurations consisting of three laminate layers. As for the coir layer, the

reinforcement structure, treatment percentage and density were decided based on the optimum results obtained in previous Sections 3.3.4.1 and 3.3.4.3. Composite manufacturing method on the other hand was chosen according to the best possible result in assisting good fibre-matrix bonding as resolved in Section 3.3.4.2. Therefore, woven reinforcement structure with density Type 1 and treated using 6% NaOH was selected as it demonstrated better impact response. Compression moulding manufacturing method was implemented as it performed good fibre-matrix bonding and absorbed better impact energy. Figure 3.14 demonstrates the configuration of the hybrid stacking of the composite laminates used in the present research.

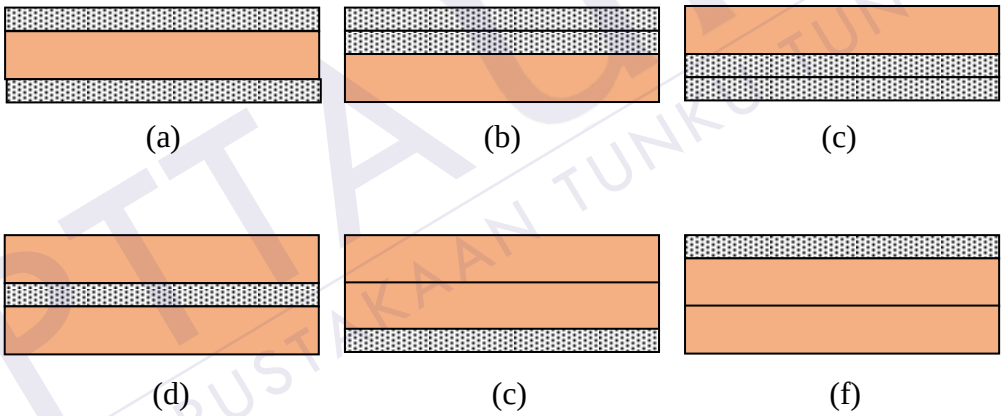

Figure 3.14: Stacking sequences of composite laminates; (a) KCK (b) KKC (c) CKK (d) CKC (e) CCK and (f) KCC

The letter “C” refers to coir ply whereas “K” denotes Kevlar ply. The first letter on each hybrid sample’s coding represent the area facing the impactor (the front face). For instance, CKK sample means that coir ply was the front face, and Kevlar ply was at the back or rear face.

3.3.3.1 Effects of hybrid laminate stacking on impact response of woven coir/Kevlar epoxy composites

The present study involved six hybrid combinations of three layers laminate as illustrated in Figure 3.14., which were KCK, KKC, CKK, CKC, CCK and KCC. The assessment included eight control samples, which were C, CC, CCC, KKK, $[K]_9$, [CK], $[CK]_2$ and $[CK]_3$. The control sample, [CK], refers to the intraply hybrid sample where coir and Kevlar yarns were mixed in the same layer. The reinforcement structure of [CK] is shown in Figure 3.15.

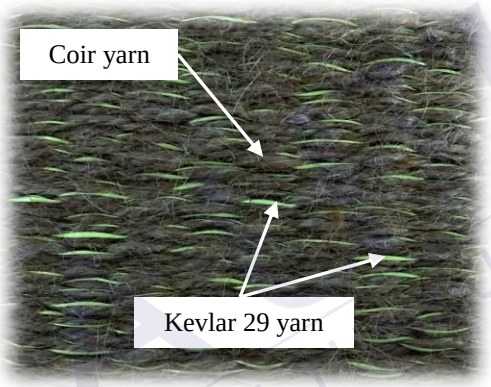

Figure 3.15: The intraply hybrid [CK] reinforcement sample

The study was performed to determine the hybrid stacking configuration, which has optimal impact resistance and absorbs more impact energy. In comparison, the hybrid composite samples were assessed under quasi-static impact (1.25 mm/s) and low velocity impact (5 m/s) to observe the compliment. Samples coding and formulations are presented in Table 3.6.

Multi-level factorial DOE was performed to investigate the effects of each factor, as well as the effects of interactions between factors on impact response. Factors and levels assigned for the DOE is shown in Table 3.7. ANOVA was

employed to determine the significant factors that predominantly influenced the impact behaviour of the composites.

Table 3.6: Samples coding and formulation of the hybrid composites with different stacking configurations and the control samples

Samples coding	Composites formulation
KCK-LV	Kevlar/Coir/Kevlar/Low velocity
KKC-LV	Kevlar/Kevlar/Coir/Low velocity
CKK-LV	Coir/Kevlar/Kevlar/Low velocity
CKC-LV	Coir/Kevlar/Coir/Low velocity
CCK-LV	Coir/Coir/Kevlar/Low velocity
KCC-LV	Kevlar/Coir/Coir/Low velocity
KCK-QS	Kevlar/Coir/Kevlar/Quasi-static
KKC-QS	Kevlar/Kevlar/Coir/Quasi-static
CKK-QS	Coir/Kevlar/Kevlar/Quasi-static
CKC-QS	Coir/Kevlar/Coir/Quasi-static
CCK-QS	Coir/Coir/Kevlar/Quasi-static
KCC-QS	Kevlar/Coir/Coir/Quasi-static
C	Coir
CC	Coir/Coir
CCC	Coir/Coir/Coir
KKK	Kevlar/Kevlar/Kevlar
$[K]_9$	9 layers of Kevlar
[CK]	1 layer of intraply hybrid coir/Kevlar
$[CK]_2$	2 layers of intraply hybrid coir/Kevlar
$[CK]_3$	3 layers of intraply hybrid coir/Kevlar

Table 3.7: Factors and levels assigned to the DOE of the effect of hybrid laminate stacking configuration

Factor	Level					
Testing	quasi-static	-	-	-	-	low velocity
Stacking conf.	KCK	KKC	CKK	CKC	CCK	KCC

3.3.3.2 Effects of different puncture speeds on coir/Kevlar hybrid composites

The optimum impact properties of two of the hybrid composite samples tested in section 3.3.5.1 were taken. The effects of four different impact speeds were evaluated on CCK and KCC to understand its impact behaviour at different incident rate. Impact speed was varied between 5 m/s to 17 m/s. Samples coding and formulations are presented in Table 3.8. Multi-level factorial DOE was performed to investigate the effect of each factor, as well as the effect of interactions between factors on impact response. Factors and levels assigned for the DOE is shown in Table 3.9. Randomisation was activated to avoid bias. ANOVA was employed to determine the significant factors that predominantly influenced the impact behaviour of the composites.

Table 3.8: Samples coding and formulation of the hybrid composite tested at different incident rates

Samples coding	Formulations
CCK-5	Coir/Coir/Kevlar tested at 5 m/s
CCK-9	Coir/Coir/Kevlar tested at 9 m/s
CCK-13	Coir/Coir/Kevlar tested at 13 m/s
CCK-17	Coir/Coir/Kevlar tested at 17 m/s
KCC-5	Kevlar/Coir/Coir tested at 5 m/s
KCC-9	Kevlar/Coir/Coir tested at 9 m/s
KCC-13	Kevlar/Coir/Coir tested at 13 m/s
KCC-17	Kevlar/Coir/Coir tested at 17 m/s

Table 3.9: Factors and levels assigned to the DOE of the effects of different incident rates

Factor	Level			
Stacking conf.	CCK	-	-	KCC
Puncture speed	5 m/s	9 m/s	13 m/s	17 m/s

3.4 Testing and characteristic analysis

Testing and characteristic analysis were divided into three main sections, which involved for yarns, dry fabrics (reinforcement) and the composites.

3.4.1 Yarns characteristic and tensile properties

The physical and tensile properties of the as received coir yarn were assessed. The physical properties such as yarn diameter, yarn linear density (or yarn fineness), yarn twist type and yarn twist direction were examined. Yarn linear density was determined by weighing specific lengths of yarn and converting the data to the appropriate units. Tex is the measuring unit for linear mass density and is defined as the mass in grams per 1000 meters (Collier and Epps, 1999). One meter long yarn was selected from the yarn package and weighed. The Tex was calculated by multiplying the weight (in grams) by 1000. The image in Figure 3.16 shows how to determine the twist type and number of twists per inch of yarn. There are two type of twists (S and Z) which reflex to the direction of the twist.

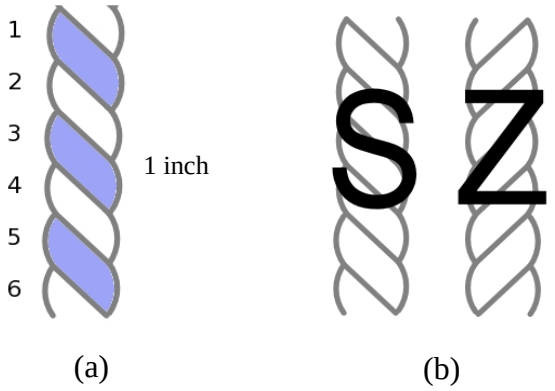

Figure 3.16: Twisted yarn; (a) number of twists per inch measurement and (b) twist type; S and Z

Yarn tensile strength test was crucial to examine the behaviour of yarns when subjected to stretching and pulling forces. When the yarn is pulled, it stretches and the amount of stretch is related to its resistance to force (Collier and Epps, 1999). Yarn tensile tests were performed using the Universal Testing Machine: Lloyd Instrument LR 30K with a gauge length of 200 mm and a crosshead speed of 1.3 mm/min to analyse its tensile strength and modulus. The yarn tensile test set up was in accordance with the set up by Gowda et al. (1999).

3.4.2 Physical characteristic of fabrics

The fabric characteristic analysis involved fabric thickness, fabric weight, fabric density, fabric wavelength and inter-yarn fabric porosity. However, fabric density, fabric wavelength and inter-yarn fabric porosity were mainly done on woven fabric structure. Fabric thickness (*t*) was measured using a digital vernier caliper. Fabric weight, on the other hand was determined by weighing fabric specimens of a pre-determined size on a balance scale. The fabric weight in grams/metre^2 (g/m^2) was calculated from the area measured. The density of the fabric was weighed relative to the thickness, expressed in grams/centimetre^3 (g/cm^3). In contrast, warp and weft densities were reported separately and expressed in warp or weft per inch. The crimp percent, *k*, as defined by ISO 7211-3 was calculated as in Equation (3.1). *L* is the distance between the two ends of the projected yarn onto the fabric plane, and *P* is the actual length of the yarn. Yarn crimp refers to the degree of yarn undulation and is a property of the weave (Lim et al. 2012).

$$K = [\,(P - L)/L\,] \times 100\% \qquad (3.1)$$

Figure 3.17 illustrates the schematic of the plain weave structure. The weft crimp wavelength, λ, was measured in order to see the crimp effect in the structure.

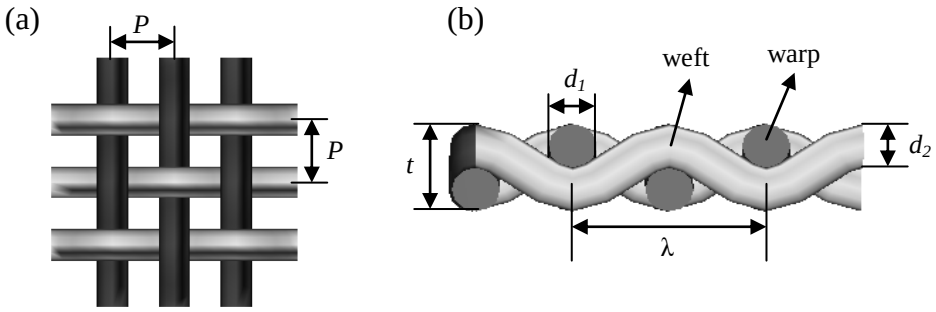

Figure 3.17: Model of plain weave fabric: (a) top view and (b) cross section view

Finally, inter-yarn fabric porosity (ε) was calculated using Equation (3.2). Porosity in fabric is defined as the ratio of the projected geometrical area of the opening across the material to the total area of the material (Cay et al., 2007).

$$\varepsilon = \frac{\text{open pore area}}{\text{total area}} = \frac{P_1 - P_2}{(P_1 + d_1)(P_2 + d_2)} \tag{3.2}$$

3.4.3 Composites characteristic analysis and testing

3.4.3.1 Composites characteristic

The thickness of the composite samples was measured using a digital vernier caliper. The thickness of each specimen was measured at six different points and the mean value was reported. On the other hand, the areal density of the specimens was measured using a digital weighing scale at the accuracy of 0.001 gram. The specimens were measured in five repetitions.

3.4.3.2 Quasi-static indentation test

A composite laminate was clamped between two steel plates, exposing a circular laminate section. A cylindrical punch with a hemispherical impactor tip was used for perforation of the laminate at 1.25 mm/s. The rate was selected according to the indentation testing specification by Li et al. (2012). An impactor tip diameter of 12.7 mm was used. The tip diameter and the exposed circular diameter (76 mm) section were in accordance with ASTM D3763 for low velocity impact test as described in Section 3.4.3.3.

3.4.3.3 Low velocity puncture impact test

Low velocity impact tests were carried out according to ASTM D3763 using Shimadzu Hydroshot Impact Test Machine at ambient temperature. The geometry of the specimens was 100mm x 100mm. The test was performed in triplicates for each specimen, and the average and standard deviation values were later reported. The testing specimens were positioned horizontally in the testing cassette of the machine's fixture. A hydraulic system actuator dropped an impactor with a nose tip of about 12.7 mm at various loading rates. The striker was equipped with a load transducer whose output was fed to a data acquisition board installed in a computer. Figure 3.18 illustrates the impact test machine.

Data analysis for determination of impact response

The load-displacement relation is the most fundamental way to describe the behaviour of composites during impact. It has been described further in Section 2.1.1. This relation can give an insight into how a composite is damaged. Most importantly, it shows how the composite absorbs the impact energy throughout the

impact process. The raw data of the impact event was converted into the force-stroke and the force-time curves displayed by the data processing impact software as illustrated in Figure 3.19.

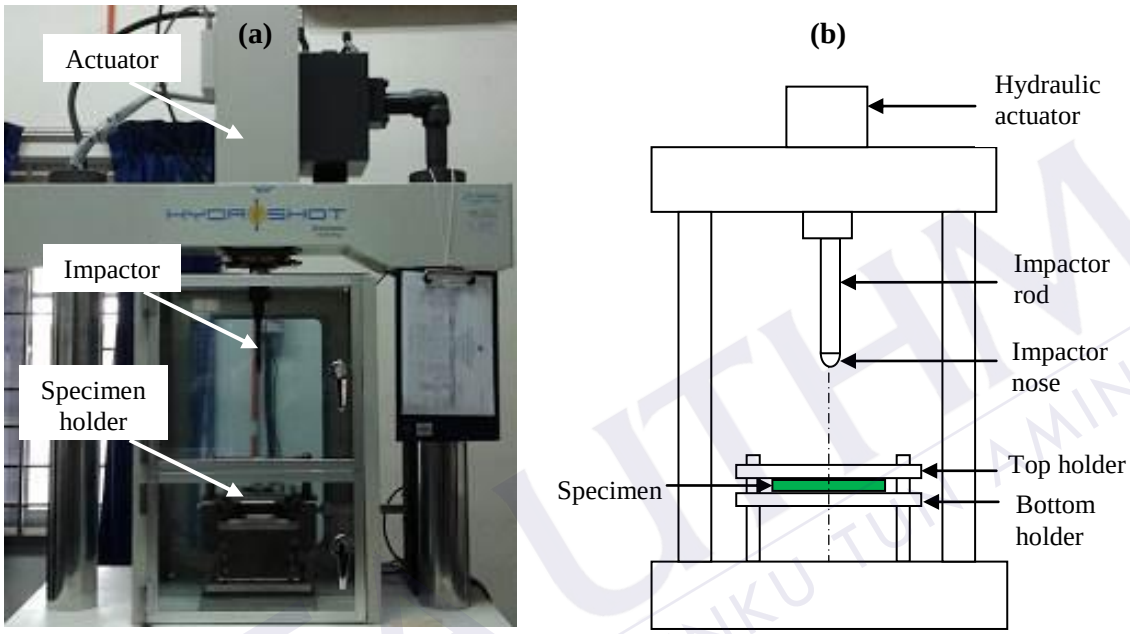

Figure 3.18: Impact test: (a) actual machine and (b) schematic diagram

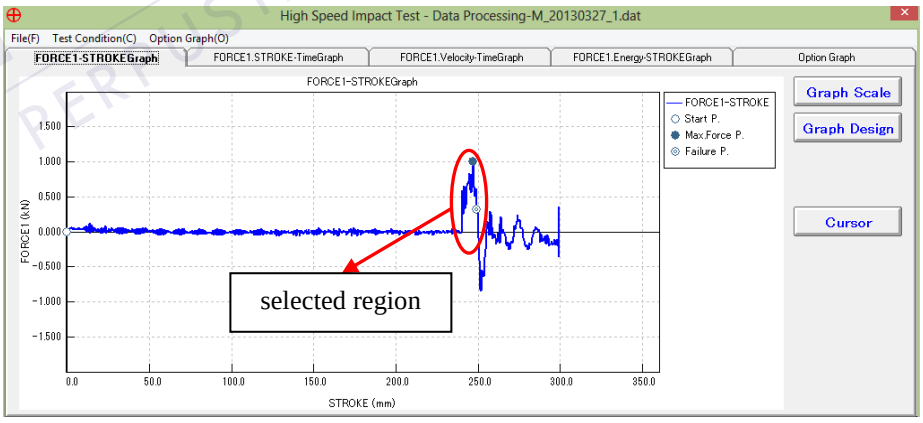

Figure 3.19: Force-stroke curve of the impact event generated by the data processing impact software

From the curve, impact response such as the first material damage, the total displacement (δ), the peak load (P_{peak}), the energy absorbed (E_a), the propagation energy (E_p) and the material's ductility index *(DI)* were obtained and calculated. As seen from Figure 3.19, the prolonged stroke before the force level started to rise occurred due to the distance travelled by the impactor before it touched the specimen. Vibration and noise were expected to be the main disturbance during the dynamic event as portrayed in the curve. The nonlinear region in the curve after the force descending region was due to the frictional forces between the impactor and the perforated composite specimen. Only the raw data from the region marked with a circle on Figure 3.19 was extracted for further analysis.

A new curve using the raw data of the marked region was then plotted using Matlab. The original graph displayed an unsmooth curve, which was expected due to high friction, vibration and noise disturbance as occurred in most of the dynamic impact curves reported earlier. Basic curve fitting was conducted to obtain smoother curve that best fit the original series of data points using the basic fitting tool in Matlab. Figure 3.20 displays the curve fitting process using Matlab.

The absorbed energy was calculated by integrating the area enveloped by the load-displacement curve. The load and displacement at maximum load point were symbolized by P_{peak} and δ_{peak}. The energy at the maximum load point can also be identified as E_m, and E_t represents the total energy absorbed by the specimen in a complete penetration. The energy dissipated after the yield point is defined as E_p (propagation energy), where $E_p = E_t - E_m$. Moreover, the ductility index, $DI = E_p/E_m$ reflects the ductility of the material. A higher ductility index means that most of the

total energy is expanded in crack propagation. Larger *DI* indicates more ductile material. The impact strength or impact toughness value in joule per meter square [J/m^2] can be obtained using Equation (3.4).

$$\text{Impact strength} = \frac{E_m}{\pi d^2 / 4} \tag{3.4}$$

Where, E_m is the energy value at maximum load point, and d is the striker diameter with a value of 12.7 mm. Figure 3.21 illustrates the identification of impact response data.

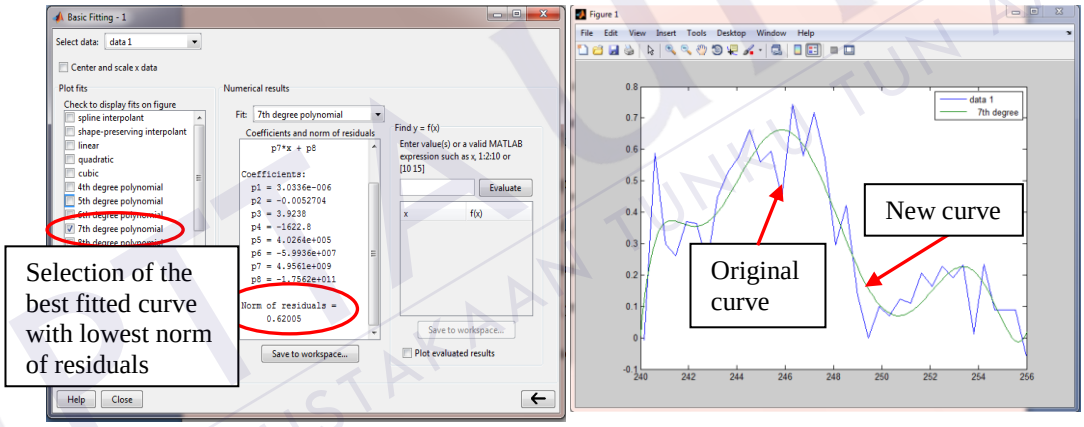

(a)

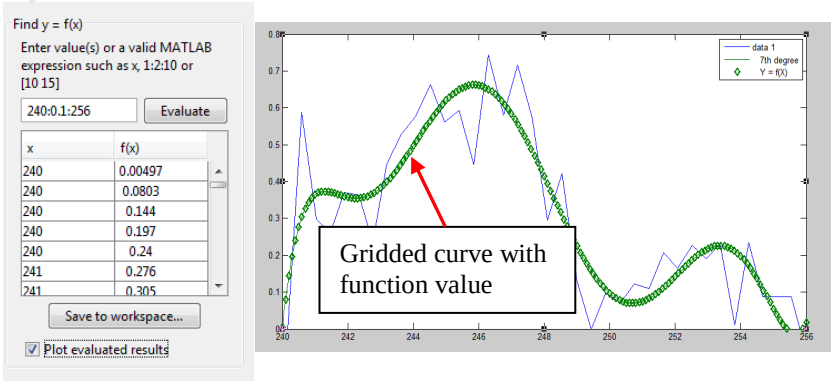

(b)

Figure 3.20: Curve fitting using Matlab; (a) basic curve fitting by selecting the lowest norm of residuals and the new curve appears on the graph, and (b) the command to generate gridded curve with function value

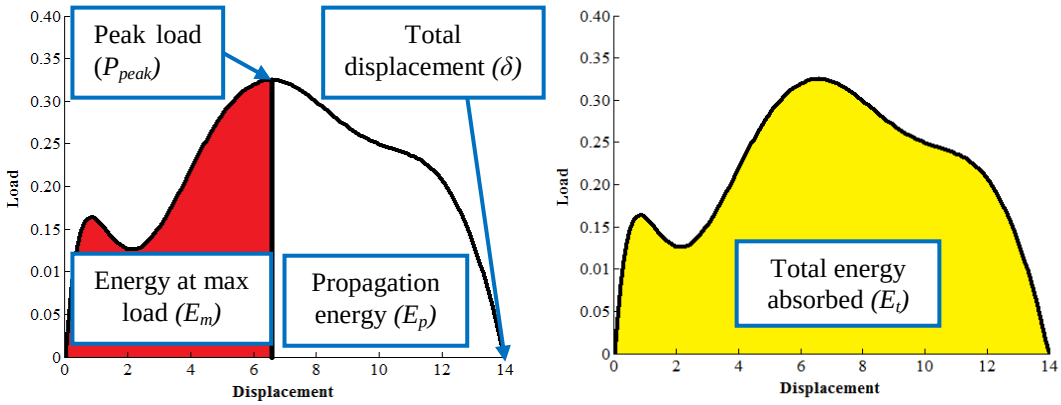

(a) (b)

Figure 3.21: The identification of the impact response data; (a) peak load, total displacement, energy at maximum load and propagation energy and (b) total energy absorbed

3.4.3.4 Composites damage assessment

Damages on composites were evaluated by several methods, including visual inspection, image processing technique for fractured area analysis and scanning electron microscope (SEM) for morphology analysis.

a) Visual inspection (vision)

The fractured surfaces and damage extent of the composites after impact loading were observed to examine the relationship between the damaged shape and the impact behaviour. Images of the impacted composite's surfaces were taken using a digital SLR camera and the radial growth scale was overlaid on the image to distinguish the damage extent of each sample.

b) Area measurement using image processing technique

An image analysis procedure was developed to determine the area of composite damage. The detailed procedure was well explained in Nunes et al. (2004). A flatbed scanner was used to scan the damaged samples, and the images

were processed in Matlab software with its image-processing tool. Samples were scanned at 600 dpi (dots per inch). On the other hand, fractured samples with uneven surfaces were imaged using a digital SLR camera prior. Gauge image with known dimension was placed beside the samples to convert the measurement unit from pixel to mm. The images were then transferred into Adobe Photoshop software for damage region editing (Figure 3.22) before further analysis in Matlab. Programming commands (Figure 3.23) were developed in Matlab in order to remove unwanted particles, detect the damaged edges and calculate the respective areas and perimeters.

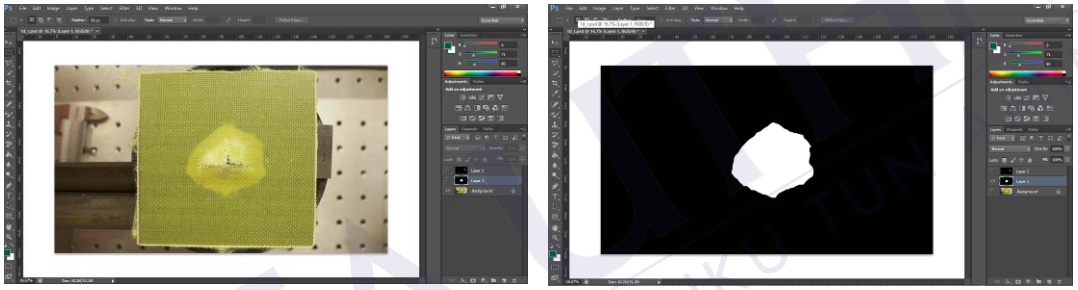

(a) (b)

Figure 3.22: Damage region editing using Adobe Photoshop; (a) original image from digital SLR camera and (b) fractured region filling

c) Morphology analysis using Scanning Electron Microscope (SEM)

Microscopic cross-section investigation by fractography and ultrasonic scanning techniques are the most relevant techniques for post-impact damage evaluation of the textile composite at present (Padaki et al., 2008). The morphology of impact fracture surfaces of the composites was observed by scanning electron microscope (SEM) at room temperature. It was performed using a Hitachi Tabletop Microscope TM-1000 with specified magnification. Gold coating of a few nanometres in thickness coated the impact fracture surfaces. The samples were viewed perpendicularly to the fractured surfaces.

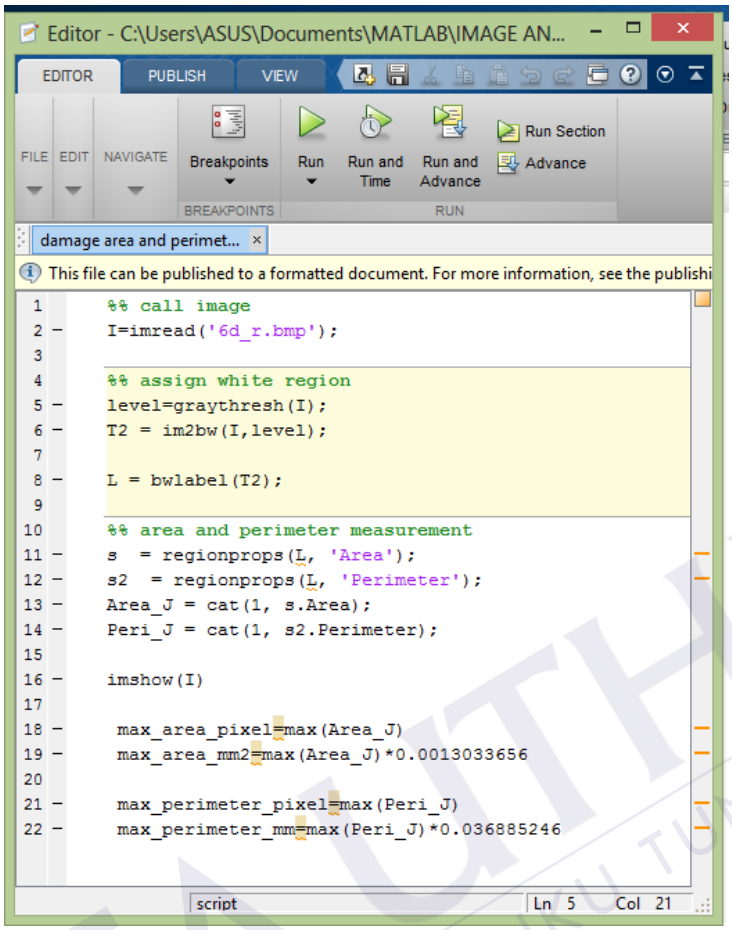

Figure 3.23: Matlab command for the detection of damage region and measurement of damage area and perimeter

3.5 Statistical analysis

Statistical analysis helps to organize data as well as highlighting the weak and strong points in a research. Besides summarizing the data, statistical analysis is a descriptive method that shares and manipulates variables if the experiments has to be repeated with the aim of improving the specifications of the samples or product. The advantage of this method is that it can be used to determine the relationship between the research variables, as well as a basis for prediction. In this research, Minitab R.14 software was used for statistical analysis.

3.5.1 Analysis of variance (ANOVA)

ANOVA was employed to analyse whether there is any significant difference between group (level) means and their associated procedures (such as "variation" among and between groups). ANOVA also pointed out the most significant group that predominantly influenced the response. A p-value of less than 0.05 indicates that there are differences among the means at 0.05 level of significance. From ANOVA analysis, grouping information using Tukey's Group Range Test (TGRT) was used to find means that are significantly different from each other in a group. On the other hand, R^2 (r-squared) or coefficient of determination indicates how well data points fit a line or curve. It provides a measure of how well the observed outcomes are replicated by the model in term of the proportion of the total variation of outcomes explained by the model. Moreover, the normal probability plot is a graphical technique for normality testing. Its function is to assess whether or not a data set is approximately normally distributed.

3.5.2 Factorial design analysis

Factorial design is one of the most effective methods in experiments involving the study of the effects of two or more factors (Montgomery, 2009). A 'factor' is another name for an independent variable. This method is a powerful design of experiments (DOE) method, which provides an efficient and systematic approach to evaluate the main and interaction effects of the studied parameters. This method offers a useful information on the influence of input parameters on response parameters (Reyes et al., 2002). Factorial design includes all possible experimental

trials. Therefore, misleading conclusions can be avoided. In the first place, factors or parameters of study need to be identified, followed by the selection of the levels during which each factor will be examined.

In the present study, the main effects plot was used to observe the change in the response of a system due to the factor (be it quantitative or qualitative) as that factor moves from a low to a high value. For instance, in a factorial design with two factors, there will be two potential main effects. In contrast, interaction effects plot was employed to witness the effect of one factor on the response changes depending on the level of other factors. It is understood that interaction occurred when there are two or more factors interacting with each other and giving effect on the response (Ahmad, 2009).

CHAPTER 4

RESULTS AND DISCUSSION

4.1 Yarn characteristics and properties

The physical and tensile properties of both coir and Kevlar 29 yarns were measured and the average value was displayed in Table 4.1. The linear density value from Table 4.1 shows that the size of coir yarn was bigger than Kevlar. Larger yarns increase the weight and thickness of fabrics. However, it also contribute to higher strength (Collier and Epps, 1999). The man made Kevlar 29 yarns in the present study comes in the form of untwisted structure. In contrast, the coir yarn comes in 2-ply spun twisted in S-direction.

Table 4.1: Physical and tensile properties of coir and Kevlar 29 yarns

Properties	Coir Yarn	Kevlar 29
Diameter (mm)	1.5	0.5
Linear density (Tex)	923	110
Twist type	2-ply spun	-
Twist direction	S	-
Tensile maximum load (N)	84	98
Tensile strength at break (MPa)	47	497
Tensile modulus of elasticity (GPa)	3.3	33.1
Tensile strain at break (%)	3.3	2.3

The table also shows that Kevlar 29 yarn outperformed coir yarn tremendously in tensile properties. The average tensile strength of coir and Kevlar 29 yarns was 47 MPa and 497 MPa, respectively. The tensile modulus of both yarns also differed greatly where coir yarn exhibited 3.3 GPa, while Kevlar 29 showed 33.1 GPa on average. Nevertheless, the tensile strain at break for coir yarn was

slightly higher with an average value of 3.3%, whereas it was 2.3% for Kevlar 29. Kevlar is prized for their high tensile properties due to the long chain-like molecule known as polymer, which consists of repeating units called the monomers (Yang, 1991). Polymers for a synthetic type of yarns like Kevlar 29 do not occur naturally, but it was produced in the laboratory or a chemical plant. Although yarns from natural fibre consist of polymers, they are actually a biologically-produced compound that cannot be modified.

4.2 Fabric characteristic

Proper selection of fabric structure is crucial in order to ensure good properties of final products. Table 4.2 displays the physical characteristic of the woven (Type 1 and Type 2), cross-ply and angle-ply coir fabric produced as well as the purchased woven Kevlar 29. The calculations for crimp percent, weft crimp wavelength and inter-yarn fabric porosity are only relevant for woven structure. The result shows that the crimp percent of the woven fabric structure was low (< 20 crimp%),which is an advantage as higher crimp results in the deterioration of mechanical properties (Lim et al., 2012). Moreover, inter-yarn fabric porosity has an effect on the penetrability through the thickness matrix. Appropriate woven porosity allows good penetration of the matrix through the woven fabric structure (Cay et al., 2007).

As shown in Table 4.2, for woven coir fabrics, shorter weft crimp wavelength was obtained by weaving the Type 2 fibre, which resulted in greater crimp percent than in Type 1. This condition correlated well since Type 2 weft yarns need to

interlace more warp yarns in a fabric plane. This justifies the fact that fewer weft yarns are obtained for Type 2 because of the tight interweave structure, which restricts the insertion of more weft yarns. The results are in accordance with the finding by Peled et al. (1998), whereby woven fabric density influences yarn wavelength. However, contrary to the present result, they found that increasing the weft density decreases the wavelength. This is understandable because warp density was not constant in this study. If warp density was constant, the distance between two identical points of waveform will get closer with the increasing of weft yarn, resulted to the decreased in weft crimp wavelength.

Table 4.2: Characteristics of coir fabric and Kevlar 29 fabric

Characteristic	Coir				Woven Kevlar 29
	Woven Type 1	Woven Type 2	Cross-ply	Angle-ply	
Thickness, t (mm)	4.0	2.7	3.2	3.2	0.3
Weight (g/m^2)	1039	1020	930	950	200
Warp density (warp/10mm)	1	2	6	6	9
Weft density (weft/10mm)	18	11			9
Crimp percent, k (%)	2	5	-	-	1.25
Weft crimp wavelength, λ (mm)	20	10	-	-	2.5
Inter-yarn fabric porosity, ε	0.35	0.10	-	-	0

4.3 Composite properties

In this section, impact response and damage assessment of coir composites were first evaluated. The evaluation included observations on the effects of different laminated coir structure on the composites, the effects of different composite manufacturing methods, and finally, the effects of woven fabrics modifications and

woven fabric density on the composites' impact behaviour. Once the optimum properties of the coir composites were obtained, the next evaluation proceeded. The next evaluation involved studying impact response and damage assessment of the hybrid (coir/Kevlar) component, which covered the analysis of the effects of hybrid composites laminate stacking sequence and the effects of different impact incident rate.

4.3.1 Coir-epoxy composites

4.3.1.1 Effects of laminated textile structure on impact response of coir-epoxy composites

Three types of composites with different reinforcement structure as indicated in Section 3.3.1 were fabricated by vacuum bagging method. The average characteristic of samples with different reinforcement structure is illustrated in Table 4.3. From the Table, it shows that the average thickness for CPC was the highest, followed by WC and APC. On the other hand, the average areal density value for all composite types showed minor difference. APC perhaps possessed a little rise in areal density due to higher matrix content caused by the slight disorientation during structure fabrication. Fabric disorientation results in higher porosity of the reinforcement structure, which promotes matrix penetration. The differences in the areal density and thickness of the composites were attributed to the capability of resin impregnation to the fibres, as different reinforcement structure gives different interfacial compatibility and adhesion. This condition will be discussed further in Section 4.3.1.1 (b).

Table 4.3: Characteristic of samples with different reinforcement structures

Composite type	Average thickness (mm)	Average areal density (g/m^2)
WC	3.9	2500
CPC	4.4	2500
APC	3.6	2700

a) Impact behaviour

The load versus displacement plot and energy absorbed versus time plot of the composite with different reinforcement structures are shown in Figure 4.1. Each curve demonstrates the representation of each sample that was closed to the mean value. It is evident from Figure 4.1 (a) that there was a significant change in load-displacement response for different laminated textile structure. It can be noticed from Figure 4.1 (a) that there were multiple broad peaks for APC structure. Unlike WC and CPC, fewer peaks were seen on the curve. The first peak, usually, indicates the initial failure. The sudden load drop after the first peak can be explained as an immediate transition of the specimen from an unharmed state to damaged state (Zhang et al., 2013). In this case, the failure might be due to bad delamination. The second and the following peaks denoting crack growth from the initial failure as supported in Dhakal et al. (2012). A combination of matrix crack and fibre break was expected to occur on samples at this particular stage. In the initial part of the curve, APC shows the steepest curve, followed by WC and CPC. More load oscillations in APC was expected due to the expansion of damage, which resulted in the reduction of the composite stiffness. The oscillation trend represents a load distribution of the surviving composite until the impact load was fully removed. This shows that APC

exhibited the most brittle structure whereby the load was distributed by a series of damages.

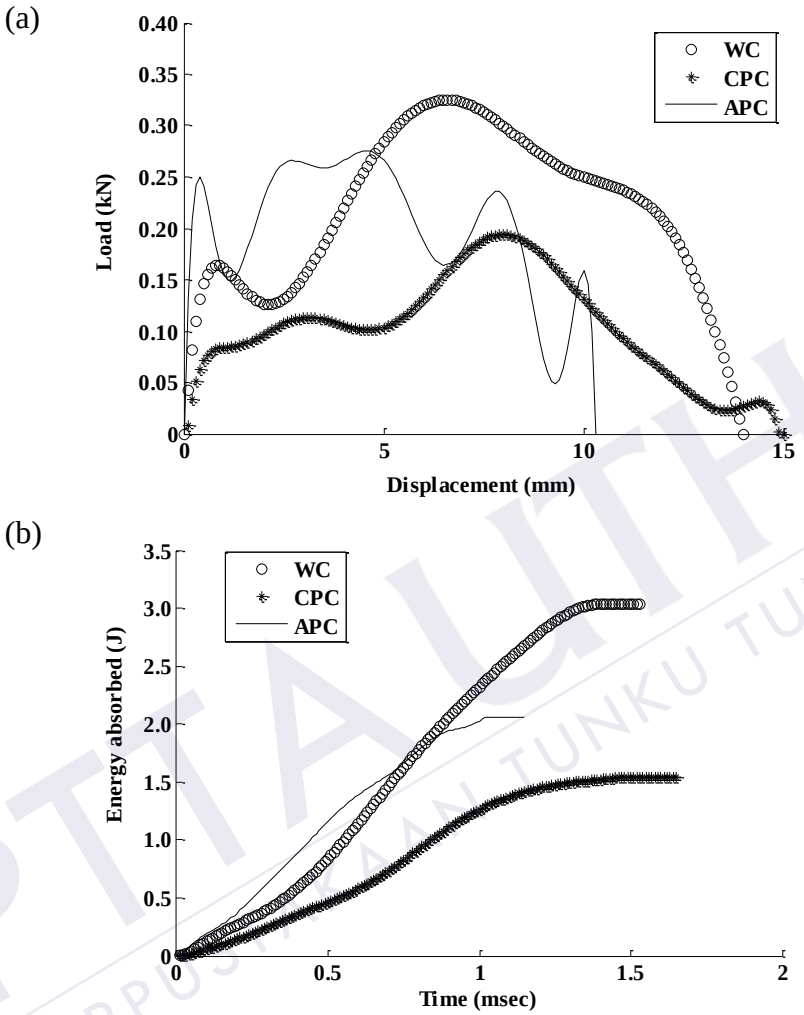

Figure 4.1: (a) Load-displacement curve and (b) energy absorbed-time curve of WC, CPC and APC

The general curve of the CPC is wide around the peak load whereas the WC curve is narrower. These revealed that WC exhibited higher stiffness compared to CPC. These results complement the research by Hosur et al. (2005), where they found that woven structure exhibits excellent resistance to impact damage attributed by the interlacing of fibres in two mutually perpendicular directions. Figure 4.1 (a) for woven coir portrayed evidence that less damage was detected as the WC curve

had fewer fluctuations. The maximum peak load for WC was the highest, followed by APC and CPC. The sudden load decreased after reaching the first peak load as portrayed by WC and CPC samples could be attributed to the critical structural damage. Figure 4.1 (a) also illustrates that the WC and CPC had higher total displacement (more than 14 mm) compared to APC structure.

Figure 4.1 (b) represents the absorbed energy versus time for composites with different reinforcement structures. The absorbed energy of all samples showed an increase with time until the energy became constant at a specific time. It was observed that the total energy absorbed increased from WC, APC and CPC. The contact time between the impactor and sample was found to decrease from CPC, WC and APC. At the very beginning of the curves for WC and CPC, the values of absorbed energy were relatively low, which can be attributed to the small dent and deformation along the thickness direction under the transverse impact load. Conversely, the absorbed energy for APC from the beginning of the curve had a rapid increase, which may suggest a serious fracture or delamination at an earlier stage on APC laminates. The second stage where the energy-time curves started to increase in slope, demonstrates an augment in deflection and internal damages. At this stage, the absorbed energy was mainly due to increased contact area between the impactor and the specimen (Zhang et al., 2013). The final stage of the curve displays that the absorbed energy was maintained at a constant value, reflecting the situation where there is no more impact energy to be absorbed by the specimen as the specimen has been fully penetrated.

For better interpretation of the experimental results, the key impact response including the maximum peak load, displacement at the peak load, total displacement, time at peak load, total time to penetration, energy absorbed to peak load, total energy absorbed, propagation energy, ductility index, specific energy absorbed to peak load, specific total energy absorbed and impact strength for the three types of sample structure are summarized in Table 4.4 and Table 4.5. The superscript letters in the columns indicate the means value grouping. The means grouping were analysed using one-way multiple comparisons Tukey's Group Range Test (TGRT) via analysis of variance (ANOVA). It can be seen from the tables that the means value for each reinforcement structure for the impact response other than the peak load, total energy absorbed, propagation energy and specific total energy absorbed were all dropped under the same mean group, which justifies the hypothesis that the variation of the reinforcement structure only have significant effects on those three responses.

It was difficult to establish any obvious conclusion just by looking at the table. With the help of ANOVA results as displayed in Table 4.6, the effects of the reinforcement structure towards the impact response could be better explained. Table 4.6 highlights that the F-value was high, and the P-value was less than 0.05 for the peak load, propagation energy and specific total energy absorbed (highlighted with bold font). This condition indicates that the reinforcement structure has significant effects only on these key impact responses. The distribution of residuals for those three responses demonstrates a lower degree of data variability with R^2 values of 0.84, 0.72 and 0.72. Therefore, the data obtained from the experiment can be accepted as normal and stable. It is also obvious that the reinforcement structure gave

Table 4.4: Mean scores of impact response of coir composites with different reinforcement structures

Sample type	Peak load (kN)	Displacement at peak load (mm)	Total displacement (mm)	Time at peak load (msec)	Total time (msec)	Energy absorbed to peak load (J)	Total energy absorbed (J)
WC	0.32±0.02[a]	5.67±0.72[a]	15.00±1.25[a]	0.62±0.09[a]	1.64±0.14[a]	1.30±0.07[a]	3.09±0.43[a]
CPC	0.18±0.02[b]	6.47±2.57[a]	14.90±0.85[a]	0.72±0.27[a]	1.65±0.10[a]	0.73±0.32[a]	1.53±0.01[b]
APC	0.31±0.05[a]	6.10±1.80[a]	11.83±2.74[a]	0.68±0.21[a]	1.32±0.32[a]	1.29±0.45[a]	2.28±0.74[ab]

* Means with same superscript letters in column are not significantly different at the (P≥0.05).
* Each result is the average value derived from three replicates

Table 4.5: Mean scores of propagation energy, ductility index, specific energy absorbed and impact strength of coir composites with different reinforcement structures

Sample type	Propagation energy (J)	Ductility index	Specific energy absorbed to peak load (J/kg)	Specific total energy absorbed (J/kg)	Impact strength (kJ/m^2)
WC	1.79±0.36[a]	1.37±0.20[a]	0.51±0.03[a]	1.22±0.17[a]	10.22±0.56[a]
CPC	0.80±0.31[b]	1.52±1.46[a]	0.29±0.13[a]	0.61±0.00[b]	5.76±2.52[a]
APC	0.99±0.32[ab]	0.78±0.16[a]	0.48±0.17[a]	0.85±0.28[ab]	10.13±3.57[a]

* Means with same superscript letters in column are not significantly different at the (P≥0.05).
* Each result is the average value derived from three replicates

the most dominant effects on peak load (highest F-value). On the other hand, the deflection at peak load, total displacement, total time to penetration, ductility index, specific energy absorbed to peak load and impact strength of the WC, CPC and APC were similar to each other (P>0.05).

Table 4.6: ANOVA result of the impact response of coir composites with different reinforcement structures

Source	Df	SS	MS	F	P
(a) Peak load (kN)					
Reinforcement structure	2	0.03522	0.01761	16.04	**0.004**
Error	6	0.00659	0.00110		
Total	8	0.04181			
(b) Total displacement (mm)					
Reinforcement structure	2	19.44	9.72	2.97	0.127
Error	6	19.63	3.27		
Total	8	39.07			
(c) Total time (msec)					
Reinforcement structure	2	0.2049	0.1024	2.36	0.175
Error	6	0.2601	0.0434		
Total	8	0.4650			
(d) Propagation energy (J)					
Reinforcement structure	2	1.657	0.829	7.57	**0.023**
Error	6	0.657	0.110		
Total	8	2.314			
(e) Ductility index					
Reinforcement structure	2	0.919	0.460	0.62	0.567
Error	6	4.422	0.737		
Total	8	5.341			
(f) Specific total energy absorbed (J/kg)					
Reinforcement structure	2	0.5617	0.2809	7.90	**0.021**
Error	6	0.2133	0.0356		
Total	8	0.7750			
(g) Impact strength (kJ/m^2)					
Reinforcement structure	2	38.96	19.48	3.00	0.125
Error	6	39.90	6.48		
Total	8	77.86			

*DF: degree of freedom, SS: sum of squares, MS: mean square, F: F-test and P: P-value

Figure 4.2 illustrates the main effects plots of the most significantly affected responses with various composite reinforcement structures, which were the peak load, propagation energy as well as the specific total energy absorbed.

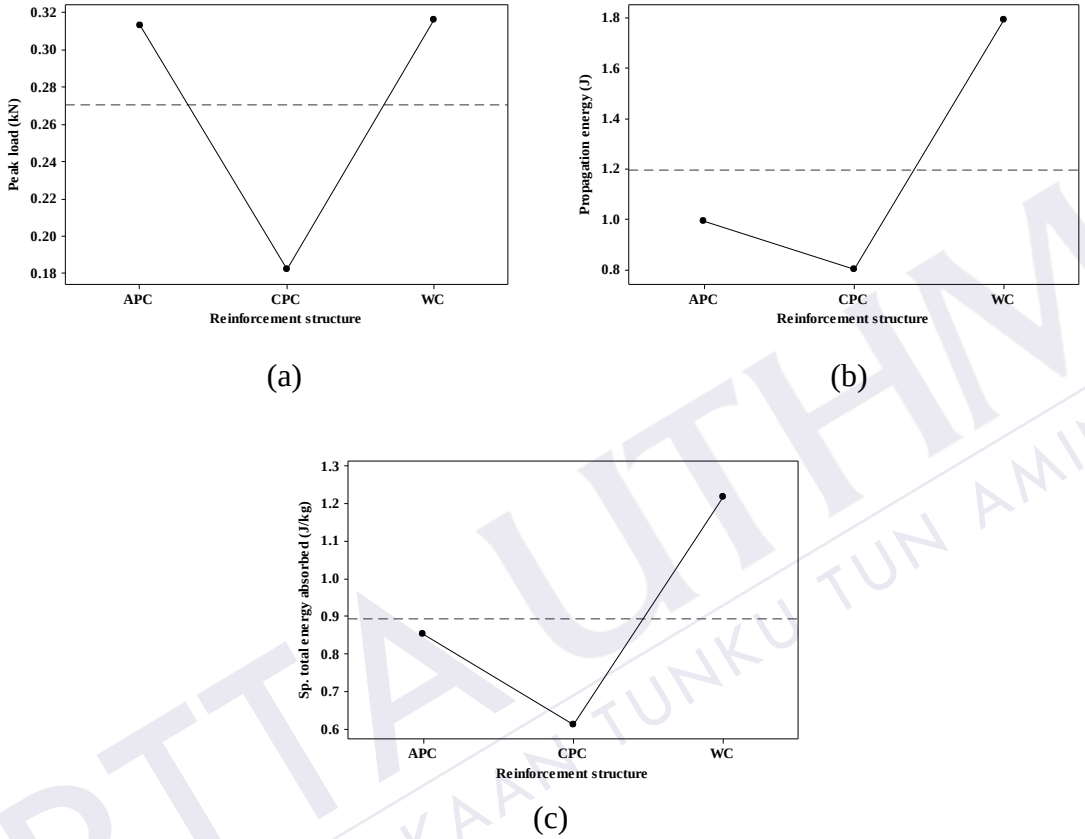

Figure 4.2: Main effects plot of coir composites with different reinforcement structures; (a) peak load, (b) propagation energy and (c) specific total energy absorbed

The CPC structure yielded the lowest value for all three impact responses. WC and APC exhibited almost the same peak load, whereas WC outperformed APC in propagation energy, and the specific total energy absorbed. The results were as expected where woven structure provides structural integrity to the composites to resist higher impact load, thus absorbing greater impact energy. Comparatively, APC indicated greater impact performance compared to CPC. This is probably due to increased number of fibres (fibres that act as load bearing) in APC that have contact

with the impactor or at the critical section (Kaleemulla and Siddeswarappa, 2009). Figure 4.3 illustrates the schematic of load bearing fibres for CPC and APC structures.

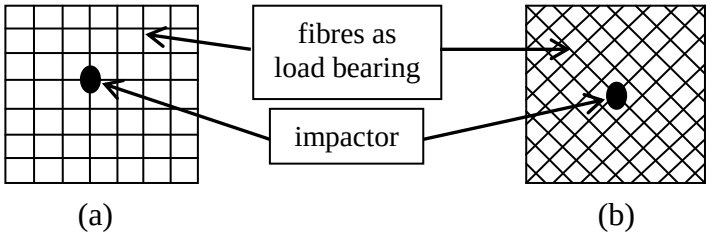

Figure 4.3: Schematic of load bearing fibres for; (a) CPC and (b) APC

b) Damage assessment and morphology analysis

Images of the perforated specimens are given in Figure 4.4. Damages on WC composites were found to be uneven with bigger clean crack hole. Higher energy is needed to break the interlaced yarns before the full penetration takes place on WC specimen. Energy from the impactor dissipates (indicated by the highest energy propagation in WC composites), owing to a wider damage on the composite structure. These observation agrees well with the research by Karakuzu et al. (2010) on continuous glass/epoxy composites. It can also be seen that the damage extended to a wider area in warp direction, which is expected due to the imbalance number of yarns in both warp and weft directions. The direction with higher density (in this case, weft) contributes to better impact resistance as indicated by shorter damage. Low density (in this case, warp) favours crack growth during impact loading, therefore resulting in a longer damage. As for CPC and APC, it was revealed that a smaller fracture area with half broken clusters remained. Easy perforation on CPC and APC was anticipated as the capability to absorb impact energy in both structures is low.

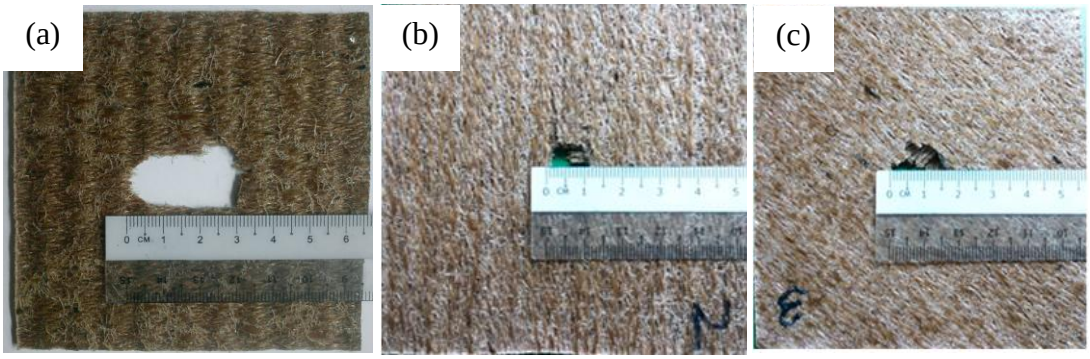

Figure 4.4: Composites fractured image after impact test;
(a) WC, (b) CPC and (c) APC

SEM micrographs of the cross-section of the fractured coir composites surfaces can be seen in Figure 4.5. Figure 4.5 (a) shows the presence of aggregation at the surfaces. The most influential damages on WC samples were matrix crack and fibre breakage. These types of defect are apparent on composite structures due to the direct contact between the specimen and the impactor. As the impactor moves through the thickness of the composites, it pushes the fibres aside, breaking the fibres and the matric failure occurs (Yahaya et al., 2014). Fibre-matrix bonding of WC composite was considerably good as matrix debris was seen covering the fibres. In contrast, both CPC and APC exhibited similar fracture mode. They suffered severe interlayer delamination. Figure 4.5 (b) illustrates the SEM micrograph of fractured CPC sample. SEM image for APC could not be taken because it easily break when cutting. APC structure exhibited very low deformation upon stress as well as obtaining the lowest energy absorbed compared to WC and CPC. These condition denotes that the APC structure was very brittle. Poor interfacial bonding of fibre-matrix was detected on CPC and APC composites as fibres were not adequately covered by matrix. In comparing Figure 4.5 (a) for WC and (b) for CPC, it is clearly seen that matrix was nicely covered around the fibre in WC sample. Whereas, SEM

image for CPC shows that the image of fibres was more prominent and matrix debris was less detected. Yarns on the top and the bottom surfaces were badly split, especially on the impacted area.

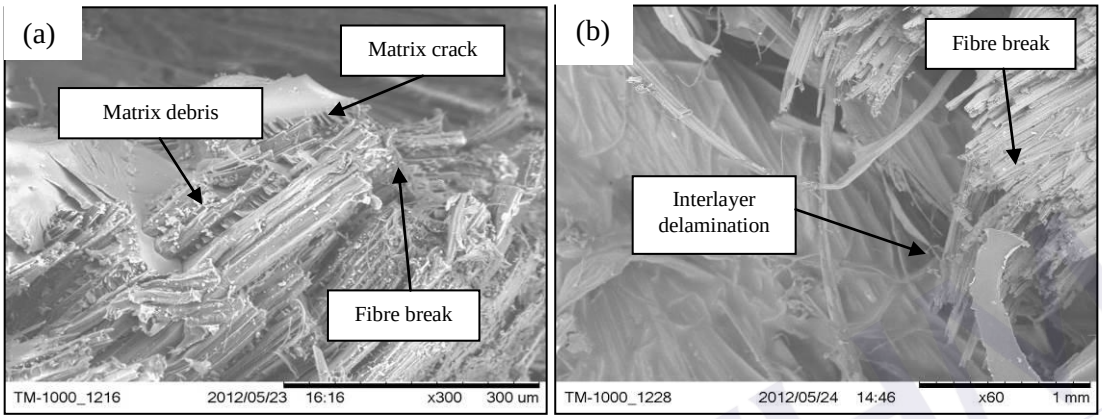

Figure 4.5: SEM of cross-sectional area of; (a) WC and (b) CPC fractured samples

WC was expected to have higher fracture size due to intermingled yarns in the warp and the weft directions. This intersection of fibres creates energy roadblocks, resulting in reduced energy dissipation rate (Heinecke, 2007). As a result, stress is dispersed to a greater area, which initiates crack propagation and enlarging the fracture area. On the other hand, poor interfacial bonding of CPC and APC composite structures made them very weak and fragile structures, which decreased their ability to resist impact as reported in the previous section.

4.3.1.2 Effects of different composite manufacturing methods on impact response of woven coir-epoxy composites

Selecting the composite manufacturing method is important to gain compromise between the time taken, the cost of the manufacturing process and the strength of the material obtained from the process. In this particular section, woven coir composite was fabricated by compression moulding and vacuum bagging as

detailed in Section 3.3.2.2 to investigate its response to penetration impact. The details on the average characteristics of the composite are given in Table 4.7. It was noticed from the table that although the woven coir composite fabricated by compression moulding (CM-WC) was lower in thickness, it obtained higher areal density compared to the composites fabricated by vacuum bagging (VB-WC). This condition was expected due to the effects of fibre-resin compaction in CM-WC composites.

Table 4.7: Characteristic of CM-WC and VB-WC samples

Composite type	Average thickness (mm)	Average areal density (g/m^2)
CM-WC	3.1	3300
VB-WC	3.9	2500

a) Impact behaviour

The representative load versus displacement curve and energy absorbed versus time curve of the composite samples produced using different manufacturing methods are given in Figure 4.6. It is evident from Figure 4.6 (a) that there was a significant change in the load-displacement response for different composite manufacturing processes. CM-WC curve exhibited higher initial slope than that in VB-WC sample, which suggests that CM-WC is stiffer than VB-WC. The trend of the ascending section in both samples was almost the same, except CM-WC had higher peak load of over 0.6 kN. The slight change in slope in the figure explained crack initiations in both samples. Although VB-WC achieved lower peak load, the maximum displacement was higher than that of CM-WC, which shows that VB-WC propagated higher impact energy before the total penetration on the sample.

(a)

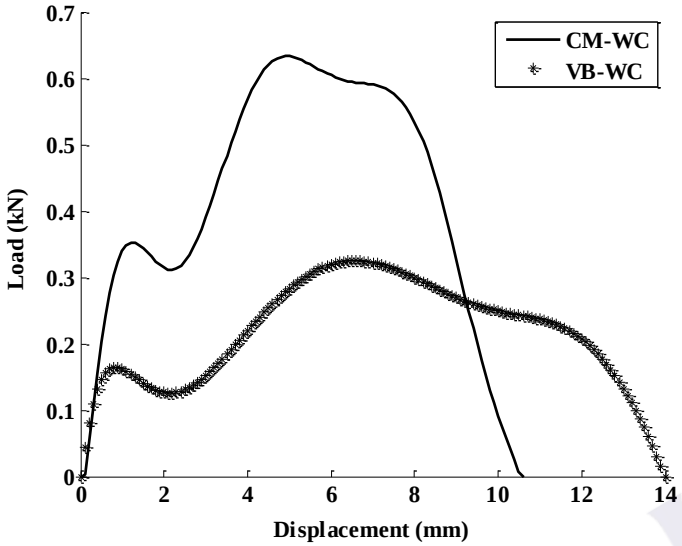

(b)

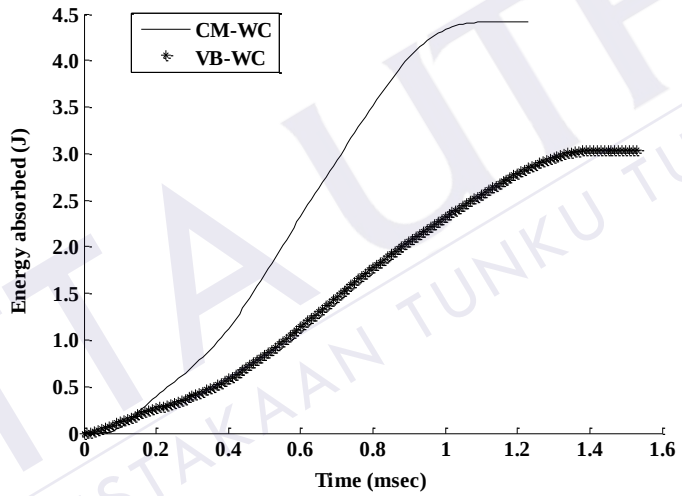

Figure 4.6: (a) Load-displacement curve and (b) energy absorbed-time curve of CM-WC and VB-WC

The steady increment of absorbed energy with time for CM-WC and VB-WC are shown in Figure 4.6 (b). It can be seen that higher absorbed energy was obtained by CM-WC samples, although the time contact between the impactor and the sample was found to decrease as compared to VB-WC. A narrower curve was illustrated by CM-WC, which may indicate greater damages developed in the sample.

Table 4.8 and Table 4.9 summarizes the impact response data for both composites including the maximum peak load, displacement at the peak load, total displacement, time at peak load, total time to penetration, energy absorbed to peak load, total energy absorbed, propagation energy, ductility index, specific energy absorbed to peak load, specific total energy absorbed and impact strength. The data represent the average value and standard deviation for the three repetition tests for each sample. The means grouping using TGRT were analysed and displayed as superscripts in each column. Table 4.8 and Table 4.9 showed an obvious finding as the superscripts for impact responses; displacement, time, propagation energy and ductility index had similar letters. These results indicate that there was no significant effect in the composite manufacturing methods towards those responses. Moreover, for energy absorbed in a sample, if the weight of each sample was accounted, which is designated as the specific energy absorbed, it also demonstrates no significant effects. A similar observation was reported by Sreekumar et al. (2007), where they conducted research on sisal leaf fibre/polyester composites. They found that different composite fabrication methods gives significant effect mainly on strength and modulus of composites, whereas no substantial effect was recorded for elongation percentage.

Table 4.10 highlights the ANOVA results which better illustrate the effects of the composite manufacturing methods on the impact response of coir composites. It was found that the composite manufacturing methods had the most dominant effect on the peak load of coir composites. This was based on the ANOVA results for the peak load, which indicate the highest F-value and a P-value of less than 0.05. Different composite manufacturing methods also contributed to significant effects on

Table 4.8: Mean scores of impact response of coir composites with different composite manufacturing methods

Sample type	Peak load (kN)	Displacement at peak load (mm)	Total displacement (mm)	Time at peak load (msec)	Total time (msec)	Energy absorbed to peak load (J)	Total energy absorbed (J)
CM-WC	0.64±0.05[a]	6.33±0.95[a]	11.97±1.59[a]	0.71±0.11[a]	1.34±0.18[a]	2.66±0.63[a]	4.69±0.55[a]
VB-WC	0.32±0.02[b]	5.67±0.72[a]	15.00±1.25[a]	0.62±0.09[a]	1.64±0.14[a]	1.30±0.07[b]	3.09±0.43[b]

* Means with same superscript letters in column are not significantly different at the (P≥0.05).
* Each result is the average value derived from three replicates

Table 4.9: Mean scores of propagation energy, ductility index, specific energy absorbed and impact strength of coir composites with different composite manufacturing methods

Sample type	Propagation energy (J)	Ductility index	Specific energy absorbed to peak load (J/kg)	Specific total energy absorbed (J/kg)	Impact strength (kJ/m^2)
CM-WC	2.02±0.72[a]	0.82±0.44[a]	0.80±0.19[a]	1.40±0.17[a]	20.97±4.95[a]
VB-WC	1.79±0.36[a]	1.37±0.20[a]	0.51±0.03[a]	1.22±0.17[a]	10.22±0.56[b]

* Means with same superscript letters in column are not significantly different at the (P≥0.05).
* Each result is the average value derived from three replicates

the impact strength of the coir composites as the P-value was less than 0.05. The results can be claimed as stable as the degree of data variability (R-square) was considered high (0.96 and 0.78) for both impact responses.

Table 4.10: ANOVA result of the impact response of coir composites with different composite manufacturing methods

Source	Df	SS	MS	F	P
(a) Peak load (kN)					
Manufacturing method	1	0.15682	0.15682	105.44	**0.001**
Error	4	0.00595	0.00149		
Total	5	0.16277			
(b) Total displacement (mm)					
Manufacturing method	1	13.80	13.80	6.76	0.060
Error	4	8.17	2.04		
Total	5	21.97			
(c) Total time (msec)					
Manufacturing method	1	0.1320	0.1320	5.05	0.088
Error	4	0.1045	0.0261		
Total	5	0.2365			
(d) Propagation energy (J)					
Manufacturing method	1	0.081	0.081	0.25	0.645
Error	4	1.304	0.326		
Total	5	1.384			
(e) Ductility index					
Manufacturing method	1	0.451	0.451	3.84	0.122
Error	4	0.470	0.118		
Total	5	0.922			
(f) Specific total energy absorbed (J/kg)					
Manufacturing method	1	0.0506	0.0506	1.80	0.251
Error	4	0.1125	0.0281		
Total	5	0.1632			
(g) Impact strength (kJ/m^2)					
Manufacturing method	1	173.4	173.4	13.99	**0.020**
Error	4	49.6	12.4		
Total	5	222.9			

*DF: degree of freedom, SS: sum of squares, MS: mean square, F: F-test and P: P-value

The main effects plots of the two most significant responses (peak load and impact strength) are given in Figure 4.7. Coir composites fabricated by the compression moulding method (CM-WC) was found to give a significant increase on peak load and impact strength. Peak load in CM-WC increased by almost 100% compared to VB-WC. On the other hand, a difference of about 50% was distinguished for impact strength. The toughness of the materials determines the amount of energy that can be absorbed (David et al., 2009). The toughness of CM-WC composite proved that it was able to resist a higher impact load, thus providing a strong impact resistance.

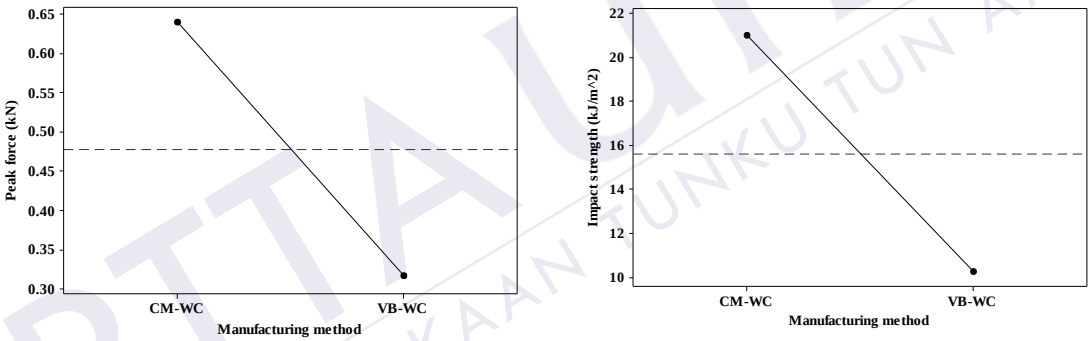

(a) (b)

Figure 4.7: Main effects plot of coir composites with different composite manufacturing methods; (a) peak load and (b) impact strength of CM-WC and VB-WC samples

b) Damage assessment and morphology analysis

Figure 4.8 represents the fracture area (front and rear surfaces) of the composite samples measured by an image processing technique. The results were based on the average of the three samples. It was noticed that the fracture area of CM-WC was slightly larger than VB-WC on both sides. The rear surface of the impacted composites also showed larger area of damage than the front surface.

However, the differences were found to be insignificant as indicated by the standard deviation error bar.

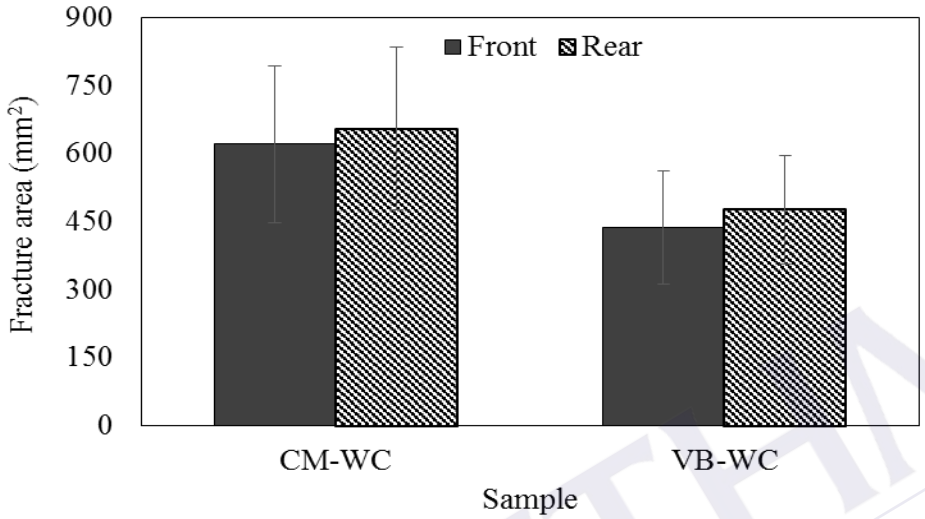

Figure 4.8: Fractured area (front and rear surface) of CM-WC and VB-WC

Figure 4.9 represents the scanned image of the fractured composite structures. It can be seen that the damage extended to a wider area in weft direction. This was expected due to the imbalanced number of yarns in the warp and the weft directions. More yarns in the weft direction helped to prevent the crack from propagating to a larger area in the warp direction. The composite manufactured by the VB process is found to result in markedly higher fibre content. It is agreed that different methods of sample preparation can cause a difference in fibre concentrations. In the VB process, the vacuum pressure concentrated the laminate and reduced the matrix content. However, fibre content does not necessarily lead to higher impact performance as the matrix composition and the bond between fibres and matrix also govern the composite properties (Behr et al., 2000). Increasing amount of fibre content may cause the reduction of the amount of matrix filling the gap between fibres and plies which eventually cause poor toughness of the samples (Ho and Lau, 2012). A better

way to observe and explain fibre-matrix adhesion and failure mechanism is through SEM observation.

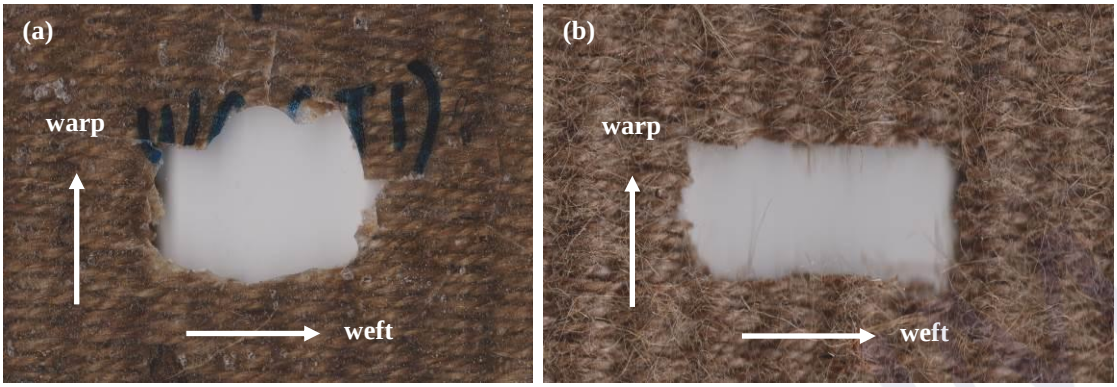

Figure 4.9: Scanned image of fractured composites; (a) CM-WC and (b) VB-WC

SEM images of the top surface and the cross-sectional area of the fracture are displayed in Figure 4.10. It was clearly observed that CM composite samples exhibited better fibre-matrix adhesion, as the matrix covered the fibres (Figure 4.10 (a)). The fibre surface was cleaner in Figure 4.10 (b), indicating poor adhesion between coir and epoxy resin. Findings from the image explain why composites with higher fibre content are not better mechanically, as the impregnation of fibres with matrix polymer plays an important factor. It is agreed that by improving the adhesion characteristic, surface tension and surface roughness increase, resulting in improved mechanical properties (Faruk et al., 2012; Wan et al., 2000). Compaction of the fabric laminate plies in the composite triggers the consolidation phase of the fabrication process. Besides improving adhesion characteristics, compaction causes reduced voids between individual plies, resulting in superior mechanical behaviour.

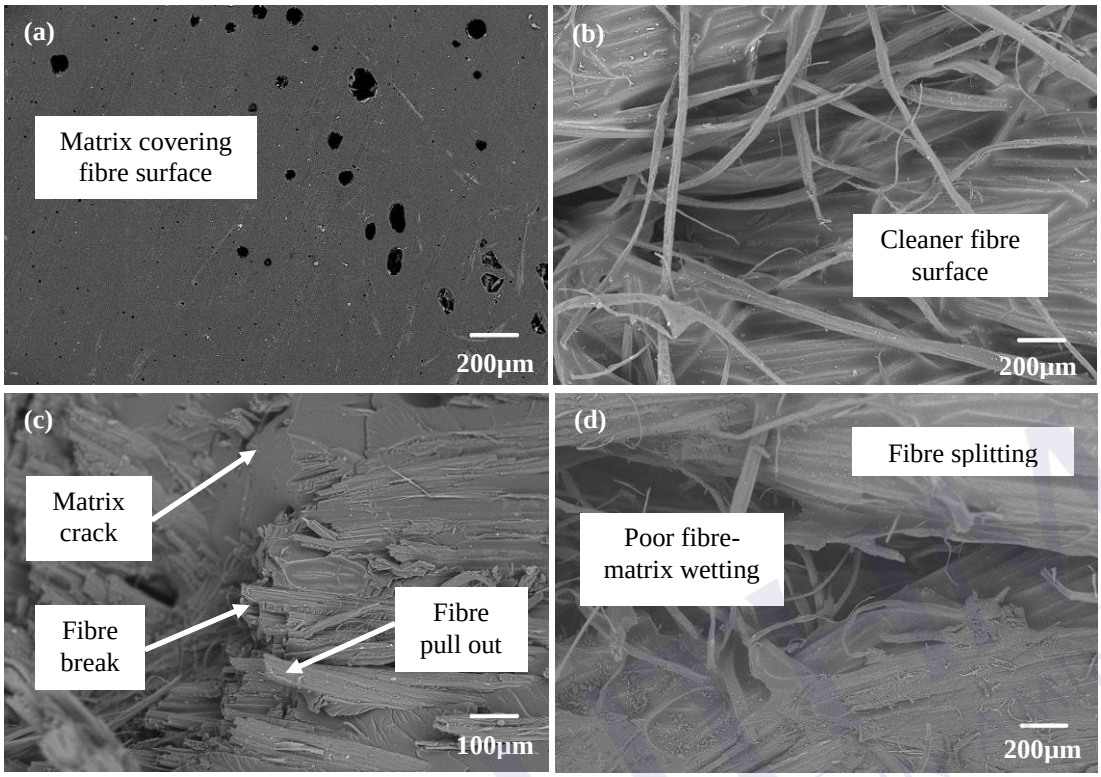

Figure 4.10: SEM images of; (a) top surface of CM, (b) top surface of VB, (c) fractured area of CM and (d) fractured area of VB

The predominant failure modes of CM composites were found to be fibre breakage, matrix cracking and fibre pull-out, as illustrated in Figure 4.10 (c). Both the matrix and the reinforcement act to resist impact, dissipate the impact energy and delay perforation of fractures as they have good bonding performance. The impact energy also dissipates via fractures and debonding of the reinforcement. Hence, bigger fractures contribute to better energy absorption. The method of resisting impact and dissipating energy shows contrasting results in VB composite samples. Substantial fibre splitting or fibrillation is observed in Figure 4.10 (d), which indicates poor wetting between the fibres and the matrix. Higher fibre content was seen in VB composites. Fibrillation was also apparent due to severe contact pressure between the fibre plies. This phenomenon can reduce the strength of the composite sample. With high fibre content, fibre agglomeration takes place. When impact is

applied on the composite, the load will be distributed unevenly between non-agglomerated and agglomerated fibres and the impact energy is absorbed mainly by the fibre (Sreekumar et al., 2007). A decrease in energy transfer from the fibre to the matrix will occur due to fibre agglomeration and an increase in fibre-to-fibre contact as less resin was found in the composite system (Idicula et al., 2005).

4.3.1.3 Effects of woven fabric modification and structure density on impact response of coir-epoxy composites

Woven coir was fabricated in two different woven densities and treated in four different NaOH solution percentages to observe the effects on impact performance. The average characteristic of the samples is depicted in Table 4.11. It was noted that the thickness of the samples and the areal density increased with increasing treatment percentage. Moreover, comparatively, Type 2 composite structure demonstrated lower thickness and areal density compared to Type 1 composite structure. The differences between Type 1 and Type 2 composites are shown in Section 3.3.1.1.

Table 4.11: Characteristic of samples with different treatment percentages and woven densities

Composite type	Average thickness (mm)	Average areal density (g/m^2)
WCT1-0	3.2	3300
WCT1-6	3.4	3400
WCT1-9	3.1	3400
WCT1-12	3.6	3800
WCT2-0	2.6	2800
WCT2-6	2.9	3100
WCT2-9	3.0	3100
WCT2-12	3.4	3500

a) Impact behaviour

Figure 4.11 (a) and (b) depict the load versus displacement curve and the energy absorbed versus time curve of woven coir (WC) with different woven densities and treatment percentages. Figure 4.11 (a) shows that there was a significant change in the load-displacement response for composites of different combination of woven densities and treatment percentages. For all of the samples, the load-displacement curves portrayed a very minimal amount of elastic energy stored, whereas most of the input energy was dissipated through plastic deformation. It can be noticed from Figure 4.11 (a) that almost all curves showed a relatively high load oscillation. The trends represented damage initiation in the laminate materials as the load increased until the impact load was fully removed. It could also be seen that the highest peak load was accomplished by the WCT1-6 sample followed by WCT1-12, WCT2-6 and WCT2-12.

Moreover, the peak load for Type 1 woven composites was found to be greater than that of Type 2 composites for all different treatment percentages. Woven composite samples with Type 1 density were found to display stiffer structures as the curves were narrower compared to Type 2 structures. The curves of Type 2 woven structure were found to be wider with higher displacement. On the other hand, the effects of woven treatment percentage on both woven composites Type 1 and 2 showed compliment, where the untreated composite exhibited the lowest impact load before it rose drastically as it been treated with 6% NaOH. However, the load trend decreased at 9% treatment and improved again at 12% treatment. The displacement for all samples scattered between 9 to almost 14 mm with WCT2-6 demonstrating the highest displacement, while WCT1-12 the lowest.

(a)

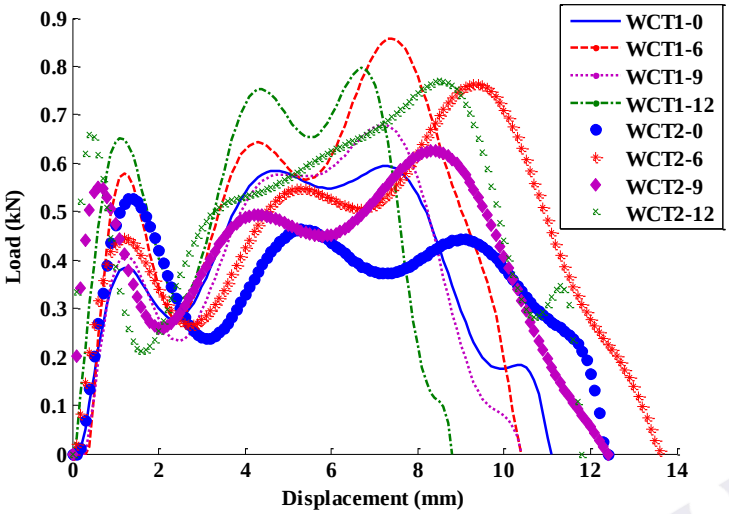

(b)

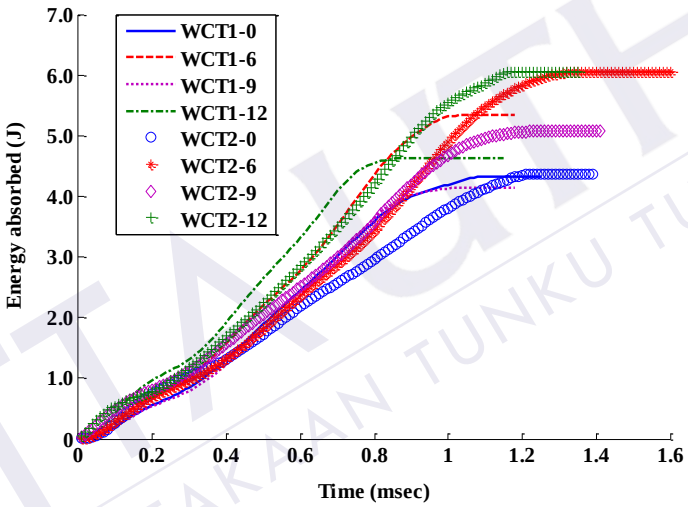

Figure 4.11: (a) Load-displacement curve and (b) energy absorbed-time curve of woven coir with different woven densities and treatment percentages

Figure 4.11 (b) clearly indicates that treating woven coir fabric structure helps to improve energy absorption in the composite materials. The energy absorbed for samples WCT2 treated with 6 and 12 percent of NaOH was found to achieve the highest energy absorbed. WCT1-6 was nearly approaching the maximum energy absorbed by both samples. Moreover, as expected, untreated woven composite structure for both woven density types had the lowest energy absorption. As a whole, it can be seen that the density for Type 2 composites demonstrated better energy

absorbed compared to that of Type 1 for all treatment percentages. As referred to Figure 4.11 (a), most of the samples of Type 2 density could prolong damage propagation in the laminate before the impact load was fully removed. The area under the load-displacement curve of woven Type 2 was larger compared to Type 1 structure. Therefore, the energy absorbed would be higher. This condition indicates that Type 2 woven composites are a tougher material, where greater amount of energy is needed to break it.

As discussed in Section 3.4.3.3, the details of the impact response can be extracted from the load-displacement curve to better interpret the results. The impact response data were entered into the factorial design table in Minitab software for further analysis. The responses include the maximum peak load, displacement at the peak load, total displacement, time at peak load, total time to penetration, energy absorbed to peak load, total energy absorbed, propagation energy, ductility index, specific energy absorbed to peak load, specific total energy absorbed and impact strength are summarized in Table 4.12 and Table 4.13. Here, the average of the three tested samples was taken. It was difficult to establish any obvious conclusion just by looking at the table. With the help of factorial ANOVA in Table 4.14, the effects of woven density and treatment towards impact response could be better explained.

Factorial ANOVA helps to study the effects of each factor (woven density and treatment percentage) as well as provides an insight into the factors dependence and independence. Based on the corresponding F-values and P-values, it was seen that the woven density parameter effect was significant on the maximum peak load, total displacement, total time to penetrate, propagation energy and specific total

energy absorbed. On the other hand, the other parameter (treatment percentage) provided a significant effect towards maximum peak load, propagation energy, ductility index, specific total energy absorbed and impact strength. Hence, the main effects plots for those parameters are displayed in Figure 4.12 to visualize the effect. On the contrary, it was noted that the effects of woven density on impact strength was comparatively negligible as the P-value was too high.

It should also be noted from Table 4.14 that the interaction effects between woven density and treatment percentage was present on the total displacement, specific total energy absorbed and impact strength, which implies that the setting of woven density structure in the material should also take into account the volume of treatment percentage allowed due to their significant combined effects. Figure 4.13 displays the interaction plot of the responses involved.

It is observed from Figure 4.12 (a) that a greater maximum peak load was achieved by woven Type 1 density composite, which was expected due to higher crimp formation by Type 2 density. The crimping of yarns/fibres may provide the required mechanical anchoring as claimed by Peled et al. (1998). Higher crimp means higher intersections between yarns on the fabric structure. As tensile loading forms on the yarns induced by the transverse puncture load, the energy "roadblocks" are created at these intersection of yarns, which reduces the maximum load that it can obtain (Heinecke, 2007).

Meanwhile, it was noticeable that Type 2 woven composite structure promoted better maximum displacement and longer duration before it was fully

Table 4.12: Mean scores of impact response of coir composites with different woven densities and treatment percentages

Sample type	Peak load (kN)	Displacement at peak load (mm)	Total displacement (mm)	Time at peak load (msec)	Total time (msec)	Energy absorbed to peak load (J)	Total energy absorbed (J)
WCT1-0	0.64 ± 0.05^{abc}	6.33 ± 0.95^{bc}	11.97 ± 1.59^{b}	0.71 ± 0.11^{bc}	1.34 ± 0.18^{b}	2.66 ± 0.63^{bc}	4.69 ± 0.55^{b}
WCT1-6	0.77 ± 0.13^{ab}	7.63 ± 0.87^{ab}	10.57 ± 0.29^{b}	0.87 ± 0.10^{ab}	1.20 ± 0.03^{b}	3.99 ± 0.26^{ab}	5.37 ± 0.18^{b}
WCT1-9	0.66 ± 0.02^{abc}	6.00 ± 1.06^{bc}	11.67 ± 3.67^{b}	0.57 ± 0.28^{bc}	1.32 ± 0.41^{b}	2.73 ± 0.30^{bc}	4.36 ± 0.59^{b}
WCT1-12	0.85 ± 0.12^{a}	7.47 ± 0.47^{ab}	10.13 ± 0.45^{b}	0.85 ± 0.06^{abc}	1.15 ± 0.05^{b}	4.02 ± 0.25^{ab}	5.33 ± 0.74^{b}
WCT2-0	0.51 ± 0.05^{c}	2.70 ± 3.06^{c}	12.73 ± 1.04^{ab}	0.31 ± 0.35^{c}	1.43 ± 0.12^{ab}	0.78 ± 0.84^{c}	4.08 ± 0.26^{b}
WCT2-6	0.72 ± 0.06^{abc}	11.33 ± 2.00^{a}	18.50 ± 4.03^{a}	1.28 ± 0.23^{a}	2.10 ± 0.46^{a}	5.22 ± 1.44^{a}	7.90 ± 1.90^{a}
WCT2-9	0.59 ± 0.10^{bc}	9.33 ± 2.06^{ab}	13.37 ± 2.03^{ab}	0.93 ± 0.03^{ab}	1.52 ± 0.24^{ab}	3.62 ± 0.37^{ab}	4.96 ± 0.09^{b}
WCT2-12	0.78 ± 0.01^{ab}	8.13 ± 1.10^{ab}	11.70 ± 1.55^{b}	0.93 ± 0.13^{ab}	1.34 ± 0.18^{b}	4.30 ± 0.60^{ab}	5.98 ± 0.65^{ab}

* Means with same superscript letters in column are not significantly different at the ($P\geq0.05$).
* Each result is the average value derived from three replicates

penetrated, as well as better energy propagation and specific total energy absorbed. Displacement or deformation of a structure under loading is closely related to its stiffness. A small deformation region has great stiffness. The load-displacement curve in Figure 4.11 (a) indicates that woven composite structure T1 exhibited higher stiffness as the curve had steeper inclination in its elastic phase. Higher load levels on Type 1 woven composite might also cause badly degraded internal structure, which leads to minimal deformation. Higher deformation in Type 2 woven composite allows more time for energy propagation. Therefore, an increase in energy propagation was observed for Woven composite Type 2 structure. A specific energy absorption was also expected to increase as more structural area can be covered in longer duration.

Table 4.13: Mean scores of propagation energy, ductility index, specific energy absorbed and impact strength of coir composites with different woven densities and treatment percentages

Sample type	Propagation energy (J)	Ductility index	Sp. energy absorbed to peak load (J/kg)	Total specific energy absorbed (J/kg)	Impact strength (kJ/m^2)
WCT1-0	2.02 ± 0.72^{ab}	0.82 ± 0.44^{b}	0.81 ± 0.19^{bc}	1.42 ± 0.17^{b}	20.97 ± 4.95^{bc}
WCT1-6	1.38 ± 0.39^{b}	0.35 ± 0.11^{b}	1.17 ± 0.08^{ab}	1.58 ± 0.05^{b}	31.42 ± 2.01^{ab}
WCT1-9	1.63 ± 0.79^{ab}	0.62 ± 0.35^{b}	0.80 ± 0.09^{bc}	1.28 ± 0.17^{b}	21.53 ± 2.40^{bc}
WCT1-12	1.32 ± 0.49^{b}	0.32 ± 0.10^{b}	1.06 ± 0.07^{ab}	1.40 ± 0.19^{b}	31.62 ± 1.96^{ab}
WCT2-0	3.29 ± 0.92^{a}	9.97 ± 8.87^{a}	0.28 ± 0.30^{c}	1.46 ± 0.09^{b}	6.16 ± 6.59^{c}
WCT2-6	2.68 ± 0.82^{ab}	0.53 ± 0.19^{b}	1.68 ± 0.46^{a}	2.55 ± 0.61^{a}	41.11 ± 11.34^{a}
WCT2-9	1.34 ± 0.34^{b}	0.38 ± 0.14^{b}	1.17 ± 0.12^{ab}	1.60 ± 0.03^{b}	28.51 ± 2.88^{ab}
WCT2-12	1.69 ± 0.16^{ab}	0.40 ± 0.07^{b}	1.23 ± 0.17^{ab}	1.71 ± 0.19^{b}	33.83 ± 4.76^{ab}

* Means with same superscript letters in column are not significantly different at the ($P\geq0.05$).
* Each result is the average value derived from three replicates

Table 4.14: Factorial ANOVA result of the impact response of coir composites with different woven densities and treatment percentages

Source	Df	SS	MS	F	P
(a) Peak load (kN)					
Woven density	1	0.040156	0.040156	6.44	**0.022**
Treatment %	3	0.215907	0.071969	11.54	**0.000**
Woven density*treatment %	3	0.005808	0.001936	0.31	0.818
Error	16	0.099769	0.006236		
Total	23				
(b) Total displacement (mm)					
Woven density	1	53.7	53.7	10.72	**0.005**
Treatment %	3	39.835	13.278	2.65	0.084
Woven density*treatment %	3	49.605	16.535	3.3	**0.047**
Error	16	80.18	5.011		
Total	23				
(c) Total time (msec)					
Woven density	1	0.7107	0.7107	10.88	**0.005**
Treatment %	3	0.50981	0.16994	2.6	0.088
Woven density*treatment %	3	0.62871	0.20957	3.21	0.051
Error	16	1.04493	0.06531		
Total	23				
(d) Propagation energy (J)					
Woven density	1	2.6591	2.6591	6.64	**0.020**
Treatment %	3	5.5193	1.8398	4.6	**0.017**
Woven density*treatment %	3	2.647	0.8823	2.2	0.127
Error	16	6.4029	0.4002		
Total	23				
(e) Ductility index					
Woven density	1	31.447	31.4473	3.18	0.093
Treatment %	3	110.899	36.9664	3.74	**0.033**
Woven density*treatment %	3	94.043	31.3477	3.17	0.053
Error	16	158.089	9.885		
Total	23	394.478			
(f) Specific total energy absorbed (J/kg)					
Woven density	1	0.99764	0.99764	15.43	**0.001**
Treatment %	3	1.59353	0.53118	8.22	**0.002**
Woven density*treatment %	3	0.71158	0.23719	3.67	**0.035**
Error	16	1.03437	0.06465		
Total	23				
(g) Impact strength (kJ/m^2)					
Woven density	1	6.21	6.21	0.21	0.656
Treatment %	3	1817.8	605.93	20.11	**0.000**
Woven density*treatment %	3	544.34	181.45	6.02	**0.006**
Error	16	482.1	30.13		
Total	23				

*DF: degree of freedom, SS: sum of squares, MS: mean square, F: F-test and P: P-value

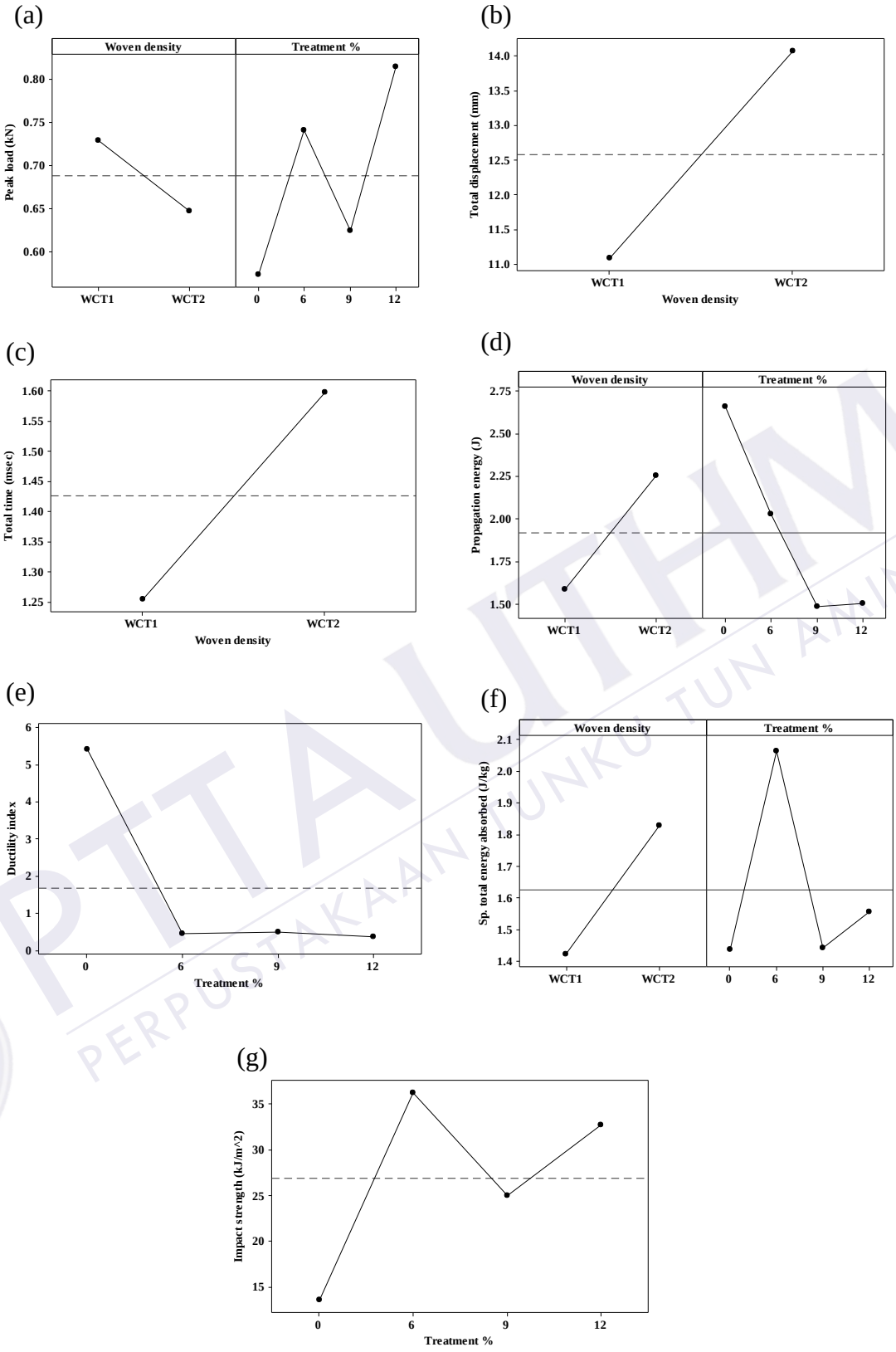

Figure 4.12: Main effects plot of impact response of coir composites with different woven densities and treatment percentages

The findings from the main effects plot of the treatment percentage parameter in Figure 4.12 show that there was a critical amount of treatment percentage beyond which the composite will lose its impact performance. It was clearly seen that the maximum peak load, specific energy absorbed and impact strength of woven composites treated by 6% NaOH solutions escalated their performances. However, for 9% NaOH treatment, the performances dropped before increasing again at 12% NaOH concentration. The performance trends up to 9% NaOH concentration was accordance with previous research conducted on coir composite. Karthikeyan and Balamurugan (2012) reported that the impact strength of coir/epoxy composite improved significantly for 6% alkali concentrations, but gradual decrease in impact strength was observed for 8% and 10%. In addition, declining tensile properties was also observed in the research by Rout et al. (2001) on coir/polyester composite for NaOH concentrations of more than 5%.

Alkaline treatment imparts surface modification on coir. Surface roughness of NF is increased by the disruption of hydrogen bonding in the network structure of the fibre. Increased surface roughness results in better mechanical interlocking of fibres. Also, treatment can remove certain amount of lignin, wax and oils covering the external surface of the fibre cell wall, thereby improving the fibre-matrix interfacial bonding. The performance reduction of woven coir composite occurs primarily because of excessive alkali concentration (Li et al., 2007). Higher concentrations of NaOH may swell the rate of hemicellulose dissolution and finally lead to strength deterioration (Rashed et al., 2006). In this study, 6% NaOH concentration was found to be a reasonable treatment percentage for woven coir/epoxy composite.

The unusual phenomenon of 12% NaOH treatment concentration was probably owed to geometry changes. Woven coir composite treated by 12% NaOH concentration has been found to shift the geometry of the woven fabric structure considerably. Rahman and Khan (2007) proved that coir fibre shrinkage increased considerably with the application of between 10% to 20% alkali concentrations at low temperature. The reason was that when strong NaOH solutions were used for fibre treatment, different Na- cellulose complexes were formed. However, this condition does not change the cellulose chain, but a large amount of NaOH and water is absorbed in the crystal structure, resulted to the swelling of fibres. By swelling, the fibre diameter increases mainly in dimension as well as lowering of crystallinity and increase in matrix accessibility (Ehrhardt et al., 2007). Increasing in fibre diameter had positive thickness effects on woven coir composite of 12% NaOH concentration, as displayed in Table 4.11. Thickness has a bigger influence on perforation resistance (Liu et al., 2000). According to Park and Jang (2003), impact properties may vary with increasing laminate thickness, and greater laminate thickness contributes to higher maximum load. These justifications show complement with the findings reported in Figure 4.12 (a).

On the other hand, energy propagation and ductility index for composite samples depleted with increasing amount of NaOH solutions (Figure 4.12 (d) and (e)). These findings represent that the material's stiffness increases as the treatment solution percentage increased, where stiffer materials usually limits the deformation, thus attributing to lower propagation energy. As a result, the material's ductility is also reduced.

The interaction plot of significant impact response is displayed in Figure 4.13. It can be seen that interactions are present for impact response of the total displacement, specific total energy absorbed, as well as impact strength.

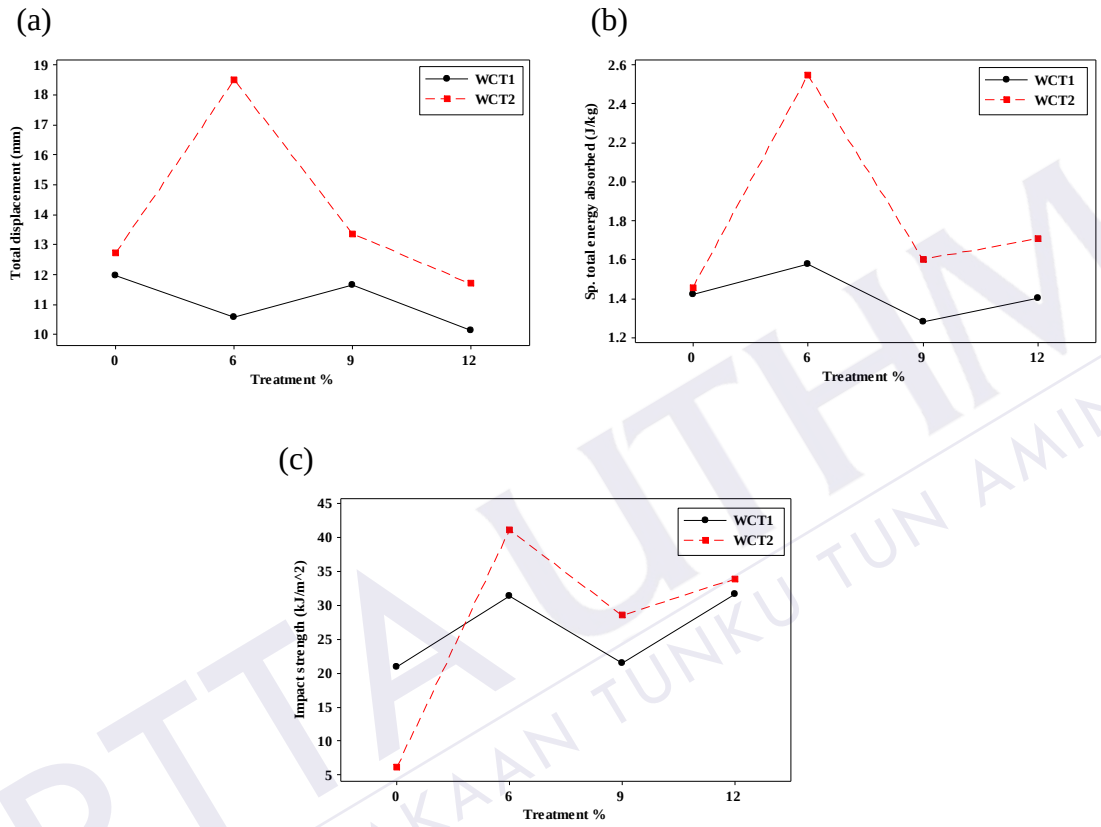

Figure 4.13: Interactions plots of impact response; (a) total displacement, (b) specific total energy absorbed and (c) impact strength of coir composites with different woven densities and treatment percentages

Figure 4.13 (a) indicates that woven Type 2 composite exhibited the highest displacement at 6% treatment. However, woven Type 1 at 6% treatment demonstrated the second lowest displacement. Moreover, the interaction plot for specific total energy absorbed in Figure 4.13 (b) shows that untreated samples had the same energy absorbed value. However, at 6% NaOH treatment, woven Type 2 dramatically outperformed Type 1 composite. As for other treatment percentages (9

and 12%), the trend was almost the same, although woven Type 2 composites showed slightly better performance. Furthermore, woven Type 1 composite showed better impact strength than Type 2 composite only for the untreated sample. Type 2 composites outperformed Type 1 for other treated samples. This condition was clearly presented in Figure 4.13 (c). All the results discussed above can be claimed as stable as the degree of data variability (R-square) was considered as acceptable (> 0.60) for the respective impact responses at 95% confidence level.

b) Damage assessment and morphology analysis

Figure 4.14 depicts the bar chart of the fractured area on front and rear faces. The results were based on the average of three samples. The distribution of residuals for those responses demonstrated a lower degree of data variability with an R-square value of 0.76 at 95% confidence level. Therefore, the data obtained from the experiment can be accepted as stable.

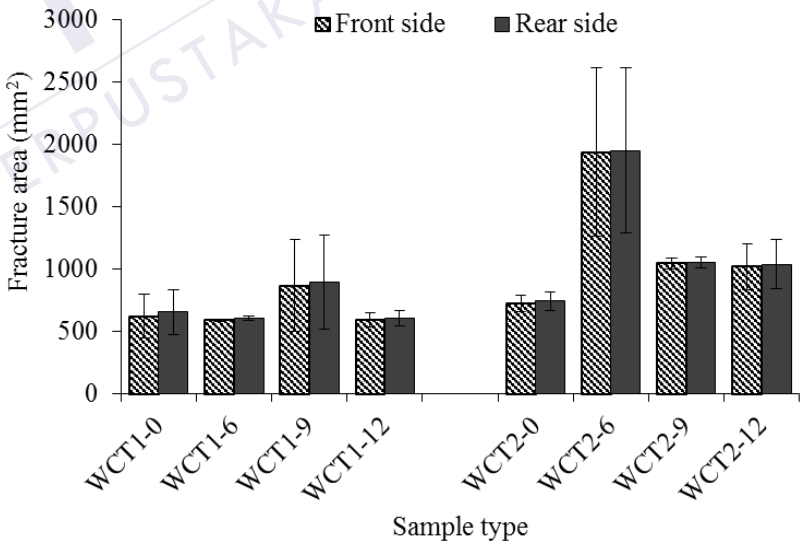

Figure 4.14: Fractured area (front and rear) of the impacted samples with different woven densities treatment percentages

Obviously, the bar chart displays that woven Type 2 structure had bigger damage area than Type 1 upon impact. Samples treated with 6% NaOH on Type 2 structure exhibited highly apparent fracture area. Whereas for Type 1, samples treated with 9% NaOH solution demonstrated the largest damage area. It was also noticeable from Figure 4.14 that the through thickness damage increased from the impacted front face towards the back face of the composites. However, the difference was found to be very little as indicated by the standard deviation error bar. Figure 4.15 represents an image of the rear face fracture on the composite samples. All samples were found to demonstrate clean segmented cracking fractures.

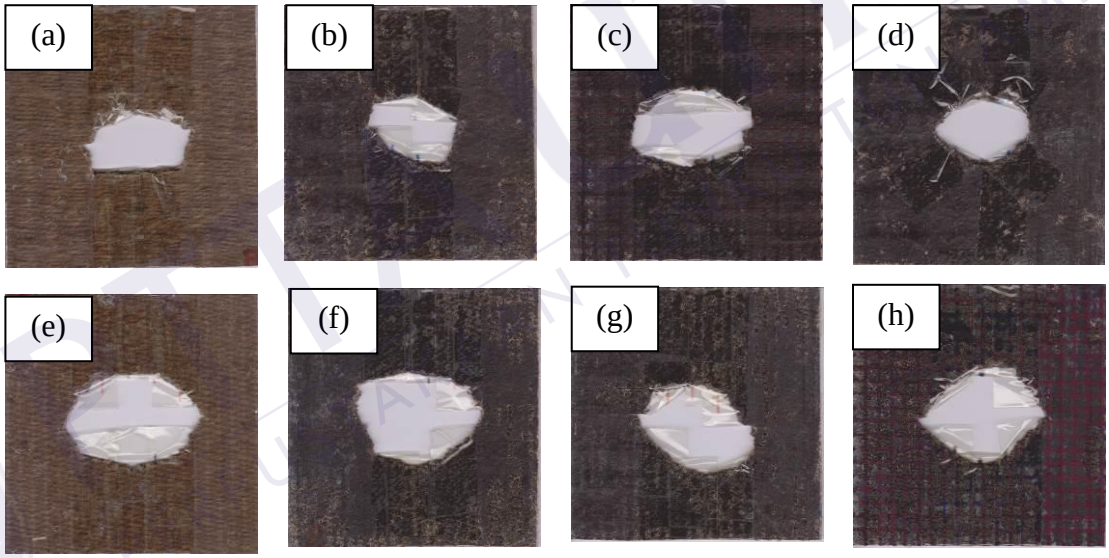

Figure 4.15: Rear fractures on composites with different woven densities and treatment percentages; (a) WCT1-0, (b) WCT1-6, (c) WCT1-9, (d) WCT1-12, (e) WCT2-0, (f) WCT2-6, (g) WCT2-9, (h) WCT2-12

The morphologies of dry woven coir fabric/mat before and after treatment are shown in Figure 4.16. Fibre opening and untwisting yarn were clearly seen on the treated woven samples. The yarns also swelled badly as the treatment percentage increased. Woven coir treated with 12% NaOH solution exhibited the worst swelling effect, resulting in increased composite thickness as measured and displayed in Table

4.11. The increase in composite thickness led to higher peak load as the contact area increased. Thus, high peak load obtained by samples treated by 12% NaOH solution as shown in Figure 4.12 (a) had strong correlation with the thickness effects. Yarn opening allows good penetration of thermoset matrix besides removing impurities on the fibre surface more effectively. However, excessive amount of alkaline solution should be avoided as it can interfere with the composite properties as discussed in the previous section. Hence, in this particular case, woven coir fabric treated by 6% NaOH solution had proven to offer the most sufficient fibre-matrix bonding as it delivered the highest impact strength and absorbed impact energy better.

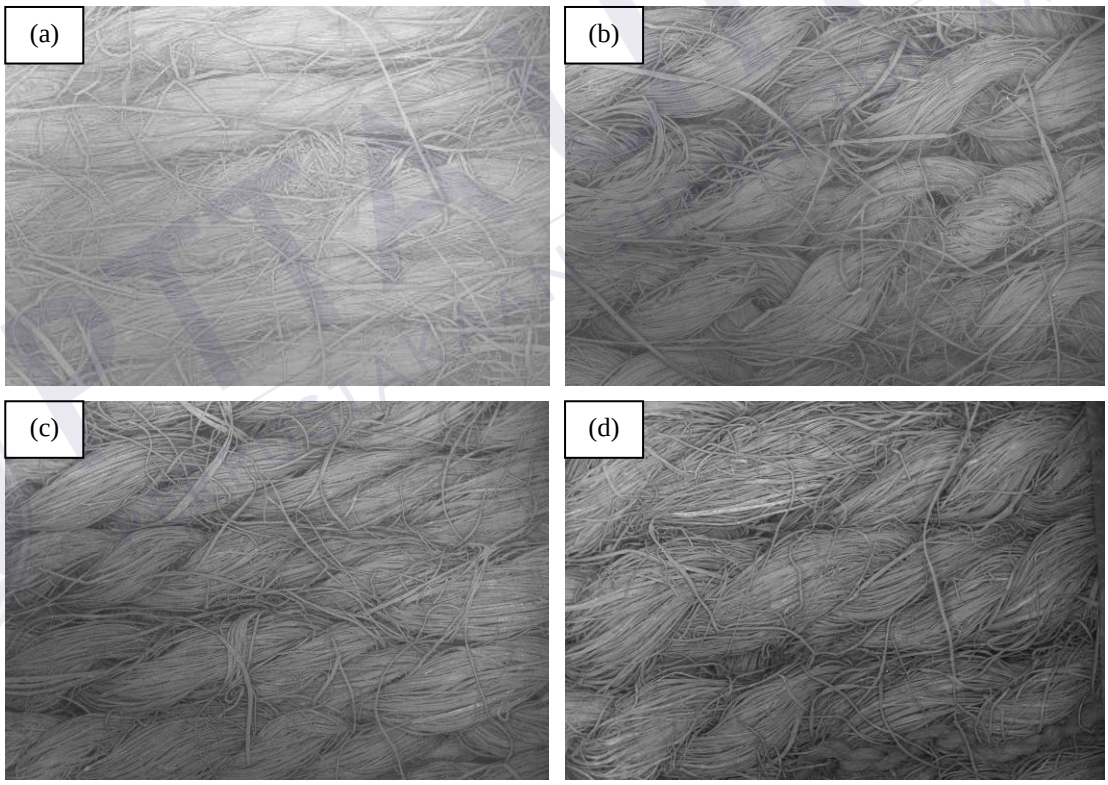

Figure 4.16: Morphology of dry woven coir fabric/mat before and after treatment at 11x; (a) untreated, (b) 6% NaOH, (c) 9% NaOH and (d) 12% NaOH

It can be seen that almost all samples exhibited brittle failure behaviour since they were fragmented and had multiple cracking upon impact load. Careful examination of the impacted composite specimens revealed multiple damage modes. SEM photographs of all untreated and treated specimens are displayed in Figure 4.17. There is evidence for these specimens that a combination of matrix cracking, fibre breakage, fibre-matrix debonding and fibre pull out are the predominant failure modes. As seen in untreated samples WCT1-0 and WCT2-0, the fibre surface was irregular. Matrix failure, fibre breakage and fibre pull-out can be clearly observed, indicating weak adhesion between fibre and matrix. Matrix debris covered the specimens, suggesting poor fracture resistance of untreated composites.

SEM images of WCT1-6 and WCT2-6 showed better interfacial bonding as they performed with minor matrix cracking and debonding. Less fibre breakage was clearly visible, indicating that fibre-matrix adhesion was excellent. With regards to WCT1-9 and WCT2-9, it was noticeable that a resin-rich area was present that can lead to localised strain. Fibrillation (fibre splitting) was clearly observable in these specimens as well as matrix cracking and debonding, which can reduce strength. Specimens were badly swollen by 12% NaOH concentration as portrayed in the SEM images of WCT1-12 and WCT2-12, which can lead to increased shrinkage and better surface tension. It could be that the impact energy was dissipated via fractures and debonding of the reinforcement as the maximum load and energy absorbed increased again for this sample.

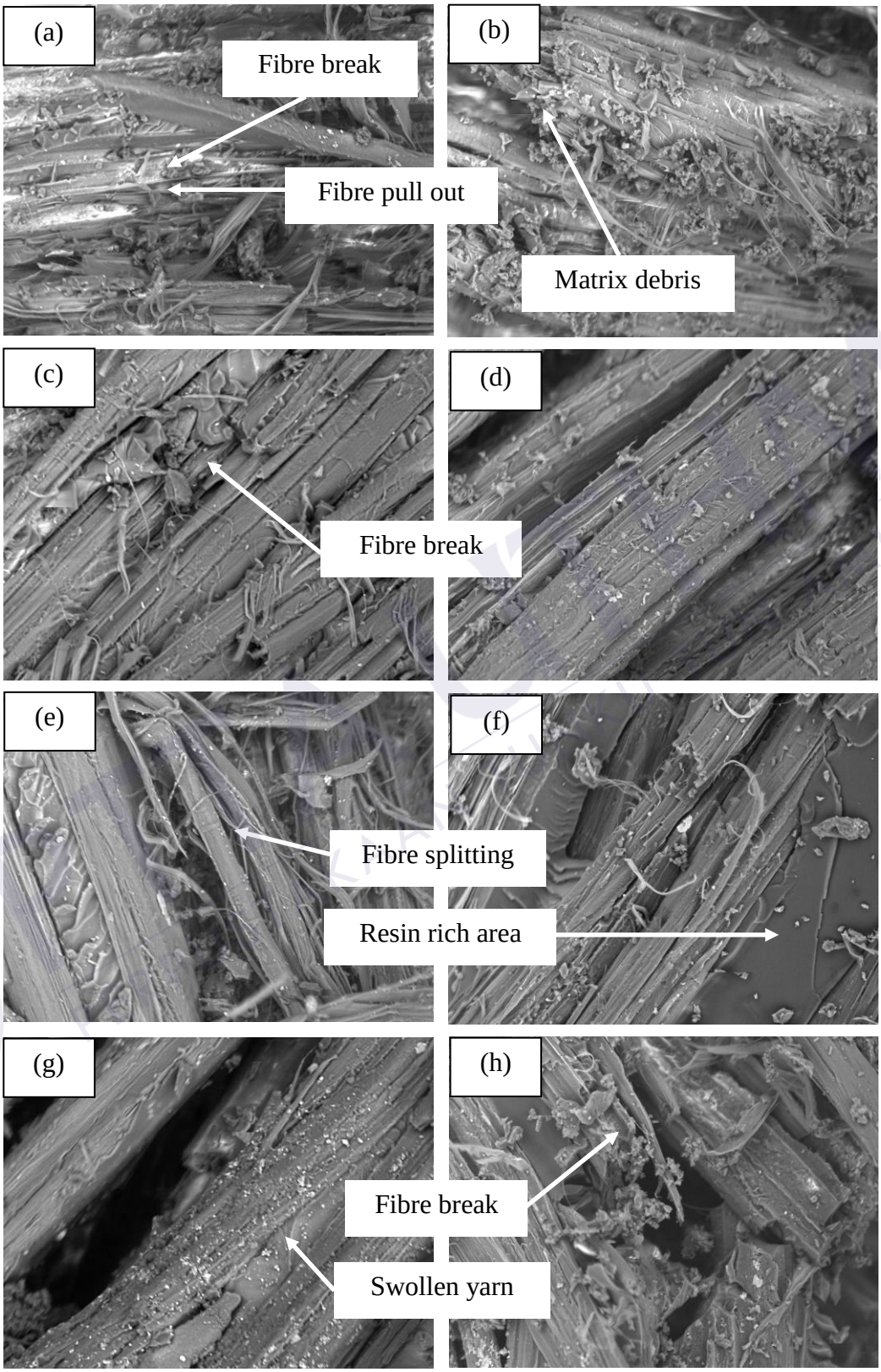

Figure 4.17: SEM of fractured surfaces for sample; (a) WCT1-0, (b) WCT2-0, (c) WCT1-6, (d) WCT2-6, (e) WCT1-9, (f) WCT2-9, (g) WCT1-12 and (h) WCT2-12, at 650X

4.3.1.4 Concluding remarks

These particular section studied the optimum impact response of coir composite to be combined with Kevlar aramids in a hybrid composite. Important parameters such as the effects of the reinforcement structure, manufacturing method, fabric density and fabric modification (treatment) were evaluated, and the results were determined. The results showed that coir in a woven structure exhibited the highest specific energy absorbed while offering better propagation energy and resisting high impact load. Composites fabricated by the compression moulding method were found to have better impact response, particularly on the peak load and impact strength. Furthermore, it is important to notice that Type 2 woven density (woven with less porosity) treated with 6% NaOH solution offered better specific energy absorbed with the highest impact strength and deflection upon impact compared to high porosity woven structure. Therefore, the above-mentioned coir fabric specification was chosen as the subsequent hybrid composite. Type 2 woven density, however, was substituted by Type 1 due to the longer time taken to produce Type 2 woven fabric. The percentage of performance difference recorded for specific total energy absorbed and impact strength were 63% and 32%, respectively. Besides, the fracture area for woven Type 1 treated with 6% NaOH was found to reduce by about 70% compared to Type 2.

4.3.2 Coir/Kevlar hybrid composites

In the current section, six different types of interply hybrid laminates were fabricated, the details of which are given in Table 4.15. The rest of the samples acted as control samples where the laminate layer was increased in order to determine the

effect of thickness. It was observed that interply layers consisting of two Kevlar plies such as KCK, KKC and CKK exhibited 42% less thickness than the composites with two layers of woven coir. On the other hand, the increase in composite thickness was anticipated as the laminate layer increase, as shown by the control sample. The thickness of three layers intraply CK and three layers coir composite was observed to precede three layers interply hybrid composite. On the contrary, three layers Kevlar laminate had less than 1 mm thickness. It was expected that the increase in thickness enhanced the overall composites areal density.

Table 4.15: Characteristic of hybrid and control samples

Composite type	Average thickness (mm)	Average areal density (g/m^2)
KCK	3.5	4100
KKC	3.5	4100
CKK	3.5	4100
CKC	6.0	6900
CCK	6.0	6900
KCC	6.0	6900
C	3.1	3300
$[C]_2$	4.9	5500
$[C]_3$	8.7	9800
$[K]_3$	0.8	1000
$[K]_9$	2.2	2500
$[CK]_1$	2.9	5500
$[CK]_2$	5.6	6300
$[CK]_3$	10.0	11300

4.3.2.1 Effects of hybrid laminate stacking configurations on low velocity impact response of hybrid coir/Kevlar composites

Low velocity impact response of hybrid composite samples made of plain woven coir and Kevlar was evaluated using an instrumented impact testing machine at 5 m/s impact speed. Very little scatter was observed on these curves, and this

consistency again emphasized the overall reliability of the present experimental procedure. Therefore, only one set of test results (out of three repetitions) was presented for each stacking type. Figure 4.18 (a) depicts the load-displacement plots for all six stacking configurations of coir/Kevlar hybrid composite panels. All samples represent an open type curve, implying the initiation of a complete perforation.

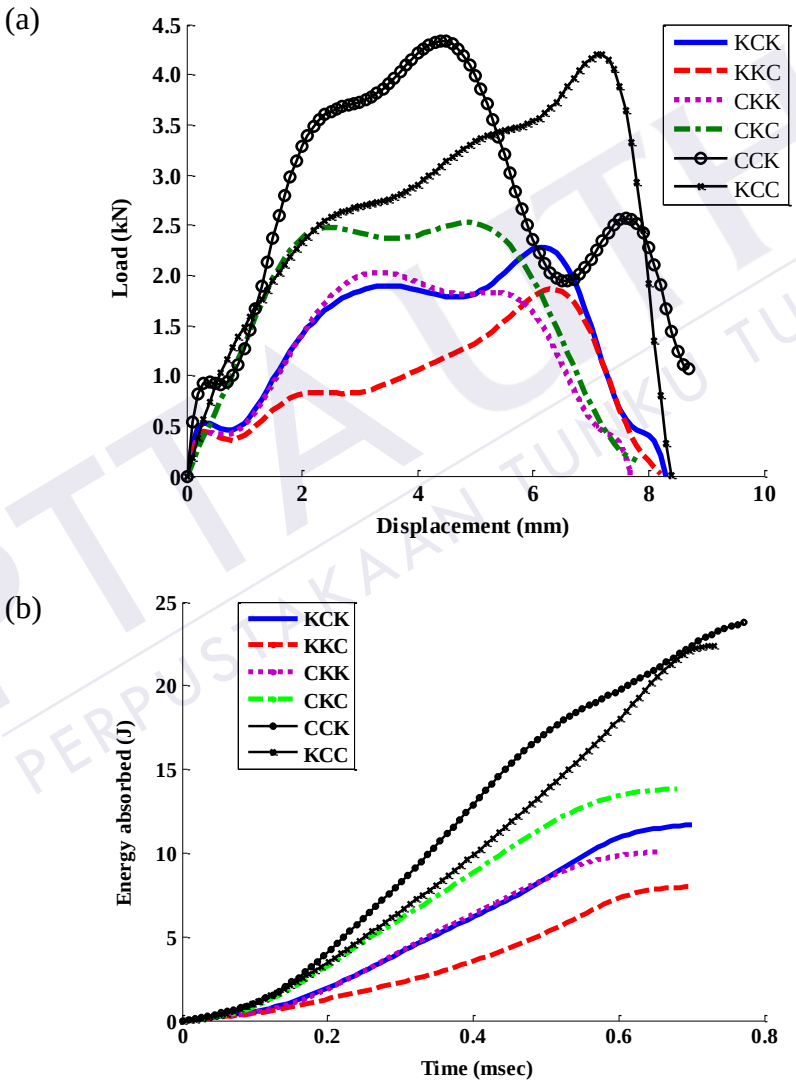

Figure 4.18: (a) Load-displacement curve and (b) energy absorbed-time curve of hybrid composites with different stacking configuration

KCK, KKC, CKK and CCK samples exhibited steeper slopes immediately upon impact. The slope showed a sudden reduction at 1.0 kN for CCK and 0.5 kN for KCK, KKC and CKK, which was expected due to the initiation of matrix crack. The stiffness then remained ascending for CCK panel up to around 3.5 kN. A load interruption was detected, which was also expected due to another combination of matrix crack and fibre breakage. After reaching its maximum load of 4.5 kN, severe unloading occurred. The steep drop likely implies the loss of contact between impactor and panel for a moment, which was expected due to serious fibre breakage and matrix crack, including a severe delamination in the composite panel. At the descending section of CCK, a slight load increment was noticeable, which was influenced by a single layer of flexible Kevlar that was placed at the rear layer of the CCK composite. Interlayer delamination between the bridging layer of coir and Kevlar was anticipated and global deformation occurrence was expected to resist penetration. From all the graphs, it was noticed that the response (particularly the bending stiffness) was dominated by the type of material placed in each layer (Yahaya et al., 2014). Coir/epoxy composites are stiffer compared to Kevlar/epoxy composites. Coir composite deforms less and therefore, carries higher load. As happened in CCK, the placement of two layers of coir on the front face imparts higher stiffness on the panel. Whereas, Kevlar composites are more flexible and absorb the impact energy through global deformation, thus carrying a lower load (Hosur et al., 2005).

It was observed from the load-displacement curve that KCC panel showed good resistance to bending fracture. The wider and higher ascending section in KCC sample indicates the presence of ductile material in the system, which increases the

material's rigidity. Slight oscillations were detected along the ascending section, which were expected due to matrix crack and delamination. Minor damage was noted in these specimens until the maximum load was reached, suggesting that the damage mode in this sample was associated with large bending stresses. A dramatic load drop then occurred corresponding to serious fibre breakage and complete perforation. As discussed earlier, the laminated stacking influenced the bending stiffness. Therefore, the placement of coir layer on the outer surface reduced the probability of greater deformation on the sample.

Lower peak load with substantial plateau load was observed in CKC, CKK and KCK, which was an indication of ductile material and the compliant nature of woven fabric composites. The oscillating load trend of the respective panels before and after reaching the maximum load was an indication of the presence of damage such as matrix crack, fibre fracture and delamination due to bending. The trend was also attributed to the combination of flexible material (which was Kevlar in this case) and the brittleness of the coir composite materials. On the other hand, less load wavering was detected in KKC, indicating that KKC exhibited good flexibility with less internal damage.

Figure 4.18 (b) illustrates the energy absorbed versus time curve for all hybrid samples, which shows that the rate of energy absorption increased with time during the initial phase. The highest energy absorption was observed for CCK followed by KCC, CKC, KCK, CKK and KKC. In general, it can be concluded that the existence of a single ply Kevlar and two layers of woven coir being placed either at the front or the back layer of the hybrid laminates system, contributed to increased material's

toughness. The penetration of coir-Kevlar hybrid involves layers of fibres with different stiffness and friction coefficient. The excellent coefficient of friction exhibited by the Kevlar layer resists the formation of a complete shear plug and prolongs the load-displacement curve (Yahaya et al., 2014).

The placement of Kevlar ply at the impacting side increased the toughness of the material. This observation was expected since Kevlar fibre has some effects in hindering the early load drop as it possesses higher tensile strength and modulus than the coir fibre. The stress on the surface layer increases and the impact load is well distributed (Park and Jang, 1997). Nevertheless, the placement of Kevlar ply at the middle of the laminates did not give a significant rise in toughness, which was expected due to poor impact resistance by a single layer of woven coir placed at the impacting side. Furthermore, bad delamination was suspected to occur while transferring the impact energy to the second layer (which, in this case, was the Kevlar layer), which can also be explained as losing the bridging strength between the woven coir layers to the Kevlar layers. The slope and the area under the load-displacement curve decreased with the presence of more than one Kevlar layers and only one layer of woven coir, hence contributing to lower energy absorbed value. Thickness is likely to be the factor for this state. Samples consisting of a single woven coir layer exhibited lower thickness. Findings from previous researchers had proven that thicker composites exhibit higher impact energy through increased peak load (Belingardi and Vadori, 2003; Park and Jang, 2003). Moreover, Caprino et al. (2003) added that the increase in thickness increases the initial rigidity of the laminates. Nonetheless, this research looked at the minimum use of Kevlar to

improve the impact properties of coir composite. Thus, promising results were achieved.

To assist a better understanding, the key impact responses including the maximum peak load, displacement at the peak load, total displacement, time at peak load, total time to penetration, energy absorbed to peak load, total energy absorbed, propagation energy, ductility index, specific energy absorbed to peak load, specific total energy absorbed and impact strength for the six types of sample configuration are summarized in Table 4.16 and Table 4.17. The normal probability plot shows an R-square value of more than 0.77 at 95% confidence level for the studied impact response, which indicates the stability and normality of the data distributions. The methods of data extraction from the load-displacement curve had been detailed in Section 3.4.3.3. It was difficult to establish any obvious conclusion just by looking at the table. The superscript in each column specifies the results of TGRT. The same small superscripts in columns in Table 4.16 and Table 4.17 indicate that the values dropped within the same deviation range. The results can be accepted as normal and stable as R-square values for the selected impact responses were more than 0.77.

It was noted from the ANOVA analysis that different coir/Kevlar stacking configurations had significant effects on the impact response, particularly peak load, total displacement, total time, propagation energy, ductility index, specific total energy absorbed and impact strength (P-value < 0.05 at 95% confidence level). Figure 4.19 demonstrates the impact responses of coir/Kevlar hybrid composites with different stacking configurations. With the help of TGRT via ANOVA analysis, the effects of different stacking configurations on impact responses could be better

Table 4.16: Mean scores for stacking configuration parameter on impact response

Sample type	Peak load (kN)	Displacement at peak load (mm)	Total displacement (mm)	Time at peak load (msec)	Total time (msec)	Energy absorbed to peak load (J)	Total energy absorbed (J)
KCK	2.20 ± 0.07^{bc}	6.23 ± 0.06^{b}	8.03 ± 0.38^{bc}	1.32 ± 0.03^{b}	1.72 ± 0.05^{c}	9.35 ± 0.11^{c}	11.47 ± 0.23^{bc}
KKC	1.82 ± 0.04^{c}	6.37 ± 0.12^{b}	8.20 ± 0.20^{bc}	1.36 ± 0.02^{b}	1.74 ± 0.04^{c}	6.01 ± 0.26^{cd}	7.90 ± 0.34^{c}
CKK	2.06 ± 0.03^{c}	3.55 ± 0.23^{d}	7.66 ± 0.15^{c}	0.75 ± 0.07^{d}	1.63 ± 0.03^{c}	3.96 ± 0.24^{d}	9.73 ± 1.20^{c}
CKC	2.78 ± 0.24^{b}	4.20 ± 0.75^{cd}	7.80 ± 0.30^{c}	0.90 ± 0.17^{cd}	1.68 ± 0.08^{c}	8.67 ± 2.04^{c}	15.29 ± 2.25^{b}
CCK	4.46 ± 0.13^{a}	4.50 ± 0.17^{c}	9.60 ± 0.90^{a}	0.97 ± 0.06^{c}	2.11 ± 0.17^{a}	13.57 ± 1.37^{b}	26.36 ± 2.25^{a}
KCC	4.14 ± 0.78^{a}	7.10 ± 0.40^{a}	8.73 ± 0.29^{b}	1.56 ± 0.08^{a}	1.92 ± 0.08^{b}	18.93 ± 4.68^{a}	22.83 ± 4.50^{a}

* Means with same superscript letters in column are not significantly different at the ($P\geq0.05$).
* Each result is the average value derived from three replicates

explained and it is presented as superscripts in Figure 4.19. The same superscript letters imply there was no significant different on the values.

Table 4.17: Mean scores for stacking configuration parameter on propagation energy, ductility index, specific energy absorbed and impact strength

Sample type	Propagation energy (J)	Ductility index	Sp. energy absorbed to peak load (J/kg)	Sp. total energy absorbed (J/kg)	Impact strength (kJ/m^2)
KCK	2.13 ± 0.34^{d}	0.23 ± 0.04^{c}	2.28 ± 0.03^{ab}	2.80 ± 0.06^{bc}	73.60 ± 0.85^{c}
KKC	1.88 ± 0.09^{d}	0.31 ± 0.01^{bc}	1.47 ± 0.06^{cd}	1.93 ± 0.08^{d}	47.34 ± 2.01^{cd}
CKK	5.77 ± 1.42^{bc}	1.47 ± 0.43^{a}	0.97 ± 0.06^{d}	2.37 ± 0.29^{cd}	31.17 ± 1.92^{d}
CKC	6.61 ± 2.09^{b}	0.82 ± 0.40^{abc}	1.26 ± 0.29^{d}	2.22 ± 0.33^{cd}	68.30 ± 16.03^{c}
CCK	12.79 ± 1.54^{a}	0.95 ± 0.13^{ab}	1.97 ± 0.20^{bc}	3.82 ± 0.33^{a}	106.85 ± 10.77^{b}
KCC	3.90 ± 0.39^{cd}	0.22 ± 0.07^{c}	2.74 ± 0.68^{a}	3.31 ± 0.65^{ab}	149.03 ± 36.85^{a}

* Means with same superscript letters in column are not significantly different at the ($P\geq0.05$).
* Each result is the average value derived from three replicates

Figure 4.19 (a) clearly represent the laminates, which comprises two layers of woven coir exhibiting high peak load, where CCK samples showed the highest. This was followed closely by KCC samples. The results show good agreement with the research by Yahaya et al. (2014) on kenaf/aramid hybrid composites, where they reported that the placement of kenaf at the innermost (front) layers gave the maximum penetration force. CCK composites also had the highest displacement and longer time to failure followed by KCC as seen in Figure 4.19 (b) and (c). Meanwhile, other hybrid samples showed minor difference in both responses. Figure 4.19 (d) clearly displays that the highest propagation energy is observed in CCK sample. Fibre type and its placement in the laminates were found to give a crucial effect on the properties, as substantial differences in energy propagation among

different stacking configurations were obtained. Proper stacking is needed to avoid the reduction of bridging strength in the composite system.

CKK composites exhibited the highest ductility index compared to other hybrid laminates (Figure 4.19 (e)). Two layers of woven Kevlar, placed at the back face of the laminates provided better ductility on the composites due to the high modulus carried by Kevlar fibres. The ability to delay the failure after the maximum load is noticeable in CKK. Although it is well known that coir composite is very much stiffer, the incorporation of a single Kevlar layer help to improve its ductility as shown by CCK and CKC.

When comparing the performance of energy absorbers in materials, the most useful property is the energy absorbed per unit mass. This is known as the specific energy absorption (SEA). Figure 4.19 (f) shows that CCK samples obtained the highest specific total energy absorbed with 3.8 J/kg followed by KCC at 3.3 J/kg. This again shows a good agreement with research on kenaf/aramid hybrid composites by Yahaya et al. (2014) who reported that natural fibre at the front layers and aramids at the outer layers offers maximum energy absorption. KCK samples were seen to correlates well with the specific total energy absorbed value of 2.8 J/kg. In contrast, KKC exhibited the least value, indicating that when considering energy absorption, a composite structure with higher percentage of coir in a woven layer form, at an equivalent weight, can still achieve better performance. SEA was more significantly affected by the strain to failure than the modulus (Bailey, 2005). Therefore, it shows agreement with the results produced as the strain to failure exhibited by the coir yarn is higher than the Kevlar yarn.

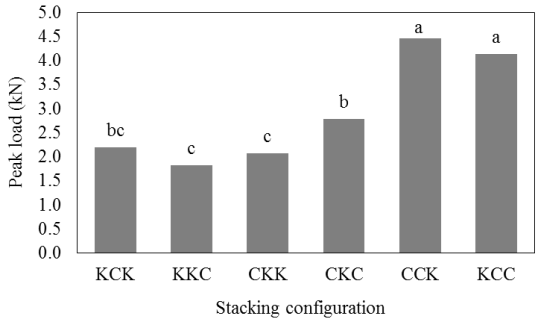

(a)

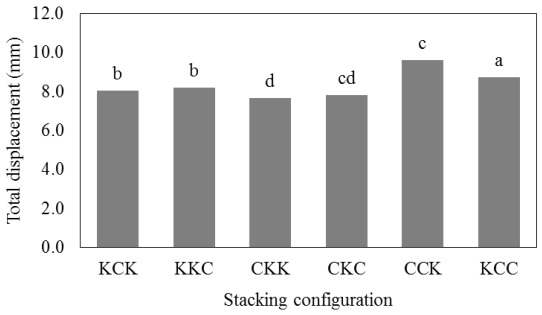

(b)

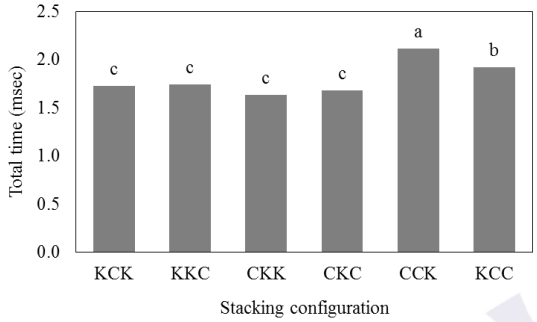

(c)

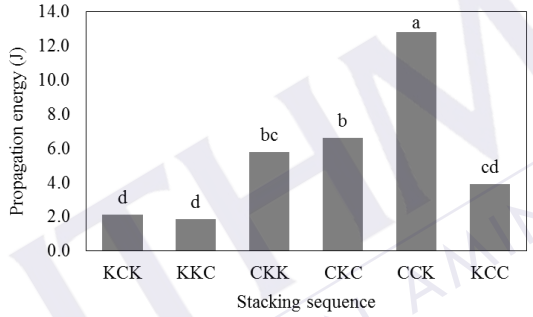

(d)

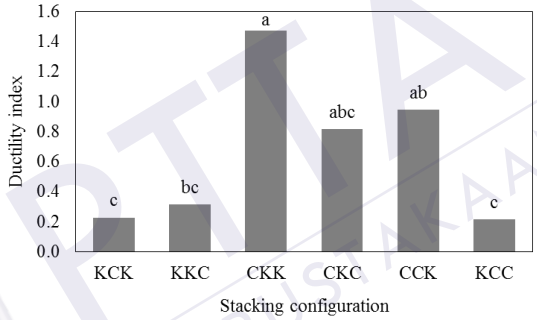

(e)

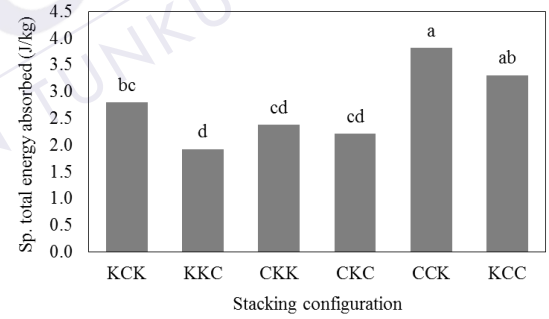

(f)

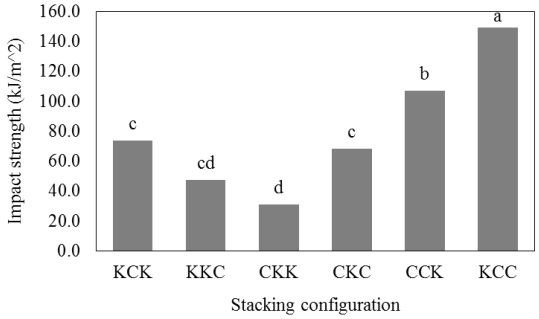

(g)

Figure 4.19: Impact response of coir/Kevlar hybrid composite with different stacking configurations

Figure 4.19 (g) clearly demonstrates that the impact strength of the composite improved with increased content of woven coir layer. KCC samples achieved an impact strength up to 150 kJ/m^2. The interaction between neighbouring fibres appeared to affect the impact strength of the composite system. As explained prior, having Kevlar layer at the front face of the sample improved the materials rigidity, hence increasing material toughness with the blends of high stiffness coir.

4.3.2.2 Comparisons of low velocity impact and quasi-static indentation test

Quasi-static indentation test was conducted at 1.25 mm/s and the results were compared to the impact behaviour. Besides, the validity of the impact test data can be checked by comparing the results from both tests (Ramakrishnan, 2009), which is supported by Li et al. (2012) who concluded that quasi-static indentation testing can be used to represent low-velocity testing as the research results showed no distinct difference.

The load-displacement curve is given in Figure 4.20. Generally, it was observed that the trend of the curves for quasi-static indentation test and low-velocity impact test at 5 m/s were in fairly good superimposition. The most resemblance trend was observed in KCC sample as shown in Figure 4.20 (f), which indicates that the process curves of the two tests had damage equivalence. A change in stiffness at the very beginning of the quasi-static curve was detected in KCK, KKC, CKK and CCK samples. This condition was associated with the contact stresses between the indenter and the specimen. As the indenter first touches the specimen's panel, it begins to dent into the specimen. As the indenter goes deeper into the specimen, the contact stresses are spread out, and the bending displacements predominate.

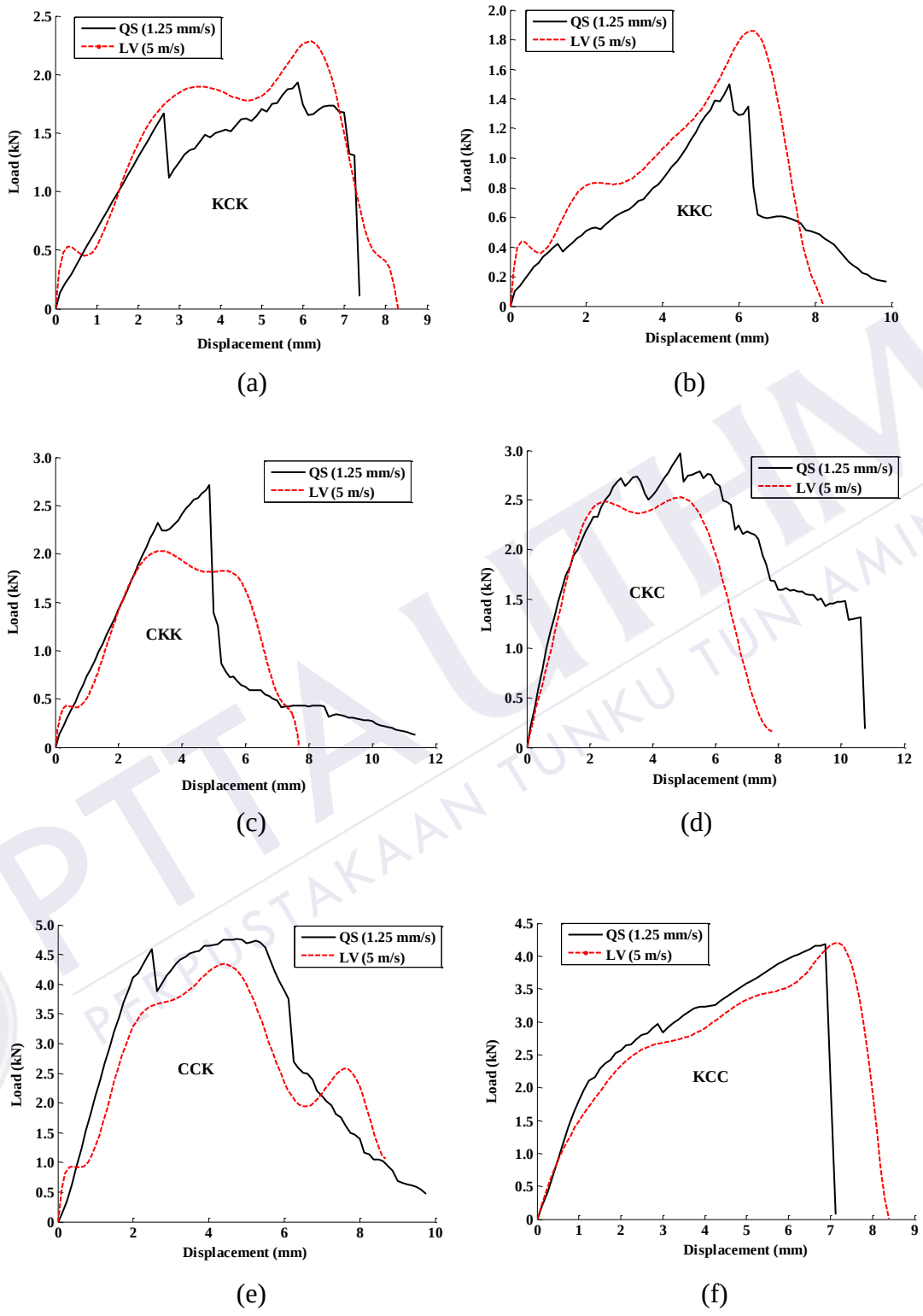

Figure 4.20: Load-displacement curve of coir/Kevlar hybrid composite (comparison between quasi-static and low-velocity curves)

The total displacement upon penetration for the quasi-static test was higher by about 4 mm than that of the low-velocity impact test as portrayed by KKC, CKK and CKC. It was anticipated that a relaxation phenomenon in the materials under quasi-static condition causes this difference (Segreti et al., 2004). Meanwhile, it was apparent that samples with two Kevlar layers, such as in KCK, KKC and CKK had slight difference (less than 0.8 kN) in the peak load, which was probably due to the bridging effect between all three layers and the relaxation phenomenon as mentioned earlier. Bridging refers to the inter-layer join of the hybrid composites. Poor bridging caused the presence of void in the laminate and initiate crack growth resulted to the reduction of maximum load the laminate can achieved. Relaxation on the other hand is the state where composites system can still return to its equilibrium condition and release of tension. The relaxation in composites system when react with stress load may vary for static and dynamic condition. Therefore, the peak load that the composites can achieve may produce slight difference under both conditions.

In order to assist in clear interpretation, extractions of the impact response based on the load-displacement curves were made. This measure is useful for design purposes because it allows the effects of various parameters on the dynamic response to be quantified with respect to the quasi-static response. Table 4.18 illustrates the mean scores for peak load, displacement at peak load, total displacement, time at peak load, total time, energy absorbed to peak load and total energy absorbed, whereas Table 4.19 depicts the mean scores for propagation energy, ductility index, specific energy absorbed to peak load, specific total energy absorbed and impact strength. The mean with the same superscripts in each column indicate that the value had no significant difference as the mean values were derived from three replicates.

Table 4.18: Impact and indentation mean scores for hybrid composite subjected to quasi-static and low-velocity impact

Sample type	Peak load (kN)	Displacement at peak load (mm)	Total displacement (mm)	Time at peak load (msec)	Total time (msec)	Energy absorbed to peak load (J)	Total energy absorbed (J)
KCK-QS	2.01±0.07^{def}	6.00±1.08^{bc}	8.46±0.69^{cd}	4.80±0.87^{bc}	6.77±0.55^{bc}	6.52±1.69^{de}	9.94±0.22^{e}
KKC-QS	1.54±0.05^{f}	7.08±0.14^{ab}	11.00±0.94^{abc}	5.67±0.12^{ab}	8.80±0.75^{ab}	4.31±0.28^{e}	6.65±1.04^{e}
CKK-QS	2.41±0.27^{cde}	5.13±0.57^{cde}	12.08±0.76^{ab}	4.10±0.46^{c}	9.67±0.61^{a}	5.85±1.68^{de}	9.71±1.01^{e}
CKC-QS	2.94±0.03^{c}	5.75±0.25^{bcd}	12.60±2.84^{a}	4.60±0.20^{c}	10.08±2.27^{a}	10.25±0.15^{cd}	19.57±1.84^{bc}
CCK-QS	5.01±0.37^{a}	5.67±0.52^{cd}	10.54±1.09^{abcd}	4.53±0.42^{c}	8.43±0.87^{abc}	16.80±0.37^{ab}	27.66±0.45^{a}
KCC-QS	4.22±0.09^{ab}	7.50±0.22^{a}	7.83±0.07^{d}	6.00±0.17^{a}	6.27±0.06^{c}	18.98±0.81^{a}	19.70±0.49^{bc}
KCK-LV	2.20±0.07^{cdef}	6.23±0.06^{abc}	8.03±0.38^{cd}	1.32±0.03^{d}	1.72±0.05^{d}	9.35±0.11^{cd}	11.47±0.23^{de}
KKC-LV	1.82±0.04^{ef}	6.37±0.12^{abc}	8.20±0.20^{cd}	1.36±0.02^{d}	1.74±0.04^{d}	6.01±0.26^{de}	7.90±0.34^{e}
CKK-LV	2.06±0.03^{def}	3.55±0.23^{f}	7.66±0.15^{d}	0.75±0.07^{d}	1.63±0.03^{d}	3.96±0.24^{e}	9.73±1.20^{e}
CKC-LV	2.78±0.24^{cd}	4.20±0.75^{ef}	7.80±0.30^{d}	0.90±0.17^{d}	1.68±0.08^{d}	8.67±2.04^{cde}	15.29±2.25^{cd}
CCK-LV	4.46±0.13^{ab}	4.50±0.17^{def}	9.60±0.90^{bcd}	0.97±0.06^{d}	2.11±0.17^{d}	13.57±1.37^{bc}	26.36±2.25^{a}
KCC-LV	4.14±0.78^{b}	7.10±0.40^{ab}	8.73±0.29^{cd}	1.56±0.08^{d}	1.92±0.08^{d}	18.93±4.68^{a}	22.83±4.50^{ab}

* Means with same superscript letters in column are not significantly different at the (P≥0.05).
* Each result is the average value derived from three replicates

Table 4.19: Propagation energy, ductility index, specific energy absorbed and impact strength mean scores for hybrid composite subjected to quasi-static and low-velocity impact

Sample type	Propagation energy (J)	Ductility index	Specific energy absorbed to peak load (J/kg)	Specific total energy absorbed (J/kg)	Impact strength (kJ/m^2)
KCK-QS	3.41 ± 1.72^{cde}	0.61 ± 0.49^{bc}	1.59 ± 0.41^{bcd}	2.42 ± 0.05^{cd}	51.37 ± 13.33^{de}
KKC-QS	2.34 ± 0.93^{de}	0.54 ± 0.20^{bc}	1.05 ± 0.07^{d}	1.62 ± 0.25^{d}	33.95 ± 2.19^{e}
CKK-QS	3.86 ± 0.73^{cde}	0.71 ± 0.28^{bc}	1.43 ± 0.41^{cd}	2.37 ± 0.25^{cd}	46.06 ± 13.23^{de}
CKC-QS	9.33 ± 1.82^{ab}	0.91 ± 0.18^{ab}	1.49 ± 0.02^{bcd}	2.84 ± 0.27^{bc}	80.69 ± 1.21^{cd}
CCK-QS	10.87 ± 0.72^{a}	0.65 ± 0.06^{bc}	2.43 ± 0.05^{a}	4.01 ± 0.07^{a}	132.26 ± 2.93^{ab}
KCC-QS	0.72 ± 0.58^{e}	0.04 ± 0.03^{c}	2.75 ± 0.12^{a}	2.86 ± 0.07^{bc}	149.44 ± 6.34^{a}
KCK-LV	2.13 ± 0.34^{e}	0.23 ± 0.04^{bc}	2.28 ± 0.03^{ab}	2.80 ± 0.06^{bc}	73.60 ± 0.85^{cd}
KKC-LV	1.88 ± 0.09^{e}	0.31 ± 0.01^{bc}	1.47 ± 0.06^{bcd}	1.93 ± 0.08^{d}	47.34 ± 2.01^{de}
CKK-LV	5.77 ± 1.42^{bcd}	1.47 ± 0.43^{a}	0.97 ± 0.06^{d}	2.37 ± 0.29^{cd}	31.17 ± 1.92^{e}
CKC-LV	6.61 ± 2.09^{bc}	0.82 ± 0.40^{ab}	1.26 ± 0.29^{cd}	2.22 ± 0.33^{cd}	68.30 ± 16.03^{cde}
CCK-LV	12.79 ± 1.54^{a}	0.95 ± 0.13^{ab}	1.97 ± 0.20^{abc}	3.82 ± 0.33^{a}	106.85 ± 10.77^{bc}
KCC-LV	3.90 ± 0.39^{cde}	0.22 ± 0.07^{bc}	2.74 ± 0.68^{a}	3.31 ± 0.65^{ab}	149.03 ± 36.85^{a}

* Means with same superscript letters in column are not significantly different at the ($P\geq0.05$).
* Each result is the average value derived from three replicates

Figure 4.21 was developed to provide a clear picture of the trends in impact responses for the six hybrid samples subjected to quasi-static and low-velocity impact tests. A P-value of more than 0.05 was observed in peak load, propagation energy, ductility index, specific total energy absorbed and impact strength. These results indicate that for the particular impact response, there was no distinct difference between quasi-static indentation and low-velocity impact tests on the respective hybrid samples. However, as expected earlier, the response for total displacement was vice versa. A P-value of less than 0.05 proved that quasi-static and low-velocity impact tests had different effect on samples deformation.

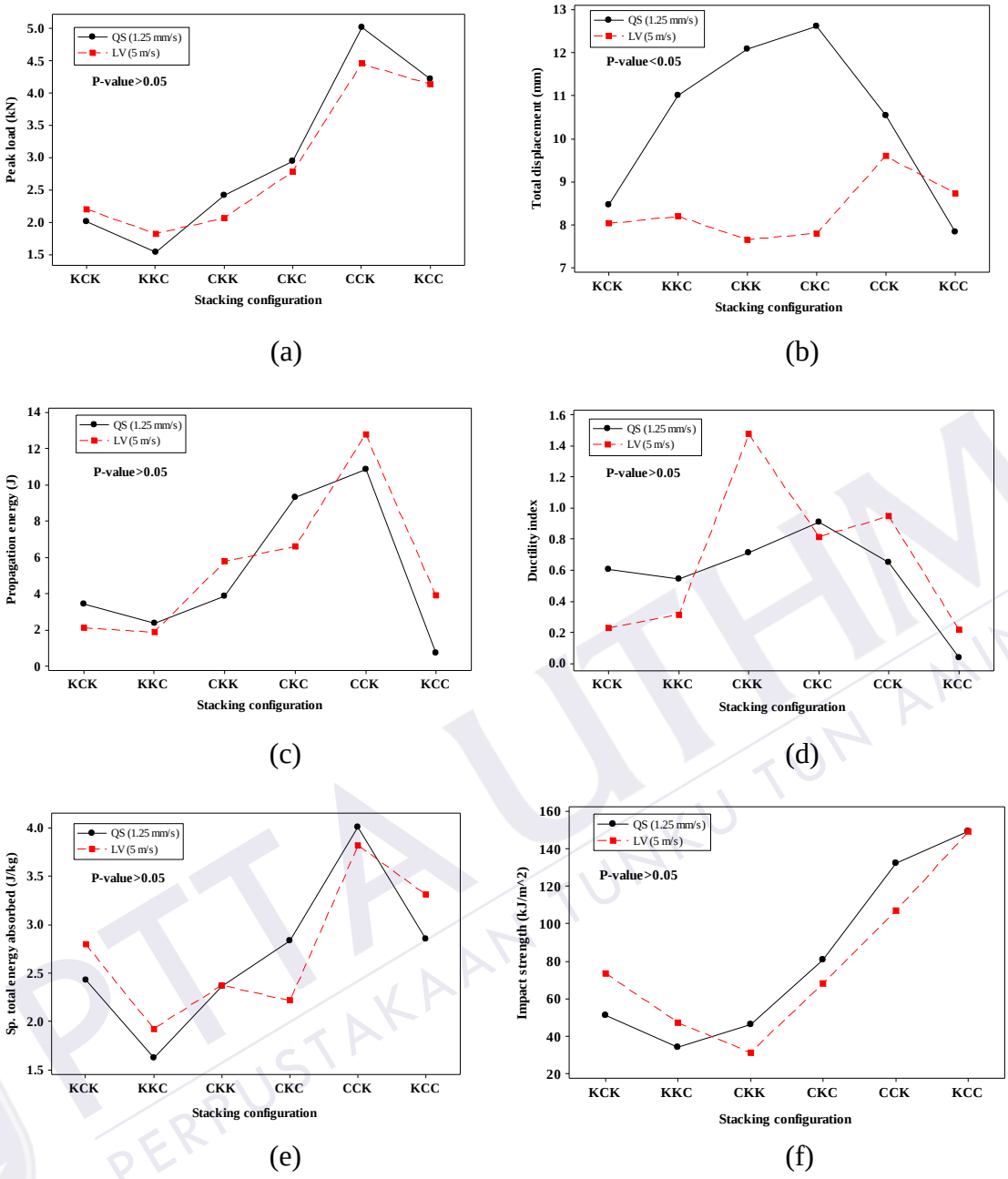

Figure 4.21: Comparison of low-velocity and quasi-static indentation responses of hybrid composite

4.3.2.3 Comparisons of impact response of hybrid and control samples

A comparison in impact responses between the control samples (CS) and the hybrid samples is essential to observe the capability of the hybrid system in delivering compensations to the ordinary composite system. Table 4.20 and Table 4.21 summarize the mean values of the impact responses with respect to different

hybrid samples and CSs. The same superscripts in each column indicate that there is no significant difference in the value. Some of the important impact response data were graphically presented for better interpretation.

Figure 4.22 shows the peak load and total displacement of the hybrid composites and the control samples. It was observed that the peak load increased with increasing layers of control samples and intraply hybrid samples. The peak load for the three laminate layers of coir/Kevlar intraply hybrid was better than the three laminate layers of 100% coir. Furthermore, the peak load for the two and three layers of coir composites was found to outperform the three laminate layers and the nine laminate layers of Kevlar. The advantage of interply hybrid CCK and KCC was evident here as the peak load approached the peak load for the three laminate layers of coir at reduced thickness and areal density. The recorded peak load difference was only 1.4 kN (31%), whereas, the thickness and the areal density differences were 45% and 42%, respectively. The thickness effect was more apparent here and agreed with other researchers (Park and Jang, 2003; Belingardi and Vadori, 2003; Cantwell and Morton, 1989).

Meanwhile, the total displacement to perforation value decreased with increasing coir layers and intraply hybrid. Contrasting behaviour was found for 100% Kevlar layer, where increased total displacement was observed as the layer increased. Poor resistance to deformation such as in Kevlar composite structure is attributed to their high modulus of elasticity that makes them more ductile than coir composite (Monteiro et al., 2008).

Table 4.20: Mean scores for hybrid and control samples on impact penetration response

Sample type	Peak load (kN)	Displacement at peak load (mm)	Total displacement (mm)	Time at peak load (msec)	Total time (msec)	Energy absorbed to peak load (J)	Total energy absorbed (J)
KCK	2.20±0.07^{ef}	6.23±0.06^{bc}	8.03±0.38^{e}	1.32±0.03^{abc}	1.72±0.05^{d}	9.35±0.11^{efg}	11.47±0.23^{fgh}
KKC	1.82±0.04^{fg}	6.37±0.12^{ab}	8.20±0.20^{de}	1.36±0.02^{ab}	1.74±0.04^{d}	6.01±0.26^{fghi}	7.90±0.34^{ghij}
CKK	2.06±0.03^{ef}	3.55±0.23^{f}	7.66±0.15^{e}	0.75±0.07^{e}	1.63±0.03^{d}	3.96±0.24^{ghi}	9.73±1.20^{fghi}
CKC	2.78±0.24^{de}	4.20±0.75^{ef}	7.80±0.30^{e}	0.90±0.17^{de}	1.68±0.08^{d}	8.67±2.04^{efgh}	15.29±2.25^{ef}
CCK	4.46±0.13^{c}	4.50±0.17^{ef}	9.60±0.90^{bcd}	0.97±0.06^{de}	2.11±0.17^{bc}	13.57±1.37^{cde}	26.36±2.25^{bc}
KCC	4.14±0.78^{c}	7.10±0.40^{ab}	8.73±0.29^{cde}	1.56±0.08^{a}	1.92±0.08^{cd}	18.93±4.68^{bc}	22.83±4.50^{cd}
C	0.89±0.77^{h}	11.30±7.63^{a}	14.01±0.57^{b}	1.29±0.87^{de}	1.58±1.20^{e}	5.66±3.99^{ghi}	7.39±5.37^{ij}
CC	2.39±2.27^{ef}	6.60±6.67^{ab}	8.60±8.97^{cde}	1.42±1.44^{ab}	1.85±1.93^{bcd}	10.85±10.28^{def}	14.04±13.36^{fg}
CCC	5.93±6.27^{b}	4.30±4.67^{def}	7.60±7.87^{e}	0.90±0.99^{de}	1.64±1.69^{d}	17.61±20.38^{b}	28.77±31.31^{b}
KKK	0.77±0.78^{h}	3.90±4.03^{ef}	10.40±9.87^{bc}	0.84±0.85^{de}	2.25±2.08^{bc}	1.52±1.63^{i}	4.10±4.10^{j}
$[K]_9$	2.30±0.09^{ef}	5.90±0.17^{bcd}	12.33±0.57^{a}	1.27±0.04^{bc}	2.69±0.13^{a}	6.51±0.06^{fghi}	15.24±0.60^{ef}
CK	0.93±0.08^{gh}	6.97±0.67^{ab}	10.57±0.38^{b}	1.47±0.16^{ab}	2.26±0.09^{b}	3.72±0.62^{hi}	6.00±0.48^{hij}
$[CK]_2$	3.45±3.57^{cd}	6.40±6.20^{bc}	8.50±8.33^{de}	1.41±1.36^{ab}	1.87±1.83^{cd}	15.59±15.54^{bcd}	19.65±19.42^{de}
$[CK]_3$	7.90±0.76^{a}	4.93±0.25^{cde}	8.50±0.89^{cde}	1.05±0.05^{cd}	1.87±0.21^{cd}	26.42±1.18^{a}	43.66±2.76^{a}

* Means with same superscript letters in column are not significantly different at the ($P \geq 0.05$).
* Each result is the average value derived from three replicates

Table 4.21: Mean scores for hybrid and control samples on propagation energy, ductility index, specific energy absorbed and impact strength

Sample type	Propagation energy (J)	Ductility index	Specific energy absorbed to peak load (J/kg)	Specific total energy absorbed (J/kg)	Impact strength (kJ/m^2)
KCK	2.13 ± 0.34^{fg}	0.23 ± 0.04^{f}	2.28 ± 0.03^{abcd}	2.80 ± 0.06^{defg}	73.60 ± 0.85^{efg}
KKC	1.88 ± 0.09^{fg}	0.31 ± 0.01^{ef}	1.47 ± 0.06^{efgh}	1.93 ± 0.08^{hi}	47.34 ± 2.01^{fghi}
CKK	5.77 ± 1.42^{def}	1.47 ± 0.43^{ab}	0.97 ± 0.06^{hi}	2.37 ± 0.29^{fgh}	31.17 ± 1.92^{ghi}
CKC	6.61 ± 2.09^{de}	0.82 ± 0.40^{cde}	1.26 ± 0.29^{fghi}	2.22 ± 0.33^{ghi}	68.30 ± 16.03^{efgh}
CCK	12.79 ± 1.54^{b}	0.95 ± 0.13^{bcd}	1.97 ± 0.20^{bcdef}	3.82 ± 0.33^{bc}	106.85 ± 10.77^{cde}
KCC	3.90 ± 0.39^{efg}	0.22 ± 0.07^{f}	2.74 ± 0.68^{a}	3.31 ± 0.65^{cd}	149.03 ± 36.85^{bc}
C	1.38 ± 0.39^{g}	0.35 ± 0.11^{ef}	1.17 ± 0.08^{ghi}	1.58 ± 0.05^{ij}	31.42 ± 2.01^{ghi}
CC	3.08 ± 0.19^{efg}	0.23 ± 0.00^{f}	1.87 ± 0.15^{cdefg}	2.43 ± 0.19^{efgh}	80.96 ± 6.65^{def}
CCC	10.94 ± 1.86^{bc}	0.56 ± 0.18^{def}	2.08 ± 0.42^{abcde}	3.20 ± 0.27^{cde}	160.44 ± 32.58^{b}
KKK	2.47 ± 0.12^{fg}	1.52 ± 0.15^{a}	1.63 ± 0.09^{defgh}	4.10 ± 0.09^{b}	12.82 ± 0.74^{i}
$[K]_9$	8.73 ± 0.64^{cd}	1.34 ± 0.11^{abc}	2.60 ± 0.02^{ab}	6.10 ± 0.24^{a}	51.25 ± 0.44^{fghi}
CK	2.29 ± 0.43^{fg}	0.63 ± 0.19^{def}	0.69 ± 0.12^{i}	1.11 ± 0.09^{j}	29.28 ± 4.89^{hi}
$[CK]_2$	3.88 ± 0.38^{efg}	0.25 ± 0.03^{ef}	2.51 ± 0.04^{abc}	3.13 ± 0.04^{cdef}	122.35 ± 2.07^{bcd}
$[CK]_3$	17.24 ± 3.37^{a}	0.66 ± 0.15^{def}	2.34 ± 0.10^{abcd}	3.86 ± 0.24^{bc}	208.07 ± 9.28^{a}

* Means with same superscript letters in column are not significantly different at the ($P\geq0.05$).
* Each result is the average value derived from three replicates

Coir composite imparts stiffness with high peak load. Coir/Kevlar hybrid in an increasing layer of intraply formation had insignificant difference in deformation before failure in comparison with the three layers coir composite, as it exhibited almost the same trend as displayed in Figure 4.22. For instance, the deformation of the backing material in armour products has certain limit to avoid injury to the human body resulting from the impact of a bullet. To pass the Level III A NIJ Standard, the back face deformation or so called the Back Face Signature (BFS) may not exceed 44 mm (Sinnppoo et al., 2009). The maximum deflection in this particular study did not exceed 12 mm, which was obtained by the nine layers of Kevlar laminate.

In comparing the coir/Kevlar interply hybrid composite with CSs and intraply hybrid, it was found that the combinations of the two types of fibres (coir and Kevlar) in an interply formation resulted in balanced properties. CCK hybrid composite demonstrated high peak load with the total displacement to perforation equal to that of the three laminate layers of Kevlar composite. However, the thickness was markedly low compared to the three laminate layers of coir and intraply hybrid samples. The red-dotted lines gave clear indication of CCK's peak load and total displacement.

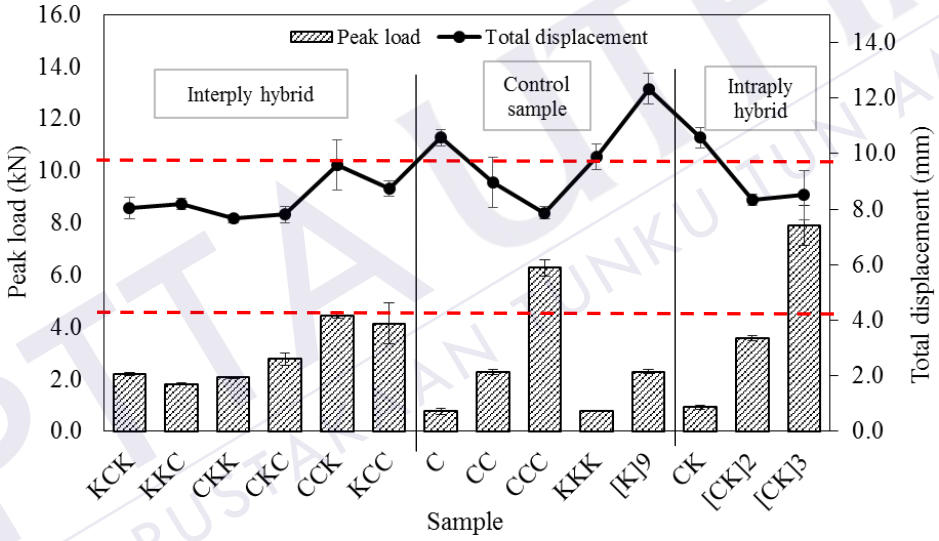

Figure 4.22: Peak load and total displacement of hybrid and control samples

Figure 4.23 reveals the trend of impact strength and total time for hybrid and control samples. Based on the results, the impact strength increased as the laminated layers increased. The improvement could be due to the increment in thickness, so that the applied stress could be transferred more effectively due to larger total fibre surface area being in contact with the matrix (Wong et al., 2010). The impact strength for coir composites was also better compared to Kevlar composite, again proving that coir composites exhibited greater toughness than the composites.

Although the incorporation of Kevlar yarns in coir in intraply hybrid improved the impact strength, the process created thicker composites compared to the interply hybrid. The red-dotted line represents the optimum properties exhibited by the interply hybrid composites. It was clearly seen that the impact strength of KCC was comparable to that of CCC at reduced thickness and weight. Besides, the impact strength of KCC was almost 200% higher than the nine layers Kevlar laminate. However, it was noticed that the thickness and areal density of KCC were 172% and 176%, respectively, higher than those of KKK.

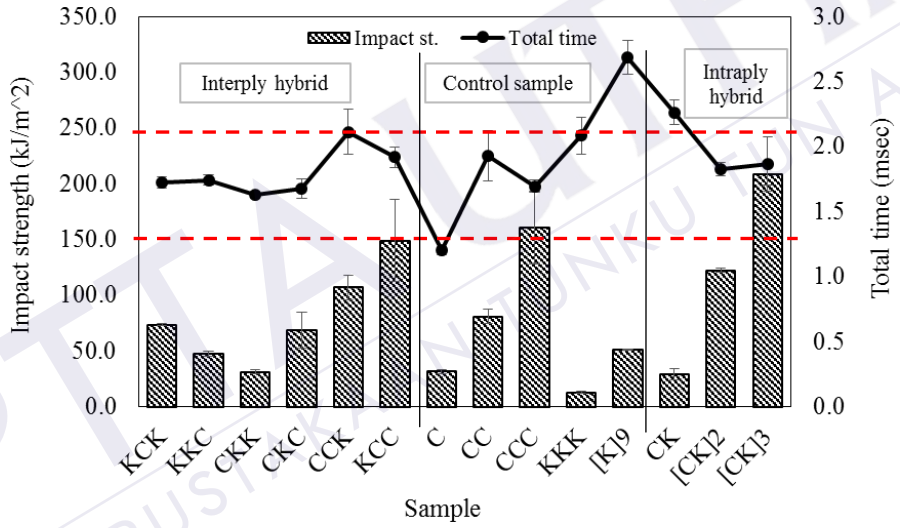

Figure 4.23: Impact strength and total time of hybrid and control samples

In general, there was variation in the total time taken before a full penetration occurred. It was anticipated that Kevlar laminated composites were capable of delaying composites perforation by deforming the structure. The interply hybrid of coir and Kevlar fabric showed a good trade-off where the results showed that KCC and CCK structures exhibited higher impact strength than the nine laminated layer of

Kevlar composite. The total time to perforation of CCK and KKK also showed similar values, which was better than that of CCC (denoted by the red-dotted line).

Figure 4.24 depicts the propagation energy and ductility index of coir/Kevlar hybrid composite and control samples. It was predominantly observed that energy propagation increased with increasing laminate layers in control and intraply hybrid samples. Low propagation energy was recorded for Kevlar laminates. It has been well documented by Reis et al. (2012) that the force-time traces of Kevlar/epoxy composites exhibit a linear curve to the point of peak force before it drops suddenly. Propagation energy is termed as the energy absorbed after the peak load. Therefore, least energy propagation was anticipated in Kevlar laminates. The insertion of only a single woven Kevlar layer in two coir layers demonstrated a substantial rise in energy propagation. The red-dotted line indicates energy propagation for CCK. It was, in fact, higher than that of the three laminates layer of coir at reduced weight and thickness. Although the three layers of intraply hybrid CK demonstrated the highest propagation energy, the samples thickness and weight almost doubled than those of interply CCK. Hence, interply hybrid was more favourable. Higher propagation energy is a primary concern, especially in aeronautic design industry as it helps delaying the total failure and fracture after an impact (Quaresimin et al., 2013).

Ductility index (DI) is useful for ranking the impact performance of different materials under similar testing condition. DI value indicates the efficiency in hindering crack propagation (Pegoretti et al., 2004). The DI are summarized in Figure 4.24 and show a great difference between 100% Kevlar composites and 100%

coir composites. The results showed that DI for three layers Kevlar laminate was 171% higher than that of the three layers of coir laminates. However, DI is not dependent on laminate thickness because variation in DI was observed in samples with different laminate layers. DI is defined as the ratio between the propagation energy (Ep) and the initiation energy (Ei). A low DI is an indication of a brittle material (Gowda et al., 1999), which was apparent in the coir laminate composite.

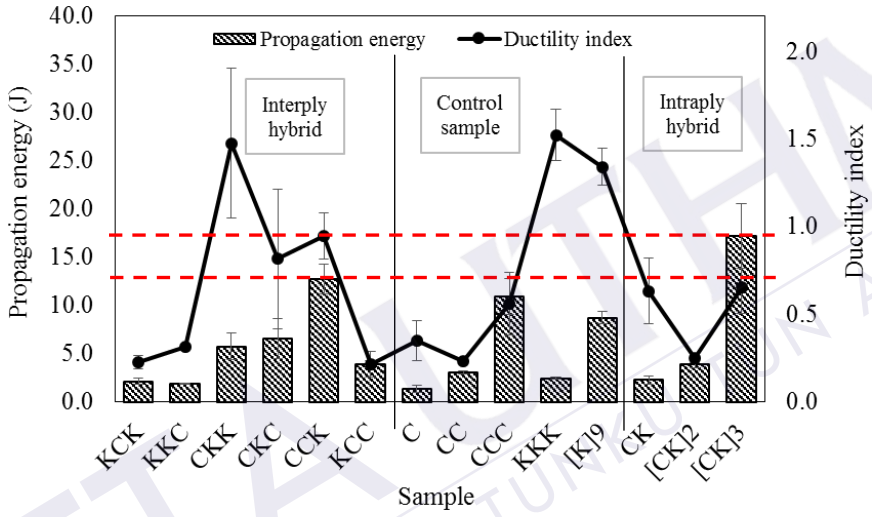

Figure 4.24: Propagation energy and ductility index of hybrid and control samples

The resistance to impact crack propagation was higher in laminates with higher percentage of Kevlar fibres, as evidenced by their DI values. A similar observation was reported by Cantwell and Morton (1991), where they found that the DI value for Kevlar composites was superior to that of the E-glass and carbon composites. Meanwhile, it is interesting to notice that the incorporation of Kevlar fabric layer to the coir with respect to interply hybrid was capable to increase the DI value to about 70% in CCK compared to that of the three layers of coir laminates (represented by the dotted red line). Pegoretti et al. (2004), agreed that hybridizing fibres in a composite system helps to improve the resistance to impact crack propagation.

Improvement in impact strength characterizes reinforcement fibres as a stress transferring medium that can absorb more impact energy effectively (Wong et al., 2010). The absorption capability of a composite structure is described as the specific energy absorption (energy per unit weight), which allows the performances of different components to be classified and compared (Quaresimin et al., 2013). Figure 4.25 represents the specific energy absorption (SEA) comparisons for different types of interply and intraply hybrids with control samples. The SEA at peak load for 100% coir performed better than 100% Kevlar control samples. However, if the total SEA was concerned, Kevlar outperformed coir composites with significant difference compared to its SEA at peak load. This condition was expected because Kevlar composites were more capable of resisting crack propagation as portrayed in their DI value.

The incorporation of Kevlar fibre in two layers intraply hybrid composite did not display any significant improvement compared to the three layers of coir composite. Nonetheless, the three layers intraply CK hybrid had the same total SEA with the three layers of Kevlar composite, and the total SEA was about 21% more than that of CCC. It was interesting to note that the total SEA for CCK interply hybrid composite was comparable to that of the three layers Kevlar laminates and three layers of intraply CK hybrid (represented by the red dotted line). CCK gained more attention as it had high SEA value with lower thickness compared to $[CK]_3$.

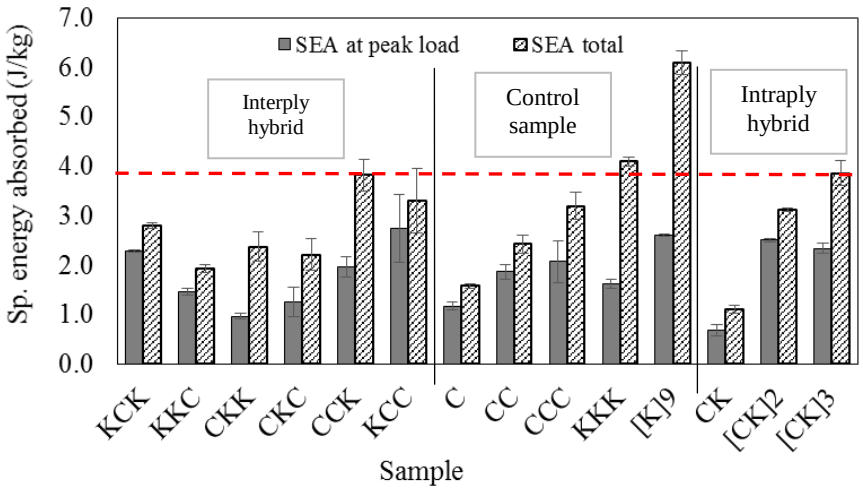

Figure 4.25: Specific energy absorbed to peak load and specific total energy absorbed of hybrid and control samples

4.3.2.4 Effects of different impact incident rates on hybrid composites

Two of the interply hybrid composites (CCK and KCC) that had optimum impact response were tested under transverse impact loading at four different loading rates; 5, 9,13 and 17 m/s, corresponding to four different energy levels. This procedure was performed to provide an insight into the effects of rate on novel coir/Kevlar hybrid composites. Transient responses for load, displacement, energy absorbed and time were recorded. The responses were plotted based on representative samples at each speed level.

The load-displacement traces for CCK and KCC composites are shown in Figure 4.26 (a) and (b). It was observed that the maximum peak load for CCK and KCC happened at almost the same displacement level, although for varying incident rates. As for CCK, it could be said that the maximum peak load and total deflection were dependent on the rate where both responses increased with increasing speed rate. A more complex observation was detected in KCC, where a slight drop in the maximum peak load was noticed at 9 m/s, and at above 9 m/s, the peak load was

almost constant. This condition was similar to the findings by Atas and Sayman (2008) who conducted experiment on E-glass laminated composite. On the other hand, panels impacted at 5 m/s and 9 m/s showed fewer load oscillations compared to the panels impacted at a speed higher than 9 m/s, which indicates that specimens impacted at higher velocity resulted in significant internal damages.

(a)

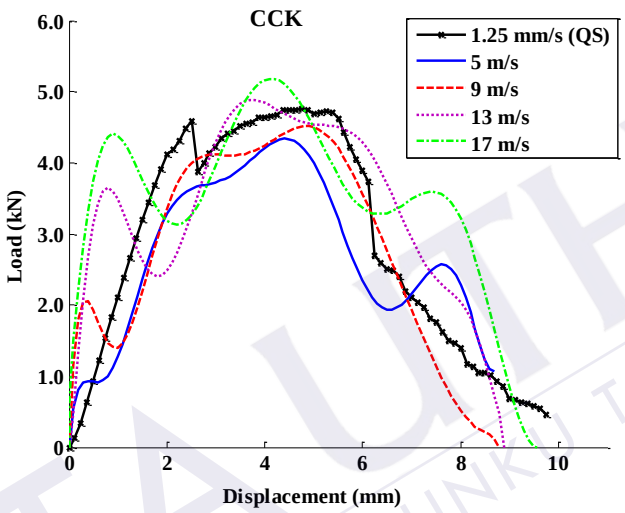

(b)

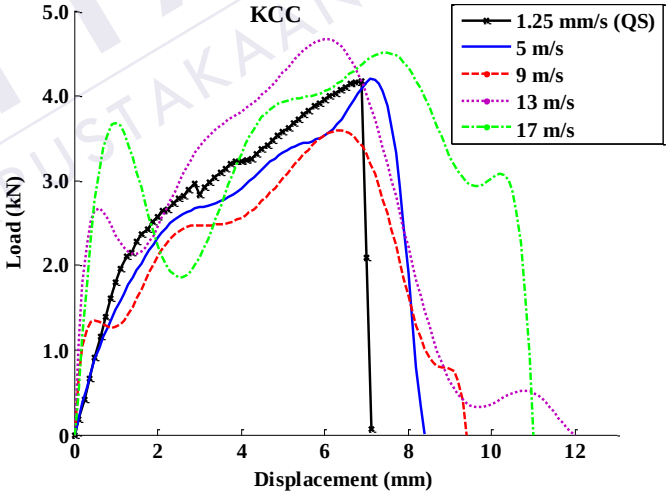

Figure 4.26: Load-displacement curve of; (a) CCK and (b) KCC at different incident rates

Both CCK and KCC samples had almost consistent ascending load trend at low velocity impact (<10 m/s). However, different trends were observed as the

impact speed increased. Higher incipient damage was detected as greater load oscillations were observed. It was expected that the panels needed higher internal fracture energy to resist higher imposed impact energy. Therefore, combinations of failure mechanisms were discovered from the load-displacement traces as indicated by load wavering. It was also revealed that both CCK and KKC lost their toughness in the earlier stage when they were impacted at higher speed (> 9m/s), whereby earlier major load drop was noticed from the traces. The issues had been well discussed by Mantena et al. (2001), in which they explained that the stress wave effect is minimal in low velocity impact (< 10 m/s), thus resulting in delayed incipient damage. The overall results permit to say that, at least for the considered materials and the range of impact speed, hybrid CCK and KCC had sensitivity towards the strain-rate effect, especially at higher impact velocity.

Traces of energy absorbed versus time for CCK and KCC hybrid panels at various incident rates, calculated from the associated load-displacement curves, are given in Figures 4.27 (a) and (b). It was observed that the amount of energy transferred from the impactor to the composite specimens at the end of impact (energy absorbed) increased with time for both types of panel. It was also noticed that higher impact speed, which corresponds to higher energy level, resulted in the increment in total energy absorbed. The time to total energy absorbed on the other hand decreased with increasing energy level. This relationship was expected, as it was also observed in other materials tested at different energy levels such as in previous works by Hosur et al. (2005), Atas and Sayman (2008) and Dhakal et al. (2012). Hosur et al. (2005) conducted a low velocity impact analysis on woven hybrid (carbon/glass) composite, whereas Atas and Sayman (2008) on did it on E-

glass laminated composite. Meanwhile, Dhakal et al. (2012) investigated the impact response of various velocities of non-woven hemp fibre reinforced unsaturated polyester composites. A sudden increase in energy absorbed as the speed increases implies a significant unstable damage in the panel (Atas and Sayman, 2008). Such a sudden damage results in a steep loss in contact load as shown in Figure 4.26.

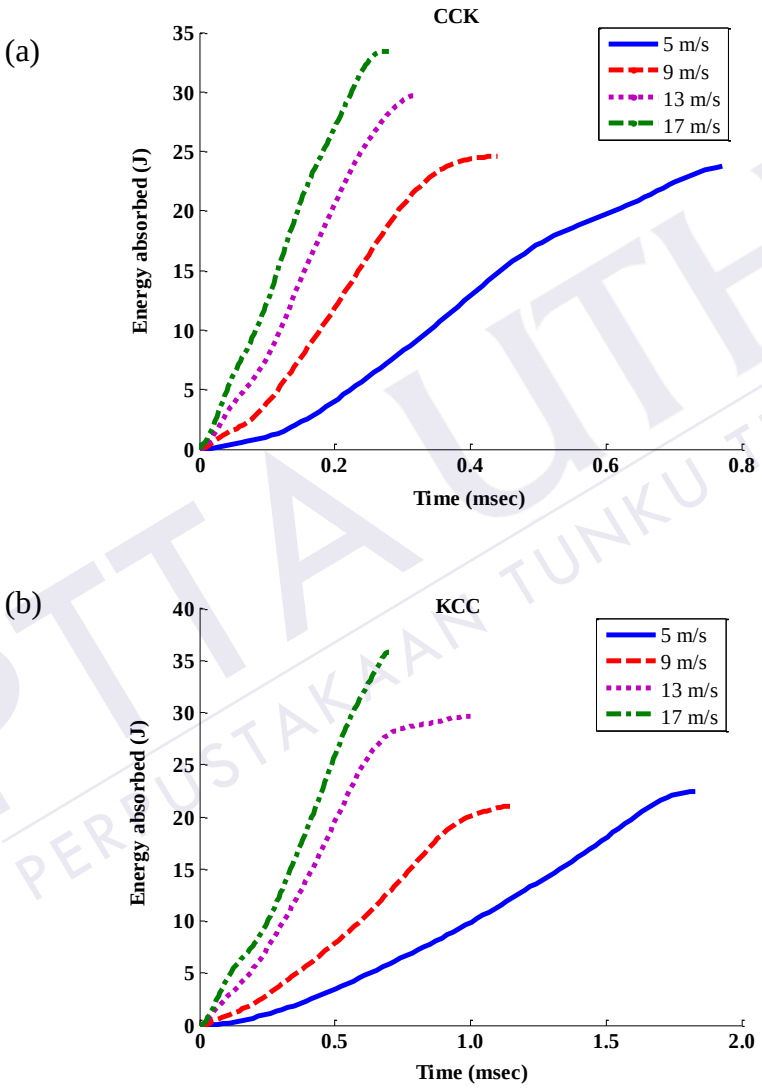

Figure 4.27: Energy absorbed-time curve of; (a) CCK and (b) KCC at different incident rates

Table 4.22 and Table 4.23 summarize the mean value of the impact responses of CCK and KCC with respect to different impact speeds. The same superscripts in each column indicate that there was no significant difference in the value based on the TGRT results. Some of the important impact response data were presented graphically to assist in better interpretation. ANOVA results proved that the difference in impact speed had a significant effect (P-value<0.05) on the impact response in term of peak load, total displacement, total time, propagation energy, ductility index and specific total energy absorbed, whereas for impact strength, the difference in impact speed showed very minimal effects (P-value>0.05).

Figure 4.28 illustrates the interaction plots of impact response at different impact incident rates. As shown in Figure 4.28 (a), the peak load for CCK was constant for impact speed below 9 m/s. However, the peak load for CCK increased with increasing impact speed above 9 m/s. A dissimilar observation was found in KCC. Declining peak load was observed in specimens tested at 9 m/s and 17 m/s. The total displacement before perforation (Figure 4.28 (b)) on the interply hybrid specimen was found to be rate dependent. As the impact speed increased, the total displacement increased as well. Nevertheless, it was noticed that the total displacement value for CCK tested at 5 m/s was reaching the 13 m/s value. This condition was expected due to the relaxation phenomenon in specimens tested at low velocity. Figure 4.28 (c) represents the total time to full penetration for both CCK and KCC. Both specimens performed as anticipated. The time taken decreased as the impact speed increased.

Table 4.22: Mean scores for CCK and KCC on impact response at different incident rates

Sample type	Peak load (kN)	Displacement at peak load (mm)	Total displacement (mm)	Time at peak load (msec)	Total time (msec)	Energy absorbed to peak load (J)	Total energy absorbed (J)
CCK-5	4.46±0.13^{ab}	4.50±0.17^{cd}	9.60±0.90^{bc}	0.97±0.06^{b}	2.11±0.17^{a}	13.57±1.37^{a}	26.36±2.25^{abcd}
CCK-9	4.45±0.33^{ab}	4.63±1.26^{bcd}	8.30±0.46^{c}	0.57±0.15^{cd}	1.02±0.05^{bc}	14.62±5.84^{a}	24.16±2.60^{bcd}
CCK-13	4.94±0.24^{a}	4.33±0.06^{d}	9.63±0.32^{bc}	0.35±0.01^{d}	0.80±0.03^{cd}	12.42±0.23^{a}	30.40±1.81^{ab}
CCK-17	5.05±0.52^{a}	5.37±0.35^{abcd}	10.93±0.90^{ab}	0.33±0.04^{d}	0.68±0.07^{d}	15.67±0.45^{a}	32.36±2.80^{a}
KCC-5	4.14±0.78^{ab}	7.10±0.40^{a}	8.73±0.29^{c}	1.56±0.08^{a}	1.92±0.08^{a}	18.93±4.68^{a}	22.83±4.50^{cd}
KCC-9	3.64±0.17^{b}	6.43±0.15^{ab}	9.47±0.80^{bc}	0.68±0.16^{c}	1.16±0.10^{b}	15.30±0.15^{a}	20.83±0.46^{d}
KCC-13	4.72±0.09^{a}	6.37±0.55^{abc}	11.93±1.10^{a}	0.52±0.04^{cd}	0.99±0.09^{bc}	19.25±2.10^{a}	29.76±0.38^{abc}
KCC-17	4.30±0.19^{ab}	7.00±1.21^{a}	11.80±0.80^{a}	0.41±0.07^{d}	0.70±0.05^{d}	17.73±5.69^{a}	32.21±3.62^{a}

* Means with same superscript letters in column are not significantly different at the (P≥0.05).
* Each result is the average value derived from three replicates

Table 4.23: Mean scores for CCK and KCC on propagation energy, ductility index, specific energy absorbed and impact strength at different incident rates

Sample type	Propagation energy (J)	Ductility index	Specific energy absorbed to peak load (J/kg)	Specific total energy absorbed (J/kg)	Impact strength (kJ/m^2)
CCK-5	12.79 ± 1.54^{abc}	0.95 ± 0.13^{abc}	1.97 ± 0.20^{a}	3.82 ± 0.33^{abcd}	106.85 ± 10.77^{a}
CCK-9	9.54 ± 3.24^{cde}	0.82 ± 0.64^{abc}	2.12 ± 0.85^{a}	3.50 ± 0.38^{bcd}	115.13 ± 45.95^{a}
CCK-13	17.98 ± 1.59^{a}	1.45 ± 0.10^{a}	1.80 ± 0.03^{a}	4.41 ± 0.26^{ab}	97.77 ± 1.80^{a}
CCK-17	16.69 ± 2.97^{ab}	1.07 ± 0.21^{ab}	2.27 ± 0.06^{a}	4.69 ± 0.41^{a}	123.37 ± 3.53^{a}
KCC-5	3.90 ± 0.39^{e}	0.22 ± 0.07^{c}	2.74 ± 0.68^{a}	3.31 ± 0.65^{cd}	149.03 ± 36.85^{a}
KCC-9	5.53 ± 0.50^{de}	0.36 ± 0.03^{bc}	2.22 ± 0.02^{a}	3.02 ± 0.07^{d}	120.50 ± 1.19^{a}
KCC-13	10.52 ± 2.47^{bcd}	0.56 ± 0.20^{bc}	2.79 ± 0.30^{a}	4.31 ± 0.06^{abc}	151.56 ± 16.50^{a}
KCC-17	14.48 ± 2.97^{abc}	0.89 ± 0.37^{abc}	2.57 ± 0.83^{a}	4.67 ± 0.53^{a}	139.58 ± 44.83^{a}

* Means with same superscript letters in column are not significantly different at the ($P\geq0.05$).
* Each result is the average value derived from three replicates

Propagation energy (Figure 4.28 (d)) and ductility index (Figure 4.28 (e)) showed similar trend for both CCK and KCC. It was seen that KCC demonstrated linear increments in both responses with respect to increasing impact speed. Meanwhile, slight reductions in propagation energy and ductility index were exhibited by CCK at 9 m/s and 17 m/s. This circumstance might relate to its failure processes and mechanisms, which will be discussed in further section. It was noticed that the value might be overestimated due to these reasons (Wang et al., 2008).

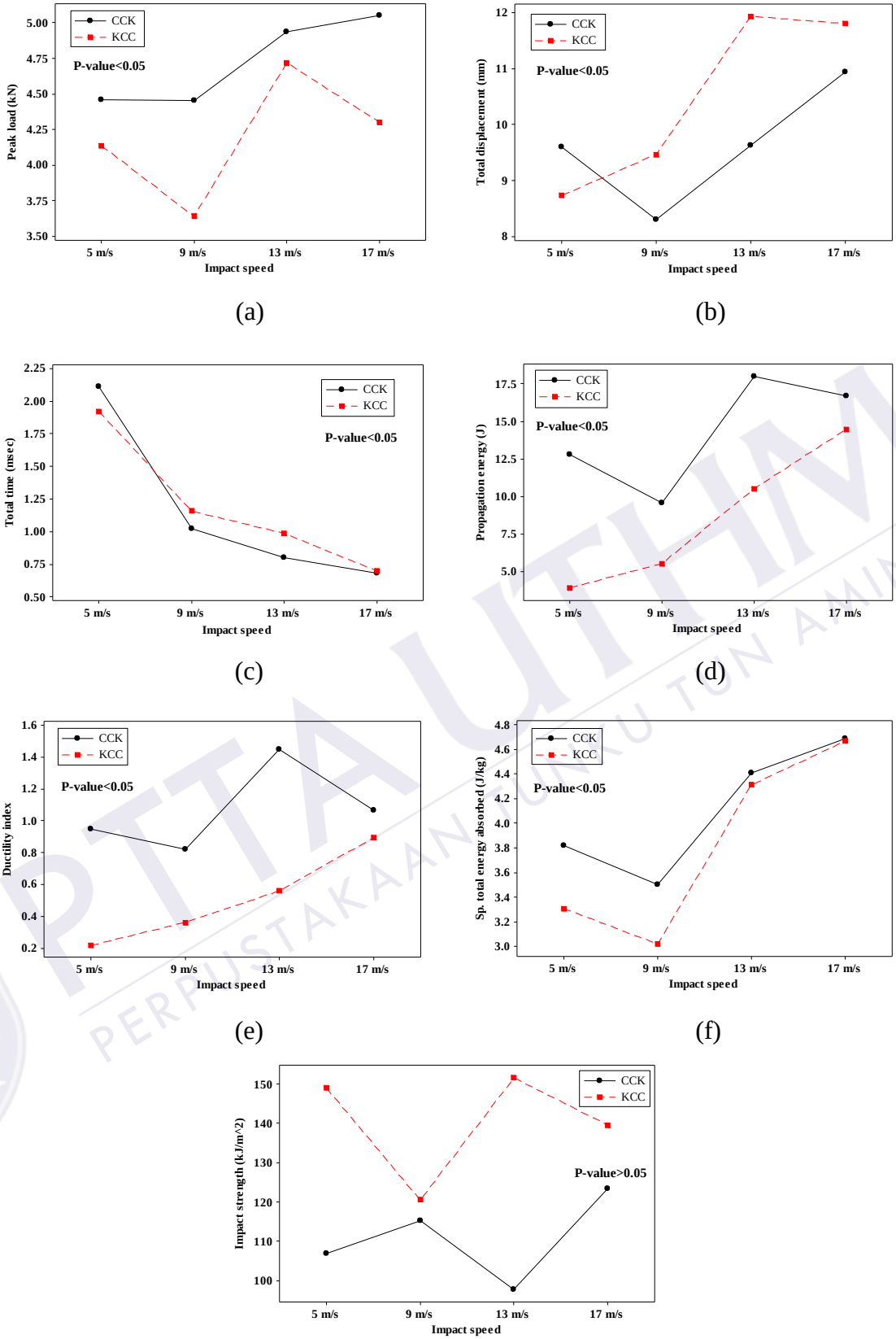

Figure 4.28: Interactions plot of impact response of CCK and KCC at different incident rates

At 9 m/s, the specific total energy absorbed (total SEA) for CCK and KCC increased with increasing impact speed (refer Figure 4.28 (f)). A similar observation was reported by Reis et al. (2012) who studied the effects of different incident rates on the Kevlar composites with filled epoxy matrix. Our results also compared well with a previous work (Kilic, 2008), which indicated that the amount of energy absorbed in laminated and sandwich composites increased with increasing impactor speed. Initially, based on the literature study, any speed below 10 m/s was categorized as low-velocity impact, whereas some defined an impact speed above 10 m/s as high or medium velocity impact. Thus, it was expected that speed transition may affect composites relaxation, which resulted in overestimating energy absorption as obtained by the specimens tested at 5 m/s. A certain amount of elastic energy may be stored in the specimen prior to failure due to this relaxation phenomenon. The dissipation of energy can occur acoustically, thermally or in the form of kinetic energy of the failed parts, which delays the process (Wang et al., 2008).

4.3.2.5 Damage assessment and morphology analysis

The fracture area of the particular interply hybrid and control samples impacted at 5 m/s are depicted in Figure 4.29. It is clearly seen from the graph that the front surface of the impacted panel exhibited low fracture area. Most of the rear fractured area of the samples was extremely high compared to the front fracture. CKK and KKK, however, exhibited only slight differences on both surfaces. As for the front surface fracture, samples having Kevlar layer on top demonstrated slightly larger damage compared to samples with coir layer on top. Table 4.24 which illustrates the visual damage of the front, rear and cross-section surfaces of the

impacted samples are significant. The damage area on the front face of the laminate resulted from the direct contact between the impactor and the samples, whereas the damage area on the rear face was due to damage propagation in order to absorb the energy transferred to the laminate. It is obviously seen from Table 4.24 that signs of inter-layer splitting was present in KCK, KKC and KCC (indicated by the bright yellowish colour). On the other hand a clean fracture area with the size of the impactor tip was noticeable in other types of sample. The same method of identifying the splitting boundaries was adopted by Icten and Karakuzu (2008) and Aktas et al. (2010) who conducted an impact behaviour study on woven laminated E-glass-epoxy composite plate. Darker boundary region was not considered as splitting damage.

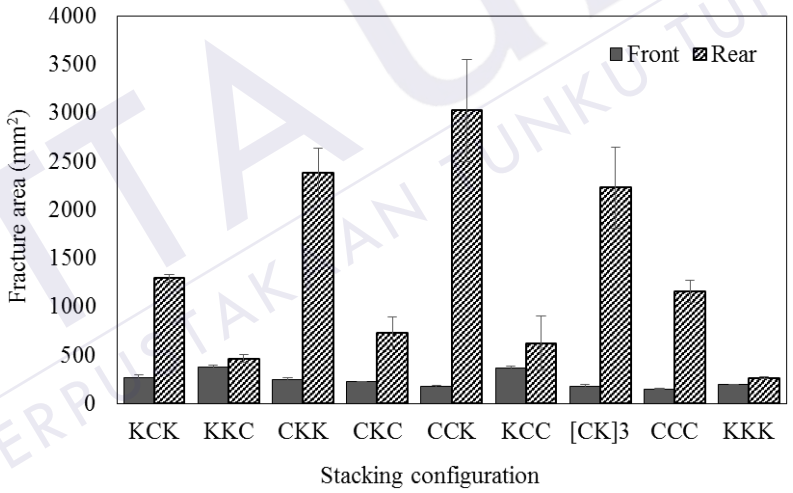

Figure 4.29: Fractured area (front and rear surface) of different hybrid composite and control samples impacted at 5 m/s

Meanwhile, on the rear impacted surfaces (refer to Figure 4.29), CCK exhibited the worst damaged area, followed by CKK and $[CK]_3$, KCK and CCC. The rest of the samples displayed considerably low rear fracture area of less than 750 mm^2. It was visible that Kevlar layer placed at the back of the samples exhibited serious delamination. The delamination part was included in the calculation of the

damaged area. Table 4.24 portrays these conditions, where it was apparent that KCK, CKK and CCK experienced severe inter-layer splitting as indicated by the bright yellow shading on the surface. KKC, CKC and KCC on the other hand, experienced segmented fracture with more yarn breakage, which contributed to the growing crack. The results were consistent with the peak load in most of the load-displacement curves displayed in the previous section where initial peak indicated initial damage and the following peak denoted crack growth. The placement of coir fabric layer on the rear face contributed to larger crack size. Severe crack size is experienced by most natural fibre composites (Jawaid and Abdul Khalil, 2011). Hemp fibre composite suffers significant crack growth upon impact as reported in Dhakal et al. (2012). Therefore, hybridization is an effective method to enhance damage resistance and tolerance.

It can be concluded that beyond the threshold energy value, impact energy was absorbed through a severe fibre break and matrix crack in samples with coir layer at the back. Whereas, for samples with Kevlar layer at the back, the failure mode was more toward interply splitting (leading to large delamination) and minor Kevlar fibre break. Hybridization of woven coir and Kevlar layer in specific configurations such as in KCC, CKC and KKC significantly improved the impact damage drawback occurring in 100% coir composite.

Table 4.24: Impact damage (front, back and cross-section surfaces) observed for panels impacted at 5 m/s

Visual damage		
Front surface	Rear surface	Cross-section surface
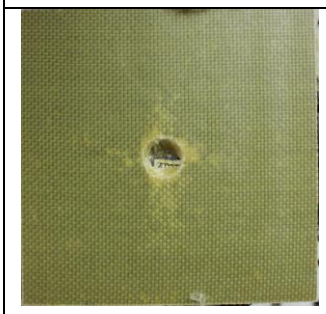		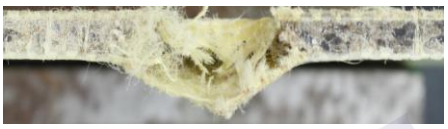
(a) KCK		
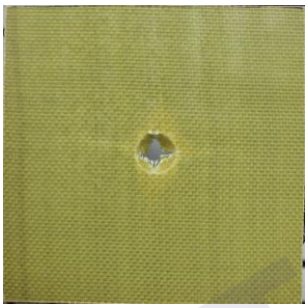	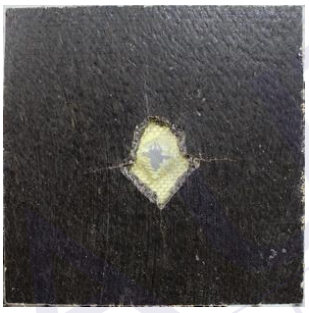	
(b) KKC		
		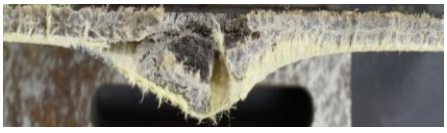
(c) CKK		
		
(d) CKC		

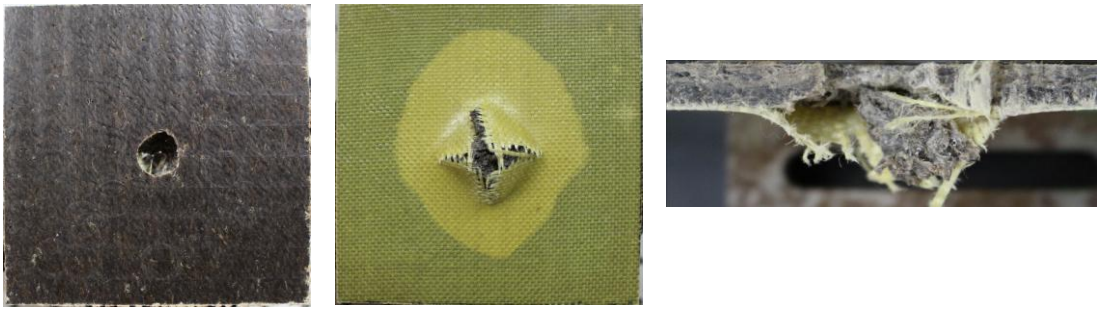

(e) CCK

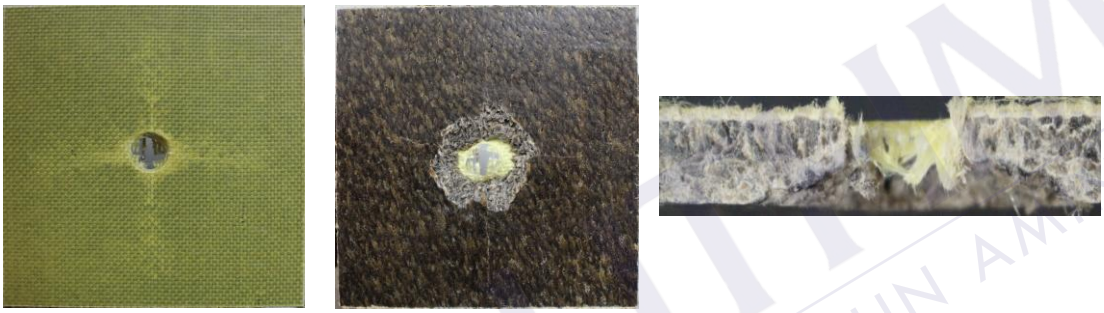

(f) KCC

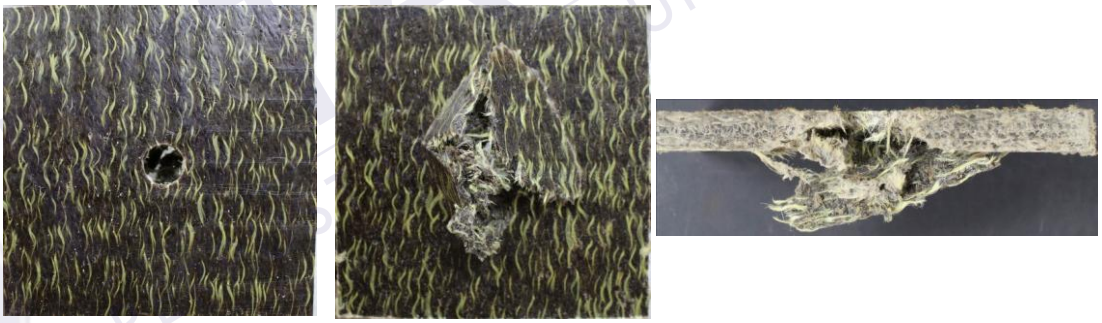

(g) $[CK]_3$

(h) CCC

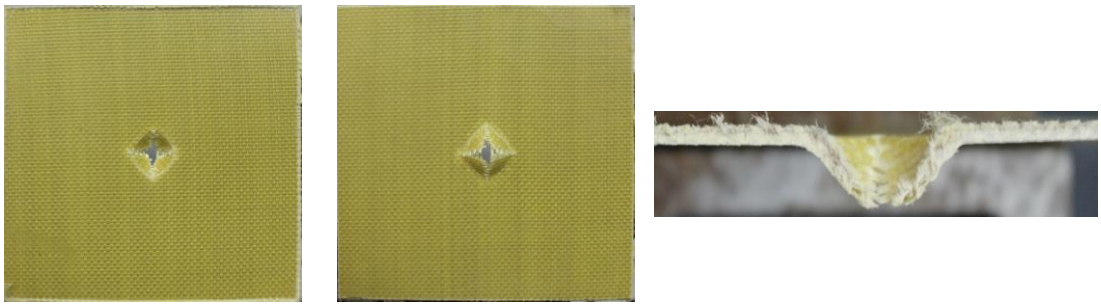

(i) KKK

Kevlar yarns as assessed in Section 4.1 indicates that it has superior tensile strength and modulus compared to coir yarn. Therefore, it was anticipated that Kevlar ply experienced lower fibre break than the coir ply. This property is very important from the point of initiation of the back surface damage in the laminate. Damage initiation on the front face impacted samples was usually dominated by matrix crack. Matrix crack initiates as either tensile or shear crack (Hosur et al., 2005). The crack will be initiated transverse to the fibres within a ply. They will propagate through the thickness and will cut through the fibres in the warp and the weft directions. If the energy available is high enough to fracture the fibre tow in a woven structure, the growth of the crack can be arrested. As a result, delamination initiation and progression will be inhibited.

In the present study, more energy was needed to penetrate through the woven Kevlar layer. Therefore, delamination damage was more apparent. Moreover, Daihua (2007) added that delaminations are enhanced by the ply stiffness mismatch. The extent of delamination depends on the portion of impact energy available to fracture the interface. Generations and propagations of a series of delaminations leads to a reduction in residual properties. Consequently, it could be seen that the impact strength of samples with higher delaminations as in KCK, CKK and CCK were much

lower. As in the case of samples having coir layer on the outer back surface, lower energy was needed to fracture the samples. Therefore, delamination could be controlled. However, delaminations help in propagating energy to a larger area, hence resulting in an increased energy absorbed in the sample.

The cross-sectional images of the fractured surface in Table 4.24 give a clear indication of the creation of damage through various failure modes. The cone formation on the back face of the target materials was clearly visible in KCK, KKC, CKK, CCK, $[CK]_3$ and KKK. As the samples were being compressed and deflected by the tip of the impactor, the samples protruded to form a dome along the rim of the circular support. Obviously, interlayer debonding was also observed in samples having Kevlar layer at the back face. These deformation mechanisms (indentation, deflection and debonding) dissipated a significant amount of impact energy prior to perforation and penetration of the impacted panels. The indication of rear face splitting and penetration was depicted by a sharp drop in load after the peak load was reached, which also signified the ultimate load that the laminate could withstand. Intraply hybrid, $[CK]_3$, was good in preventing inter-layer splitting or delamination, as occuring in interply hybrid. However, serious extension of crack size was observed with the remaining fractures hanging, held by Kevlar yarns, which experienced less fibre break compared to coir yarn. Very few Kevlar yarns break was observed on each sample as indicated on the cross-sectional images of the surface. CKK and CCK samples also showed that the segmented fracture part of coir was arrested by Kevlar layer (at the back face of the samples) due to fewer Kevlar yarns break. All in all, it can be concluded that the types of failure depended on the material and the geometric properties of the target materials.

The effects of increasing impact incident rate (impact speed) to the composites damage area were evaluated, and the results are depicted in Figure 4.30. It was found that there was no significant difference in the damaged area with increasing impact speed for both front and rear faces. The results contradicted the research by Atas and Sayman (2008) and Daihua (2007), who mentioned that more severe damage on composite panels is predicted with increasing impact energy of the impactor. However, it was noted from their research that the target materials and the specimen's clamping guide shape were different. Zhang et al. (2008) had proven that different clamping frame types affect impact response and fracture damage. Therefore, different result is anticipated.

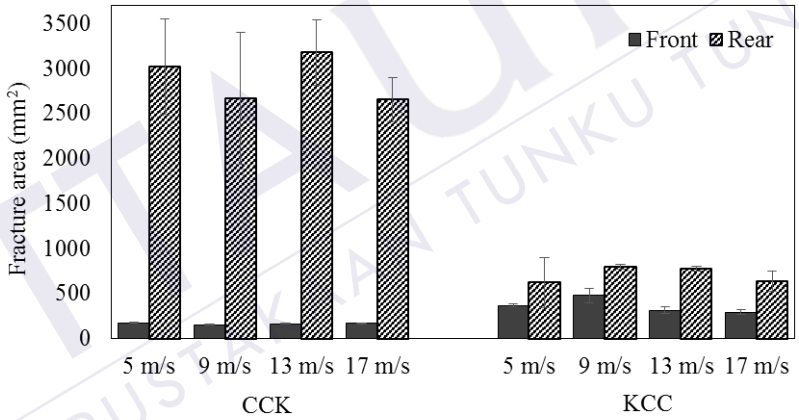

Figure 4.30: Fractured area (front and rear surface) of hybrid composite at different impact incident rates

There were various damage mechanisms resulting from the impact load as displayed visually. Figures 4.31, 4.32 and 4.33 show representative SEM images to identify these damage mechanisms that lead to structural failure. Figure 4.31 illustrates the SEM images of hybrid samples consisting of two plies of woven Kevlar and one ply of woven coir stacked in different configurations. It was observed that KCK, KKC and CKK samples experienced great fibre break and matrix crack on

coir lamina, whereas, only slight damage occurred on Kevlar lamina layer. The crack size propagated to a larger area on coir lamina as witnessed in KCK and KKC. Moreover, it was noticed that KCK and CKK samples, where there was Kevlar layer at the bottom surface exhibited inter-layer delamination. Bigger crack expansion was detected in samples having coir layer at the back.

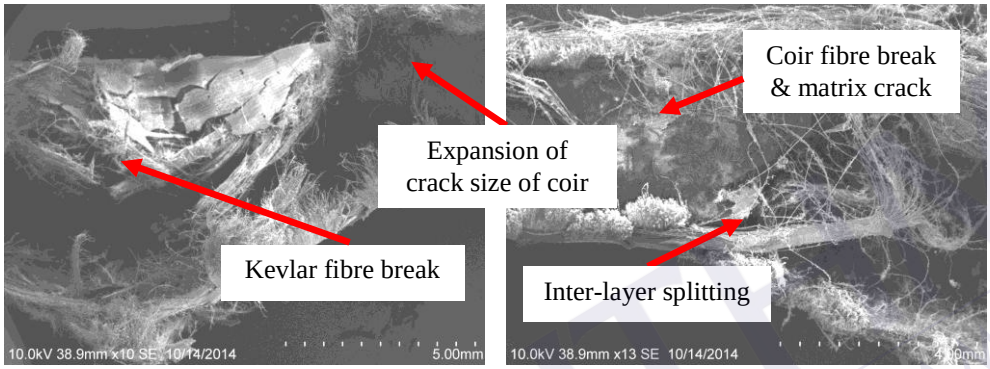

(a) KCK

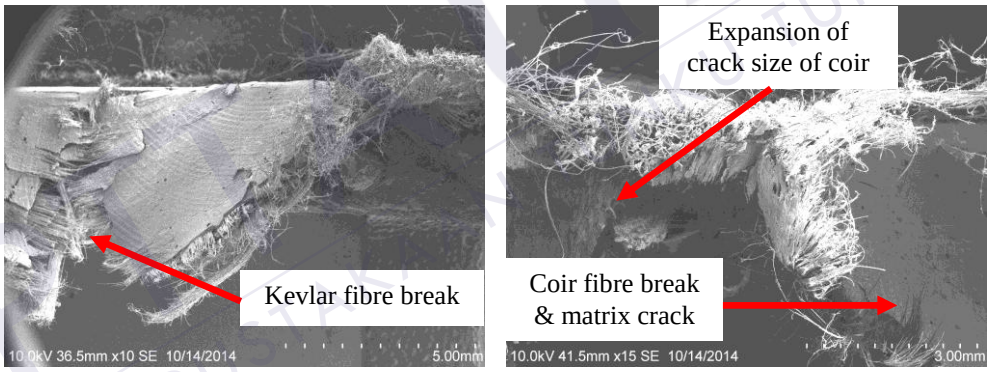

(b) KKC

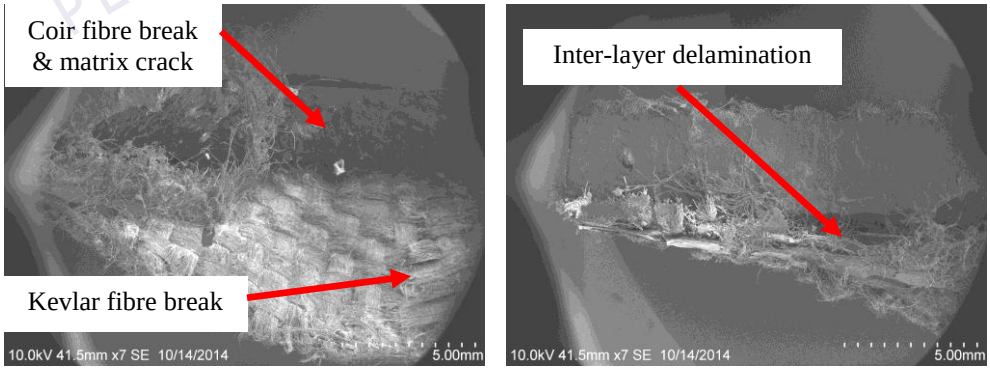

(c) CKK

Figure 4.31: SEM images of the cross-sectional fractured surfaces of; (a) KCK, (b) KKC and (c) CKK

Figure 4.32 shows the cross-sectional surface of fractured samples consisting of two layers of coir and one layer of Kevlar. Fibre break and matrix crack were the vital damage mechanisms on coir lamina. It can be seen that the expansion of crack size was increasingly bigger from front to rear faces of the sample. Penetration of impactor only caused minor fibre break to the Kevlar layer in the laminated composite. It was clearly seen in CKC samples where the Kevlar ply in the middle had less break compared to the coir plies. The placement of Kevlar at the back face of the composite caused bad delamination as shown in CCK. Good fibre-matrix adhesion was observed between woven coir layers as debonding was not visible at all.

Figure 4.33 demonstrates SEM images of the control samples. The images are expected to give a clearer indication of the damage mechanisms of each material. It was observed that the intraply hybrid $[CK]_3$ exhibited severe segmented fibre-matrix crack, which resulted in greater crack area. As for CCC, it was noticeable that the expansion of crack increased from top to bottom surfaces. Kevlar composites (KKK) on the other hand, resisted impact by the formation of dome and only slight fibre break was observed.

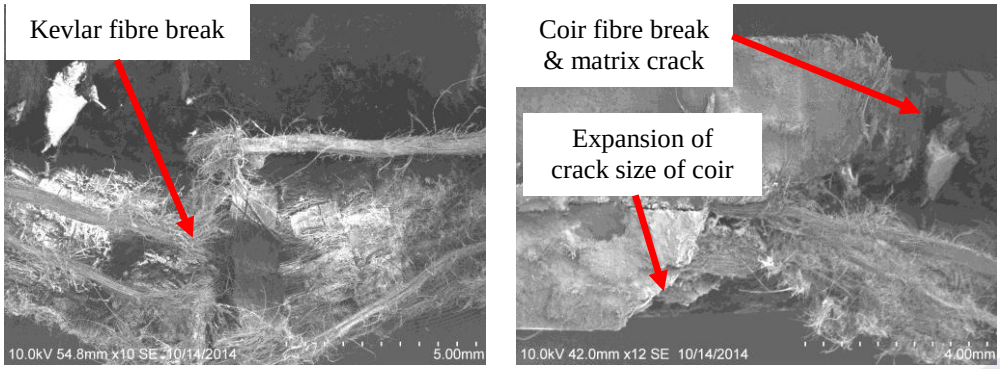

(a) CKC

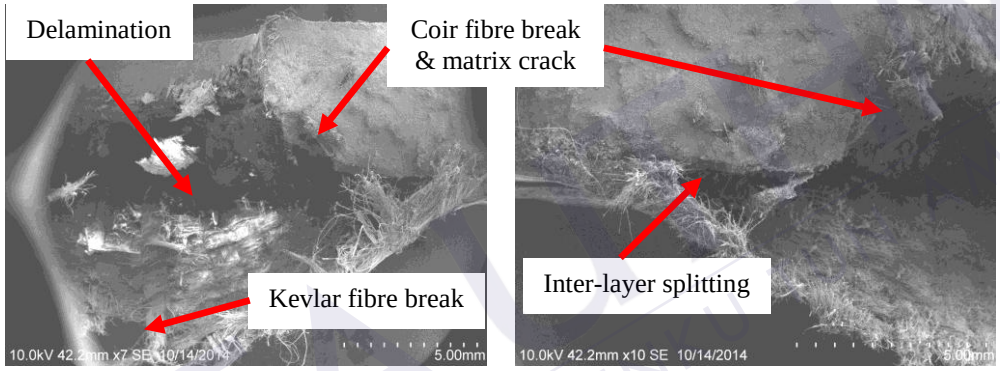

(b) CCK

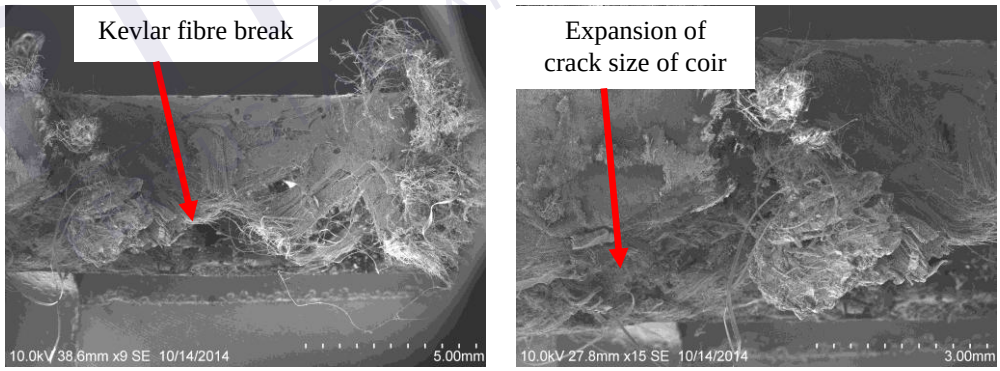

(c) KCC

Figure 4.32: SEM images of the cross-sectional fractured surfaces of; (a) CKC, (b) CCK and (c) KCC

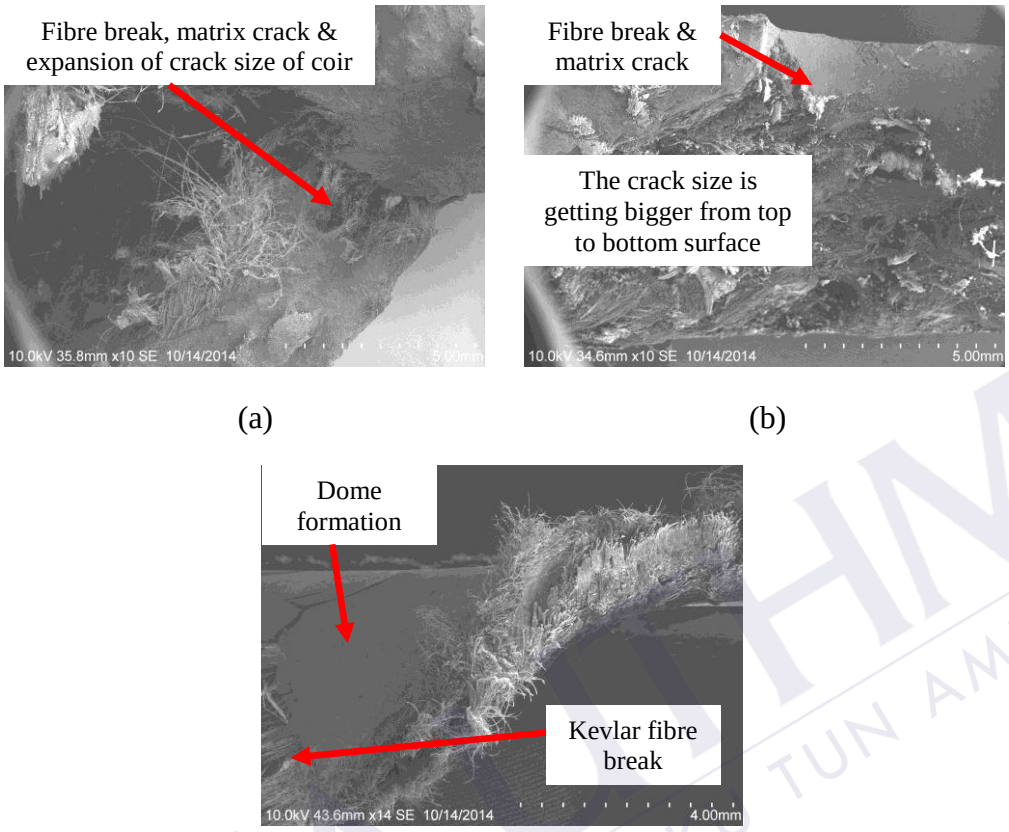

Figure 4.33: SEM images of the cross-sectional fractured surfaces of control sample; (a) $[CK]_3$, (b) CCC and (c) KKK

CHAPTER 5

CONCLUSION AND RECOMMENDATIONS

5.1 Conclusions

The specific findings and contributions of this thesis are summarized as follows:

(1) Woven structure exhibited greater propagation energy and specific total energy absorbed compared to cross-ply 0°/90° and angle-ply 45°/-45°. However, larger fracture area was observed on woven coir-epoxy composite structure.

(2) Woven coir-epoxy composite fabricated by the compression moulding method achieved higher peak load and better impact strength. Besides, they also promoted better fibre-matrix adhesion.

(3) Woven composite with more dense reinforcement structure (higher crimp percentage, lower porosity) exhibited lower peak load with high deflection upon penetration. The optimum deflection, specific energy absorbed and impact strength were achieved by the dense woven structure of coir composites at 6% NaOH treatment concentration. However, poor damage resistance was also observed.

(4) Modifying the stacking configuration of coir/Kevlar hybrid composites leads to improved impact properties. It was observed that the employment of two woven layers of coir as reinforcement in a three-layer interply hybrid coir/Kevlar composites resulted in an excellent impact response particularly

in term of peak load, total displacement, total time taken to full penetration, specific total energy absorbed and impact strength. It was interesting to note that the hybrid composite consisting of two woven coir layers with only one Kevlar layer had equivalent specific total energy absorption with 100% Kevlar laminate (at three layers).

(5) The load-displacement curve for the low velocity impact showed a good correlation with the quasi-static test conducted on coir/Kevlar hybrid laminate. Therefore, the validity of the low velocity impact test was undisputed. Total energy absorbed increased with increasing impact incident rate. The time to total energy absorbed on the other hand decreased with increasing energy level.

(6) Damage modes and tolerance of coir/Kevlar hybrid laminated structure can be greatly improved by varying its stacking configurations. It was observed that placing Kevlar layer at the front surface and coir layers at the back surface provided an optimal damage area on the composite panel. The increment in impact incident rate did not have any significant effect on the fracture area of the hybrid composite.

5.2 Recommendations for future works

Based on the results of this research, several recommendations for future work are suggested as follows, and further study is warranted.

(1) Further quasi-static and dynamic experimental testings at various range of speed can be undertaken. These additional results can be added to strengthen the present research findings.

(2) Further analysis can also be done for other impact conditions, material design and processing. Impactor shape, clamping geometry, thickness, matrix type and content, processing time, temperature and pressure during fabrication can be investigated as these factors may affect the energy absorption behaviour of the composite. The factors can be combined and DOE analysis can be performed for better results interpretation.

(3) A balanced plain woven coir structure should be considered in future works to ensure that there will be no extreme differences in the testing results. Therefore, in order to achieve a more balance warp and weft structures, the weaving device needs further improvement.

REFERENCES

Abou Nassif, G.A. (2012). Effect of weave structure and weft density on the physical and mechanical properties of micro polyester woven fabrics. Life Science Journal, 9(3), pp.1326–1331.

Abraham, T., Banik, K. and Karger-Kocsis, J. (2007). All-PP composites (PURE®) with unidirectional and cross-ply lay-ups: dynamic mechanical thermal analysis. Polymer Letters, 1(8), pp.519–526.

Abrate, S., Castanie, B. and Rajapakse, Y.D.S. (2013). Dynamic failure of composite and sandwich structures. Dordrecht: Springer.

Ahmad, Z. (2009). Impact and energy absorption of empty and foam-filled conical tubes. PhD Thesis, Queensland University of Technology.

Akber Basri, M.H., Abdu, A., Junejo, N., Abdul Hamid, H. and Ahmed, K. (2014). Journey of kenaf in Malaysia : A Review. Academic Journals, 9(11), pp.458–470.

Akil, H.M., Omar, M.F., Mazuki, A.A.M., Safiee, S., Ishak, Z.A.M. and Abu Bakar, A. (2011). Kenaf fiber reinforced composites : A review. Materials and Design, 32, pp.4107–4121.

Aktas, M., Karakuzu, R. and Icten, B.M. (2010). Impact behavior of glass/epoxy laminated composite plates at high temperatures. Journal of Composite Materials, 44(19), pp.2289–2299.

Ali, M. (2010). Coconut Fibre – A Versatile Material and its Applications in Engineering. Proceedings of the Second International Conference on Sustainable Construction Materials and Technologies, Universita Politecnica delle Marche, Ancona, Italy.

Anonymous (2013). Bio-based News [Online]. [Access on April 2015]. Available from World Wide Web: http://news.bio-based.eu/biocomposites/.

Arrakhiz, F.Z., Malha, M., Bouhfid, R., Benmoussa, K. and Qaiss, A. (2012). Tensile, flexural and torsional properties of chemically treated alfa, coir and bagasse reinforced polypropylene. Composites Part B: Engineering, 47, pp.1–7.

Atas, C. and Sayman, O. (2008). An overall view on impact response of woven fabric composite plates. Composite Structures, 82, pp.336–345.

Ayrilmis, N., Jarusombuti, S., Fuengvivat, V., Bauchongkol, P. and White, R.H. (2011). Coir fiber reinforced polypropylene composite panel for automotive interior applications. Fibers and Polymers, 12(7), pp.919–926.

Bader, M.G. and Ellis, R.M. (1974). The effect of notches and specimen geometry on the pendulum impact strength of uniaxial CFRP. Composites, 5(6), pp.253–258.

Bailey, D.A. (2005). The effect of damage on the energy absorption potential of composite structures. PhD Thesis, University of Nottingham.

Balasubramani, V. and Boopathy, S.R. (2012). Damage area prediction of laminated composite plates after low velocity impact in ANSYS. IEEE Proceedings of 7th International Conference on Intelligent Systems and Control (ISCO 2013). Coimbatore, Tamil Nadu, India.

Begum, K. and Islam, M.A. (2013). Natural Fiber as a substitute to synthetic fiber in polymer composites : A review. Research Journal of Engineering Sciences, 2(3), pp.46–53.

Behr, M., Rosestritt, M., Lang, R. and Handel, G. (2000). Flexural properties of fiber reinforced composite using a vacuum/pressure or a manual adaptation manufacturing process. Journal of dentistry, 28(7), pp.509–514.

Belingardi, G. and Vadori, R. (2003). Influence of the laminate thickness in low velocity impact behavior of composite material plate. Composite Structures, 61, pp.27–38.

Bhattacharyya, D. and Fakirov, S. (2012). Synthetic Polymer-Polymer Composites. Munich: Hanser Publishers.

Bolukbasi, A.O. and Laananen, D.H. (1995). Energy absorption in composite stiffeners. Composites, 26, pp.291–301.

Cantwell, W.J. and Morton, J. (1989). Comparison of the low and high velocity impact response of CFRP. Composites, 20(6), pp.545–551.

Cantwell, W.J. and Morton, J. (1991). The impact resistance of composite materials — a review. Composites, 22(5), pp.347–362.

Cao, J., Akkerman, R., Boisse, P., Chen, J., Cheng, H.S., de Graaf, E.F., et al. (2008). Characterization of mechanical behavior of woven fabrics: Experimental methods and benchmark results. Composites Part A: Applied Science and Manufacturing, 39, pp.1037–1053.

Caprino, G., Langella, A. and Lopresto, V. (2003). Indentation and penetration of carbon fibre reinforced plastic laminates. Composites Part B: Engineering, 34, pp.319–325.

Caprino, G. and Lopresto, V. (2001). On the penetration energy for fibre-reinforced plastics under low-velocity impact conditions. Composites Science and Technology, 61, pp.65–73.

Cay, A., Atav, R. and Duran, K. (2007). Effects of warp-weft density variation and fabric porosity of the cotton fabrics on their colour in reactive dyeing. Fibres & Textiles in Eastern Europe, 15(1), pp.91–94.

Chai, G.B. and Manikandan, P. (2014). Low velocity impact response of fibre-metal laminates – A review. Composite Structures, 107, pp.363–381.

Chathbai, A. (2007). Parametric study of energy absorption characteristics of a rectangular aluminum tube wrapped with E-glass/epoxy. Master Thesis, Wichita State University.

Cheon, S.S., Lim, T.S. and Lee, D.G. (1999). Impact energy absorption characteristics of glass fiber hybrid composites. Composite Structures, 46, pp.267–278.

Collier, B. (2000). Understanding textiles, 6th edition, Upper Saddle River, New Jersey: Prentice Hall.

Collier, B. and Epps, H.H. (1999). Textile testing and analysis. New Jersey: Merrill.

Curtis, J. Hinton, M.J., Li, S., Reid, S.R. and Soden, P.D. (2000). Damage, deformation and residual burst strength of filament-wound composite tubes subjected to impact or quasi-static indentation. Composites Part B: Engineering, 31, pp.419–433.

Daihua, Z. (2007). Low velocity impact analysis of composite laminated plates. PhD Thesis, The University of Akron.

David, N. V., Gao, X.-L. and Zheng, J.Q. (2009). Ballistic resistant body armor: contemporary and prospective materials and related protection mechanisms. Applied Mechanics Reviews, 62, p.050802(1-20).

Defoirdt, N., Biswas, S., De Vriese, L., Tran, L.Q.N., Acker, J.V., Ahsan, Q., Gorbatikh, L., Vuure, A.V. and Verpoest, I. (2010). Assessment of the tensile properties of coir, bamboo and jute fibre. Composites Part A: Applied Science and Manufacturing, 41, pp.588–595.

Dehkordi, M.T., Nosraty, H., Shokrieh, M.M., Minak, G. and Ghelli, D. (2010). Low velocity impact properties of intra-ply hybrid composites based on basalt and nylon woven fabrics. Materials & Design, 31, pp.3835–3844.

De Weyenberg, I.V., Ivens, J., De Coster, A., Kino, B., Baetens, E. and Verpoest, I. (2003). Influence of processing and chemical treatment of flax fibres on their composites. Composites Science and Technology, 63, pp.1241–1246.

Dhakal, H.N., Skrifvars, M., Adekunle, K. And Zhang, Z.Y. (2014). Falling weight impact response of jute/methacrylated soybean oil bio-composites under low velocity impact loading. Composites Science and Technology, 92, pp.134-141.

Dhakal, H.N., Zhang, Z.Y., Bennett, N. and Reis, P.N.B. (2012). Low-velocity impact response of non-woven hemp fibre reinforced unsaturated polyester composites: Influence of impactor geometry and impact velocity. Composite Structures, 94, pp.2756–2763.

Dorey, G., Sidey, G. and Hutchings, J. (1978). Impact properties of carbon fibre/Kevlar 49 fibre hydrid composites. Composites, 9, pp.25–32.

Duan, Y., Saigal, A. and Greif, R. (2003). Impact behavior and modeling of engineering polymers. Polymer Engineering and Science, 43(1), pp.112–124.

Dubrovski, P.D. and Cebasek, P.F. (2005). Analysis of the mechanical properties of woven and nonwoven fabrics as an integral part of compound fabrics. Fibres & Textiles in Easterm Europe, 13(3), pp.50–53.

Ehrhardt, A., Groner, S. and Bechtold, T. (2007). Swelling behaviour of cellulosic fibres – Part 1: Changes in physical properties. Fibres & Textiles in Easterm Europe, 15(5-6), pp.46-48.

Ellis, R.L. (1996). Ballistic impact resistance of graphite epoxy composites with shape memory alloy and extended chain polyethlyne spectra hybrid components. Master Thesis, Virginia Polytechnic Institute and State University.

Fan, H., Zhou, Q., Yang, W. and Jingjing, Z. (2010). An experiment study on the failure mechanisms of woven textile sandwich panels under quasi-static loading. Composites Part B: Engineering, 41, pp.686–692.

Faruk, O., Bledzki, A.K., Fink, H-P. and Sain, M. (2012). Biocomposites reinforced with natural fibers: 2000–2010. Progress in Polymer Science, 37(11), pp.2000–2010.

Feraboli, P., Wade, B., Deleo, F. and Rassaian, M. (2009). Crush energy absorption of composite channel section specimens. Composites Part A: Applied Science and Manufacturing, 40, pp.1248–1256.

Fink, J.K. (2008). High performance polymers. Norwich, New York: William Andrew.

Goutianos, S., Peijs, T., Nystrom, B. and Skrifvars, M. (2006). Development of flax fibre based textile reinforcements for composite applications. Applied Composite Materials, 13, pp.199–215.

Gowda, T.M., Naidu, A.C.B. and Chhaya, R. (1999). Some mechanical properties of untreated jute fabric-reinforced polyester composites. Composites Part A: Applied Science and Manufacturing, 30, pp.277–284.

Gustin, J., Joneson, A., Mahinfalah, M. and Stone, J. (2005). Low velocity impact of combination Kevlar/carbon fiber sandwich composites. Composite Structures, 69, pp.396–406.

Hachemane, B., Zitoune, R., Bezzazi, B. and Bouvet, C. (2013). Sandwich composites impact and indentation behaviour study. Composites Part B: Engineering, 51, pp.1–10.

Halvorsen, A., Salehi-Khojn, A., Mahinfalah, M. and Nakhaei-Jazar, R. (2006). Temperature effects on the impact behavior of fiberglass and fiberglass/Kevlar sandwich composites. Applied Composite Materials, 13, pp.369–383.

Hariharan, A.B.A. and Abdul Khalil, H.P.S. (2005). Lignocellulose-based hybrid bilayer laminate composite: Part I - Studies on tensile and impact behavior of oil palm fiber-glass fiber-reinforced epoxy resin. Journal of Composite Materials, 39(8), pp.663–684.

Harish, S., Peter Michael, D., Bensely, A., Mohan Lal, D. and Rajadurai, A. (2009). Mechanical property evaluation of natural fiber coir composite. Materials Characterization, 60, pp.44–49.

Heinecke, J. (2007). From fiber to armor. Law enforcement technology magazine [Online]. [Access on April 2011]. Available from World Wide Web: http://www.officer.com/article/10249724/from-fiber-to-armor.

Ho, M. and Lau, K. (2012). Design of an impact resistant glass fibre/epoxy composites using short silk fibres. Materials and Design, 35, pp.664-669.

Hosur, M.V., Adbullah, M. and Jeelani, S. (2005). Studies on the low-velocity impact response of woven hybrid composites. Composite Structures, 67, pp.253–262.

Icten, B.M. and Karakuzu, R. (2008). Effects of weaving density and curing pressure on impact behavior of woven composite plates. Journal of Reinforced Plastics and Composites, 27(10), pp.1083–1092.

Idicula, M., Malhotra, S.K., Joseph, K. and Thomas, S. (2005). Dynamic mechanical analysis of randomly oriented intimately mixed short banana/sisal hybrid fibre reinforced polyester composites. Composites Science and Technology, 65, pp.1077–1087.

Iqbal, M.A. and Gupta, N.K. (2008). Energy absorption characteristics of aluminum plates subjected to projectile impact. Latin American Journal of Solids and Structures, 5, pp.259–287.

Jacob, G.C., Fellers, J.F., Simunovic, S. and Starbuck, M. (2002). Energy absorption in polymer composites for automotive crashworthiness. Journal of Composite Materials, 36, pp.813–850.

Jang, B.Z., Chen, L.C., Wang, C.Z., Lin, H.T. and Zee, R.H. (1989). Impact resistance and energy absorption mechanisms in hybrid composites. Composites Science and Technology, 34, pp.305–335.

Jawaid, M. and Abdul Khalil, H.P.S. (2011). Cellulosic / synthetic fibre reinforced polymer hybrid composites : A review. Carbohydrate Polymers, 86, pp.1–18.

Jayabal, S. and Natarajan, U. (2010). Influence of fiber parameters on tensile, flexural, and impact properties of nonwoven coir–polyester composites. International Journal of Advanced Manufacturing Technology, 54, pp.639–648.

Jayabal, S., Natarajan, U. and Murugan, M. (2011). Mechanical property evaluation of woven coir and woven coir-glass fiber-reinforced polyester composites. Journal of Composite Materials, 45(22), pp.2279–2285.

Jones, R.M. (1999). Mechanics of composite materials. 2nd edition. Philadelphia: Taylor & Francis.

Kaczmarek, H. and Maison, S. (1994). Comparative ultrasonic analysis of damage in CFRP under static indentation and low-velocity impact. Composites Science and Technology, 51, pp.11–26.

Kaleemulla, K.M. and Siddeswarappa, B. (2009). Plane strain fracture behaviour of fabric reinforced hybrid composites under varied notch configurations. Journal of Minerals & Materials Characterization & Engineering, 8(6), pp.495–508.

Kamiya, R., Cheeseman, B.A., Popper, P. Chou, T-W. (2000). Some recent advances in the fabrication and design of three-dimensional textile preforms: a review. Composites Science and Technology, 60, pp.33–47.

Kang, T.J. and Kim, C. (2000). Impact energy absorption mechanism of largely deformable composites with different reinforcing structures. Fibers and Polymers, 1(1), pp.45–54.

Karahan, M. (2008). Comparison of ballistic performance and energy absorption capabilities of woven and unidirectional aramid fabrics. Textile Research Journal, 78(8), pp.718–730.

Karakuzu, R., Erbil, E. and Aktas, M. (2010). Impact characterization of glass/epoxy composite plates: An experimental and numerical study. Composites Part B: Engineering, 41, pp.388–395.

Karthikeyan, A. and Balamurugan, K. (2012). Effect of alkali treatment and fiber length on impact behavior of coir fiber reinforced epoxy composites. Journal of Scientific & Industrial Research, 71, pp.627–631.

Khan, G.M.A. and Alam, M.S. (2012). Thermal characterization of chemically treated coconut husk fibre. Indian Journal of Fibre & Textile Research, 37, pp.20–26.

Kilic, Y. (2008). Impact and energy absorption of laminated and sandwich composites. Master Thesis, Massachusetts Institute of Technology.

Kim, J-K. and Sham, M-L. (2000). Impact and delamination failure of woven-fabric composites. Composites Science and Technology, 60, pp.745–761.

Kumar, N.M., Reddy, G.V., Naidu, S.V., Rani, T.S. and Subha, M.C.S. (2009). Mechanical properties of coir/glass fiber phenolic resin based composites. Journal of Reinforced Plastics and Composites, 28(21), pp.2605–2613.

Kushwaha, P.K. and Kumar, R. (2010). The studies on performance of epoxy and polyester-based composites reinforced with bamboo and glass fibers. Journal of Reinforced Plastics and Composites, 29(13), pp.1952–1962.

Li, X., Tabil, L.G. and Panigrahi, S. (2007). Chemical treatments of natural fiber for use in natural fiber-reinforced composites: A review. Journal of Polymers and the Environment, 15, pp.25–33.

Li, Y., Xuefeng, A. and Xiaosu, Y. (2012). Comparison with low-velocity impact and quasi-static indentation testing of foam core sandwich composites. International Journal of Applied Physics and Mathematics, 2(1), pp.58–62.

Lim, J.S., Lee, B.H., Lee, C.B. and Han, I-S. (2012). Effect of the weaving density of aramid fabrics on their resistance to ballistic impacts. Engineering, 4, pp.944–949.

Liu, D. (2004). Characterization of impact properties and damage process of glass/epoxy composite laminates. Journal of Composite Materials, 38(16), pp.1425–1442.

Liu, D., Raju, B.B. and Dang, X. (2000). Impact perforation resistance of laminated and assembled composite plates. International Journal of Impact Engineering, 24, pp.733–746.

Liu, Q. and Hughes, M. (2008). The fracture behaviour and toughness of woven flax fibre reinforced epoxy composites. Composites Part A: Applied Science and Manufacturing, 39, pp.1644–1652.

Lu, G. and Yu, T. (2003). Energy absorption of structures and materials. Cambridge: Woodhead Publishing Limited.

Mallick, P.K. 1988. Fiber-reinforced composites. New York: Marcel Dekker.

Mantena, P.R., Mann, R. and Nori, C. (2001). Low-velocity impact response and dynamic characteristics of glass-resin composites. Journal of Reinforced Plastics and Composites, 20(6), pp.513–534.

Mishra, S., Mohanty, A.K., Drzal, L.T., Misra, M., Parija, S., Nayak, S.K. and Tripathy, S.S. (2003). Studies on mechanical performance of biofibre/glass reinforced polyester hybrid composites. Composites Science and Technology, 63, pp.1377–1385.

Mohanty, A.K., Misra, M. and Hinrichsen, G. (2000). Biofibres, biodegradable polymers and biocomposites: An overview. Macromolecular Materials and Engineering, 276-277, pp.1–24.

Mohmmed, R., Zhang, F., Sun, B. and Gu, B. (2014). Static and low velocity impact on mechanical behaviours of foam sandwiched composites with different ply angles face sheets. Journal of Composite Materials, 48(10), pp.1173–1188.

Monteiro, S.N., Terrones, L.A.H. and D'Almeida, J.R.M. (2008). Mechanical performance of coir fiber/polyester composites. Polymer Testing, 27, pp.591–595.

Montgomery, D.C. (2009). Design and analysis of experiments. 7th edition. Hoboken, New Jersey: John Wiley & Sons.

Naik, N.K. (1994). Woven fabric composites. Lancaster: Technomic Publishing Co.

Nunes, L.M., Paciornik, S. and d'Almeida, J.R.M. (2004). Evaluation of the damaged area of glass-fiber-reinforced epoxy-matrix composite materials submitted to ballistic impacts. Composites Science and Technology, 64, pp.945–954.

Nunna, S., Chandra, P.R., Shrivastava, S. and Jalan, A.K. (2012). A review on mechanical behavior of natural fiber based hybrid composites. Journal of Reinforced Plastics and Composites, 31(11), pp.759–769.

Onder, E. and Berkalp, O.B. (2011). Basic operations in weaving process [Online]. [Access on December 2012]. Available from World Wide Web: http://textilelibrary.wordpress.com/.

Othman, A.R. and Hassan, M.H. (2013). Effect of different construction designs of aramid fabric on the ballistic performances. Materials and Design, 44, pp.407–413.

Padaki, N. V, Alagirusamy, R. and Deopura, B.L. (2008). Low velocity impact behaviour of textile reinforced composites. Indian Journal of Fibre & Textile Research, 33, pp.189–202.

Park, R. and Jang, J. (2003). Effect of laminate thickness on impact behavior of aramid fiber/vinylester composites. Polymer Testing, 22, pp.939–946.

Park, R. and Jang, J. (1997). Stacking sequence effect of aramid–UHMPE hybrid composites by flexural test method. Polymer Testing, 16, pp.549–562.

Pegoretti, A., Fabbri, E., Migliaresi, C. and Pilati, F. (2004). Intraply and interply hybrid composites based on E-glass and poly(vinyl alcohol) woven fabrics: tensile and impact properties. Polymer International, 53, pp.1290–1297.

Peled, A., Bentur, A. and Yankelevsky, D. (1998). Effects of woven fabric geometry on the bonding performance of cementitious composites. Advanced Cement Based Materials, 7, pp.20-27..

Powell, D.A. and Zohdi, T.I. (2009). Attachment mode performance of network-modeled ballistic fabric shielding. Composites: Part B, 40, pp.451–460.

Powell, P.C. (1994). Engineering with fibre-polymer laminates. London: Chapman & Hall.

Pramanik, B. and Mantena, P.R. (2012). Energy absorption of nano-reinforced and sandwich composites in ballistic and low-velocity punch-shear. Open Journal of Composite Materials, 2, pp.87–96.

Prasanna, G.V. and Subbaiah, K.V. (2013). Modification, flexural, impact, compressive properties and chemical resistance of natural fibres reinforced blend composites. Malaysian Polymer Journal, 8(1), pp.38–44.

Qiao, P., Yang, M. and Bobaru, F. (2008). Impact mechanics and high-energy absorbing materials : Review. Journal of Aerospace Engineering, 21(4), pp.235-248.

Quaresimin, M., Ricotta, M., Martello, L. and Mian, S. (2013). Energy absorption in composite laminates under impact loading. Composites Part B: Engineering, 44, pp.133–140.

Rahman, M. (2013). Impact resistance of laminated hybrid composite panels composed of compliant and rigid plies. PhD Thesis, The University of New South Wales.

Rahman, M.M and Khan, M.A. (2007). Surface treatment of coir (Cocos nucifera) fibers and its influence on the fibers' physico-mechanical properties. Composites Science and Technology, 67, pp.2369–2376.

Ramakrishnan, K.R. (2009). Low velocity impact behaviour of unreinforced bi-layer plastic laminates. Master Thesis, The University of New South Wales.

Rashed, H.M.M.A., Islam, M.A. and Rizvi, F.B. (2006). Effects of process parameters on tensile strength of jute fiber reinforced thermoplastic composites. Journal of Naval Architecture and Marine Engineering, 3, pp.1–6.

Reid, S.R. and Zhou, G. (2000). Impact behaviour of fibre-reinforced composite materials and structures. Cambridge, England: CRC Press, Woodhead Publishing Limited.

Reis, P.N.B., Ferreira, J.A.M., Santos, P., Richardson, M.O.W. and Santos, J.B. (2012). Impact response of Kevlar composites with filled epoxy matrix. Composite Structures, 94, pp.3520–3528.

Reyes, A., Langseth, M. and Hopperstad, O.S. (2002). Crashworthiness of aluminum extrusions subjected to oblique loading: experiments and numerical analyses. International Journal of Mechanical Sciences, 44, pp.1965–1984.

Richardson, M.O.W. and Wisheart, M.J. (1996). Review of low-velocity impact properties of composite materials. Composite Part A: Applied Science and Manufacturing, 27A, pp.1123–1131.

Rout, J., Misra, M., Mohanty, A.K., Nayak, S.K. and Tripathy, S.S. (2003). SEM observations of the fractured surfaces of coir composites. Journal of Reinforced Plastics and Composites, 22(12), pp.1083–1100.

Rout, J., Misra, M., Tripathy, S.S., Nayak, S.K. and Mohanty, A.K. (2001). The influence of fibre treatment on the performance of coir-polyester composites. Composites Science and Technology, 61, pp.1303–1310.

Santosa, S., Banhart, J. and Wierzbicki, T. (2001). Experimental and numerical analyses of bending of foam-filled sections. Acta Mechanica, 148, pp.199–213.

Santulli, C. (2007). Impact properties of glass/plant fibre hybrid laminates. Journal of Materials Science, 42, pp.3699–3707.

Santulli, C., Janssen, M. and Jeronimidis, G. (2005). Partial replacement of E-glass fibers with flax fibers in composites and effect on falling weight impact performance. Journal of Materials Science, 40, pp.3581–3585.

Sathishkumar, T.P., Naveen, J. and Satheeshkumar, S. (2014). Hybrid fiber reinforced polymer composites - a review. Journal of Reinforced Plastics and Composites, 33(5), pp.454–471.

Satyanarayana, K.G., Sukumaran, K., Mukherjee, P.S., Pavithran, C. and Pillai, S.G.K. (1990). Natural fibre-polymer composites. Cement & Concrete Composites, 12, pp.117–136.

Segreti, M., Rusinek, A. and Klepaczko, J.R. (2004). Experimental study on puncture of PMMA at low and high velocities, effect on the failure mode. Polymer Testing, 23, pp.703–718.

Seyam, A. and El-Shiekh, A. (1990). Mechanics of woven fabrics: Part I: Theoretical investigation of weavability limit of yarns with thickness variation. Textile Research Journal, 60(7), pp.389–404.

Seyam, A. and El-Shiekh, A. (1994). Mechanics of woven fabrics: Part IV: Critical review of fabric degree of tightness and its applications. Textile Research Journal, 64(11), pp.653–662.

Shengqing, Z. and Boay, C.G. (2013). Damage and failure mode maps of composite sandwich panel subjected to quasi-static indentation and low velocity impact. Composite Structures, 101, pp.204–214.

Sindhu, K., Joseph, K., Joseph, J.M. and Mathew, T.V. (2007). Degradation studies of coir fiber/polyester and glass fiber/polyester composites under different conditions. Journal of Reinforced Plastics and Composites, 26(15), pp.1571–1585.

Sinnppoo, K., Arnold, L. and Padhye, R. (2009). Application of wool in high-velocity ballistic protective fabrics. Textile Research Journal, 80, pp.1083–1092.

Sivapragasam, A. (2008). Coconut in Malaysia – current developments and potential for re-vitalization. Proceedings the 2nd International Plantation Industry Conference and Exhibition (IPICEX2008), Shah Alam, Malaysia.

Sreekala, M.S., George, J., Kumaran, M.G. and Thomas, S. (2002). The mechanical performance of hybrid phenol-formaldehyde-based composites reinforced with glass and oil palm fibres. Composites Science and Technology, 62, pp.339–353.

Sreekumar, P.A., Joseph, K., Unnikrishnan, G., and Thomas, S. (2007). A comparative study on mechanical properties of sisal-leaf-fibre reinforced polyester composites prepared by resin transfer and compression moulding techniques. Composites Science and Technology, 67, pp.453-461.

Srivastava, A., Majumdar, A. and Butola, B.S. (2011). Improving the impact resistance performance of Kevlar fabrics using silica based shear thickening fluid. Materials Science and Engineering: A, 529, pp.224–229.

Stronge, W.J. (2000). Impact Mechanics. Cambridge: Cambridge University Press.

Thwe, M.M. and Liao, K. (2003). Durability of bamboo-glass fiber reinforced polymer matrix hybrid composites. Composites Science and Technology, 63, pp.375–387.

Ursenbach, D.O., Vaziri, R. and Delfosse, D. (1995). An engineering model for deformation of CFRP plates during penetration. Composite Structures, 32, pp.197–202.

Venkata Reddy, G., Venkata Naidu, S. and Shobha Rani, T. (2008). Impact properties of kapok based unsaturated polyester hybrid composites. Journal of Reinforced Plastics and Composites, 27(16-17), pp.1789–1804.

Verma, D., Gope, P.C., Shandilya, A., Gupta, A. and Maheshwari, M.K. (2013). Coir fibre reinforcement and application in polymer composites : A Review. Journal of Materials and Environmental Science, 4(2), pp.263–276.

Wambua, P., Vangrimde, B., Lomov, S. and Verpoest, I. (2007). The response of natural fibre composites to ballistic impact by fragment simulating projectiles. Composite Structures, 77, pp.232–240.

Wambua, P., Ivens, J. and Verpoest, I. (2003). Natural fibres: can they replace glass in fibre reinforced plastics? Composites Science and Technology, 63, pp.1259–1264.

Wan, Y.Z., Wang, Y.L., Luo, H.L., Dong, X.H. and Cheng, G.X. (2000). Effects of fiber volume fraction, hot pressing parameters and alloying elements on tensile strength of carbon fiber reinforced copper matrix composite prepared by continuous three-step electrodeposition. Materials Science and Engineering: A, 288, pp.26–33.

Wang, W., Wan, X., Zhou, J., Zhao, M., Li, Y., Shang, S. and Gao, X. (2014). Damage and failure of laminated carbon-fiber-reinforced composite under low-velocity impact. Journal of Aerospace Engineering, 27, pp.308–317.

Wang, W. and Huang, G. (2009). Characterisation and utilization of natural coconut fibres composites. Materials & Design, 30, pp.2741–2744.

Wang, X., Hu, B., Feng, Y., Liang, F., Mo, J., Xiong, J. and Qiu, Y. (2008). Low velocity impact properties of 3D woven basalt/aramid hybrid composites. Composites Science and Technology, 68, pp.444–450.

Wei, W. and Gu, H. (2009). Characterisation and utilization of natural coconut fibres composites. Materials & Design, 30, pp.2741–2744.

Wirawan, R., Zainudin, E.S. and Sapuan, S.M. (2009). Mechanical properties of natural fibre reinforced PVC composites : A Review. Sains Malaysiana, 38(4), pp.531–535.

Wong, K.J, Nirmal, U. and Lim, B.K. (2010). Impact behavior of short and continuous fiber-reinforced polyester composites. Journal of Reinforced Plastics and Composites, 29(23), pp.3463–3474.

Xiao, S., Chen, P. and Ye, Q. (2014). Prediction of damage area in laminated composite plates subjected to low velocity impact. Composites Science and Technology, 98, pp.51–56.

Yahaya, R., Sapuan, S.M., Jawaid, M., Leman, Z. and Zainudin, E.S. (2014). Quasi-static penetration and ballistic properties of kenaf–aramid hybrid composites. Materials and Design, 63, pp.775–782.

Yang, H.H. (1991). Kevlar Aramid Fiber. Chichester: John Wiley Sons & Ltd.

Yousif, B.F., Shalwan, A., Chin, C.W. and Ming, K.C. (2012). Flexural properties of treated and untreated kenaf/epoxy composites. Materials and Design, 40, pp.378–385.

Yuhazri, M. and Dan, M. (2007). Helmet shell using coconut fibre. Journal Advanced Manufacturing Technology, 1(1), pp.23–30.

Zampaloni, M., Pourboghrat, F., Yankovich, S.A., Rodgers, B.N., Moore, J., Drzal, L.T., Mohanty, A.K. and Misra, M. (2007). Kenaf natural fiber reinforced polypropylene composites : A discussion on manufacturing problems and solutions. Composites Part A: Applied Science and Manufacturing, 38, pp.1569–1580.

Zarei, H.R. and Kroger, M. (2006). Multiobjective crashworthiness optimization of circular aluminum tubes. Thin-Walled Structures, 44, pp.301–308.

Zhang, D., Sun, Y., Chen, L. and Pan, N. (2013). A comparative study on low-velocity impact response of fabric composite laminates. Materials and Design, 50, pp.750–756.

Zhang, G.M, Batra, R.C. and Zheng, J. (2008). Effect of frame size, frame type, and clamping pressure on the ballistic performance of soft body armor. Composites Part B: Engineering, 39, pp.476–489.

Zhang, J.Y., Yu, T.X., Kim, J.K. and Sui, G.X. (2000). Static indentation and impact behaviour of reformed bamboo/aluminium laminated composites. Composite Structures, 50, pp.207–216.

Zhang, S-Y., Wang, C-G., Fei, B-H., Yu, Y., Cheng, H-T. and Tian, G-L. (2013). Mechanical function of lignin and hemicelluloses in wood cell wall revealed with microtension of single wood fiber. Bioresources, 8(2), pp.2376–2385.

LIST OF PUBLICATION

Publications

Azrin Hani, A.R., Hashim, M.S., Lim, T.Y., Mariatti, M. and Ahmad, R. (2015). Impact behaviour of woven coir-epoxy composite: Effects of woven density nd woven fabric treatment. Journal of Materials: Design and Applications. [Accepted, Impact factor: 0.746]

Azrin Hani, A.R., Shaari, M.F., Mohd Radzuan, N.S., Hashim, M.S., Ahmad, R. and Mariatti, M. (2013). Analysis of woven natural fiber fabrics prepared using self-designed handloom. International Journal of Automotive and Mechanical Engineering, 8, pp.1197-1206. [Scopus indexed]

Azrin Hani, A.R., Ahmad, R. and Mariatti, M. (2014). Impact behaviour of woven coir-epoxy composite prepared by compression moulding and vacuum bagging methods. Journal of Applied Science and Agriculture, 9(11), pp. 333-340. [ISI indexed]

Azrin Hani, A.R., Mariatti, M., Roslan, A., Mohd Nazrul, R. and Othman, A.R. (2013). Influence of woven and cross-ply laminates on mechanical properties of coir epoxy composite. Applied Mechanics and Materials, 315, pp.136-140. [Scopus indexed]

Azrin Hani, A.R., Chan, T.S., Ahmad, R. and Mariatti, M. (2013). Impact and flexural properties of imbalance plain woven coir and kenaf composite. Applied Mechanics and Materials, 271-272, pp.81-85. [Scopus indexed]

Azrin Hani, A.R., Ahmad, R. and Mariatti, M. (2013). Influence of laminated textile structures on mechanical performance of NF-epoxy composites. World Academy of Science, Engineering and Technology, 78, pp.861-867.

Azrin Hani, A.R., Roslan, A., Mariatti, J. and Maziah, M. (2012). Body armor technology: A review of materials, construction techniques and enhancement of ballistic energy absorption. Advanced Materials Research, 488-489, pp.806-812. [Scopus indexed]

Azrin Hani, A.R., Ahmad, R., Mariatti, J., Roslan, M.N. and Ariffin, S. (2011). Mechanical properties evaluation of woven coir and Kevlar reinforced epoxy composites. Advanced Materials Research, 277, pp.36-42. [Scopus indexed]

Presentations

Azrin Hani, A.R., Ahmad, R. and Mariatti, M. (2014). Impact behaviour of woven coir-epoxy composite prepared by compression moulding and vacuum bagging methods. International Conference on Agriculture, Biotechnology, Science and Engineering, Ho Chi Minh City, Vietnam, 29-30 August, 2014.

Azrin Hani, A.R., Ahmad, R. and Mariatti, M. (2013). Influence of laminated textile structures on mechanical performance of NF-epoxy composites. The International Conference on Aerospace, Mechanical, Automotive and Materials Engineering, Istanbul, Turkey, 20-21 June, 2013.

Azrin Hani, A.R., Shaari, M.F., Mohd Radzuan, N.S., Hashim, M.S., Ahmad, R. and Mariatti, M. (2013). Analysis of woven natural fiber fabrics prepared using self-designed handloom. 2nd International Conference on Mechanical Engineering Research, Gambang, Kuantan, Pahang, 1-3 July, 2013.

Azrin Hani, A.R., Chan, T.S., Ahmad, R. and Mariatti, M. (2013). Impact and flexural properties of imbalance plain woven coir and kenaf composite. The 3rd International Conference on Frontiers of Manufacturing and Design Science, Hong Kong, 11-13 December, 2012.

Azrin Hani, A.R., Mariatti, M., Roslan, A., Mohd Nazrul, R. and Othman, A.R. (2013). Influence of woven and cross-ply laminates on mechanical properties of coir epoxy composite. The 3rd International Conference on Mechanical and Manufacturing Engineering, UTHM, Johor, Malaysia, 20-21 November, 2012.

Azrin Hani, A.R., Ahmad, R., Mariatti, J., Roslan, M.N. and Ariffin, S. (2011). Mechanical properties evaluation of woven coir and Kevlar reinforced epoxy composites. The 12th International Conference on QiR (Quality in Research), Bali, Indonesia, 4-7 July, 2011.